TABLE OF CONTENTS

Page

LIST OF TABLES

Page

LIST OF FIGURES

LIST OF ABREVIATIONS

AVR	Automatic Voltage Regulator
CCPs	Carbon Capture Plants
CPF	Continuation Power Flow
DAEs	Differential Algebraic Equations
DFIG	Doubly Fed Induction Generator
DR	Demand Response
ED	Economic Dispatch
ENVCI	Equivalent Node Voltage Collapse Index
EPSO	Enhanced Particle Swarm Optimization
ESSs	Energy Storage Systems
FIR	Fast Instantaneous Reserve
FRC	Fully Rated Converter
FTS	Full Time Scale
FVSI	Fast Voltage Stability Index
GA	Genetic Algorithm
GEM	Generator Equivalent Model
GSA	Gravitational Search Algorithm
GSC	Grid-Side Converter
HDE	Hybrid Differential Evolution
IB	Impedance Index
ISO	Independent System Operator

LFF	Load Flow Feasibility
LMPs	Local Marginal Prices
LS	Load Shedding
LVRT	Low Voltage Ride Through
LVSI	Line Voltage Stability Index
MSV	Minimum Singular Value
OLTC	On-Load Tap Changer
OPF	Optimal Power Flow
OXL	Over Excitation Limiter
PF	Power Flow
PIs	Performance Indices
PMUs	Phasor Measurement Units
PSO	Particle Swarm Optimisation
QSS	Quasi Steady State
RESs	Renewable Energy Sources
RPD	Reactive Power Dispatch
RSC	Rotor-side converter
SFR	System Frequency Response
SIR	Sustained Instantaneous Reserve
SOC	State of Charge
SOPF	Stochastic Optimal Power Flow
SVC	Static VAR Compensator
TEI	Thevenin Equivalent Impedance

TH	Threshold Value
TV	Tangent Vector
UFLS	Under-Frequency Load Shedding
VCPI	Voltage Collapse Proximity Indicator
VSC-OPF	Voltage Stability Constrained Optimal Power Flow
VSM	Voltage Stability Margin
WECC	Western Electricity and Coordinating Council
WF	Wind Farm
WG	Wind Generator

INTRODUCTION

Nowadays, voltage stability assessment is an important issue in power systems due to a large number of blackouts in different countries. The main goal of an independent system operator (ISO) is to run the power system operation without any voltage stability collapse at low cost or high revenue. Many voltage stability indices (VSIs) have been presented that have a role to evaluate the voltage instability risk and to predict the voltage collapse point.

In the recent decades, the electric power industry has changed from the monopoly which was controlled by a government to a free competition environment. Many regulations have been changed to be adaptable to this new environment in different areas. Thus, voltage stability assessment carried out by an ISO should be revised and reformulated. It is an undeniable fact that the power system should operate close to the limits of stable conditions, because of minimizing the total costs. Therefore, some factors will be come out which may trigger the long-term voltage instability such as a stressed power system, insufficient fast reactive power resources, on-line load tap changers (OLTCs) response and so on. Several elements have an impact on the voltage control which are OLTCs, generators, over excitation limiters (OXLs), static and switchable capacitor/reactor banks and static VAR control (SVC) (Canizares, 2002).

Voltage instability is a local and a nonlinear phenomenon. When a high voltage variation occurs, the power system may lose the loads in some areas or the elements such as transmission lines and generators (Cutsem et Vournas, 1998). The sequence of cascading events with voltage instability may result in a phenomenon which is named *voltage collapse.* The outcome of this phenomenon is a blackout or a low-voltage operation. Most reasons of voltage collapse are based on failing to provide reactive power demands (Canizares, 2002; Eremia et Shahidehpour, 2013):

- Inability to provide reactive power by generators and SVC due to the reactive power limits;

- Increase of reactive power loss on the congested transmission lines;
- Behavior of OLTCs until hitting their limits;
- Increase of active power loading;
- Dynamics of load recovery;
- Contingencies such as line tripping or generator outage.

The voltage collapse events can cause extensive power system outages. Thus the number of power system outages worldwide, which are increasing yearly, should be reduced. Figure 0.1 presents a summary of extensive power system outages over the recent half-century. Figure 0.2 shows the approximate percent of extensive outages over the recent half-century based on different locations as the US & Canada, Europe, and the rest of the world (International)(Wikipedia, 2017). Whole outage costs are approximately calculated $75B annually in the US & Canada (McLinn, 2009).

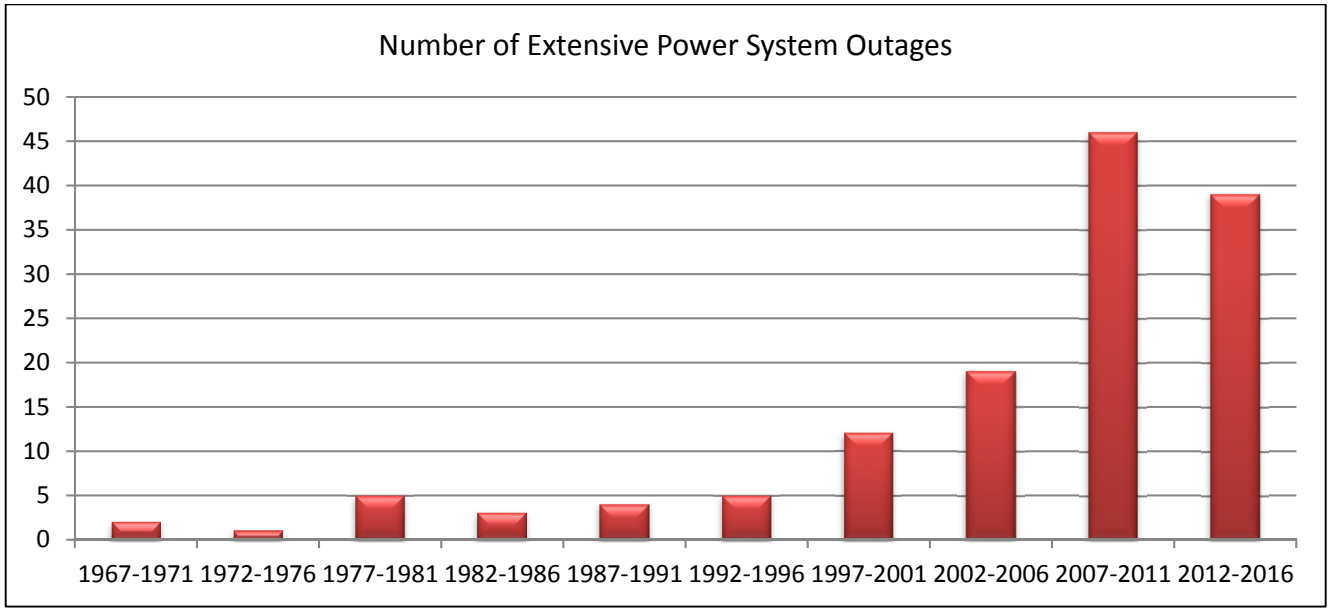

Figure 0.1 Number of extensive power system outages in worldwide

An optimal power flow (OPF) approach was first developed in 1962 by Carpentier. There are different linear and nonlinear solution methods for this approach while linear methods are inaccurate and nonlinear methods are slow and fragile. It is important to get accurate

solutions because of solving the OPF periodically each five minutes. In spite of the introduction of the OPF more than a half-century, the OPF encounters inaccurate and fragile solutions which may enforce an extra cost in billions of dollars per year to ISO (Cain, O'Neill et Castillo, December, 2012).

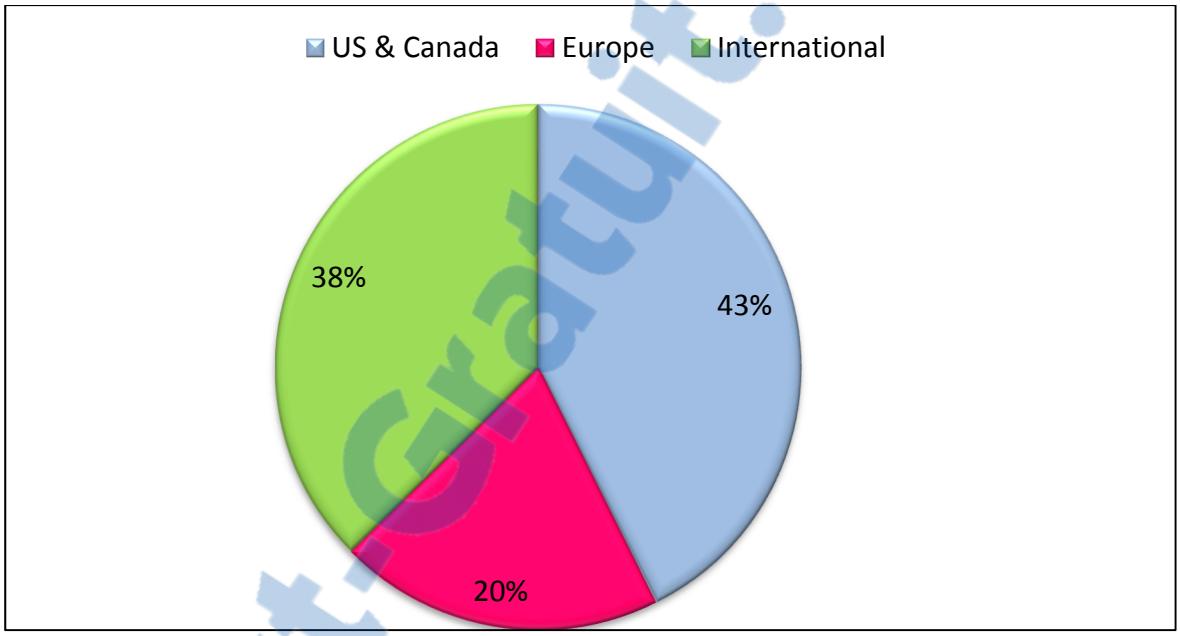

Figure 0.2 Percent of extensive power system outages in different locations

Generally, the power flow (PF) analysis shows the behavior of elements in steady state conditions. This analysis can calculate whether power system elements can satisfy the limits in steady state conditions without any contingencies or not. Moreover, the OPF analysis can reach the losses at the minimum level by calculating all the values of voltages and currents (Andersson, 2004). Variations of unpredicted resources like wind power create a high amount of uncertainties. In this situation, stochastic OPF (SOPF) can reduce the risk of outages (Bienstock, Chertkov et Harnett, 2014). The SOPF approach provides an applicable model for uncertainties in the system.

Motivation and Challenges

One of the challenges in power systems is a large number of voltage collapses which frequently occur. Therefore, voltage stability evaluation becomes crucial in power system operation and control. Voltage stability can be affected by several elements and controllers which operate in different time scales. In particular, the role of wind power generation, demand response (DR), over excitation limiter (OXL), on-load tap changer (OLTC) and generator model are significant. The proper modelling of these elements and controllers as well as using an OPF approach should be analyzed for long-term voltage stability.

VSIs can be mixed with OPF and they produce a problem which is named Voltage Stability Constrained OPF (VSC-OPF) (Avalos, Canizares et Anjos, 2008; Canizares et al., 2001; Lage, da Costa et Canizares, 2012; Milano, Canizares et Invernizzi, 2005; Rosehart, Canizares et Quintana, 2003a; 2003b; Venkatesh, Arunagiri et Gooi, 2003). These traditional VSC-OPF approaches don't consider the model of elements and efficient control ways like wind power generation, DR, OXL, OLTC and generator. Due to the dynamic behavior of power systems, using traditional VSI is not accurate and cannot predict the unstable operating point. Thus, the creation of new VSC-OPF approaches can be useful to improve the performance of ISOs.

Research Objective

The principal objective of this thesis is to choose an appropriate criteria for voltage stability evaluation in SOPF approach and to consider the worst contingency or the congested condition. Modeling of elements and control ways like a wind generator, DR, OXL and OLTC is considered in the OPF formulation.

According to the literature review and simulations that will be described in detail, the following objectives are derived from the principal goal:

- To evaluate and compare several important voltage stability indices;
- To compare different VSC-OPF approaches and represent their drawbacks;

- To introduce a novel voltage stability index that can model OLTCs, capability curve limits of traditional generators and wind generators;
- To develop a new formulation for VSC-OPF approaches with the novel voltage stability index;
- To analyze SOPF approaches with the presence of uncertainties in wind power generation;
- To investigate DR and load shedding (LS) program in SOPF approaches;
- To add a frequency restoration scheme in VSC-SOPF formula and find the effects of DR and LS program;

Methodology

The following section describes the proposed methodology to achieve the research objectives. The methodology includes the following steps:

- Comparison between different voltage stability indices such as L-index, minimum singular value and line voltage stability indices (LVSIs) is carried out. Then, VSC-OPF approaches with these indices is implemented in MATLAB and validated in several case studies. The approaches are optimized with different objective functions like minimization of the operating cost function.
- Investigating the behavior of elements and control ways, such as DR, wind generator, OLTC and OXL in the long-term voltage stability simulation with PSAT. This step will help to define new voltage stability indices for better voltage instability detection. Then, implement the VSC-OPF approach with these new indices in MATLAB and PSAT. This approach will be performed in different test systems.
- Implementing SOPF to model the uncertainties in wind power generation. A literature review is done to choose an appropriate technique to consider the uncertainties.
- Appending frequency constraints in the VSC-SOPF. These constraints are extracted from a frequency restoration scheme with three levels. Cooperating the DR and LS

program and reserve is considered in this scheme. Due to the complexity and nonlinearity of the constraints, this approach is carried out in GAMS.

Thesis Contributions

The contributions of the thesis are described as follows:

An improved impedance-based index for voltage stability analysis

An improved impedance-based (IB) index is proposed in this thesis that models doubly-fed induction generator (DFIG) capability curve limits and OLTC behavior. These factors have significant roles in the long-term voltage stability studies. The proposed IB index can detect precisely the voltage collapse, especially after the occurrence of a given contingency due to the dynamic elements of the system. It can model the DFIG reactive power capability characteristics as a variable virtual impedance which is adaptable in the dynamic studies. Therefore, the model of DFIG reactive limits can be integrated to the internal circuit of the generator and it can be appended to impedance matching theory. An OLTC model is also added to this index. The OLTC can affect both Thevenin equivalent impedance and load impedance. Thus, the IB index equation is modified by considering those impedance variations on the OLTC model. The robustness of the proposed method has been investigated by including SVC and different load types in the power systems.

A new VSC-OPF approach with proposed improved IB index

A VSC-OPF approach is studied including an improved IB index. A new approach is compared with three existing VSC-OPF approaches in stressed and single line outage conditions. These VSC-OPF approaches are, namely, based on the L-index, the minimum singular value and the voltage collapse proximity indicator (VCPI). The proposed VSC-OPF

approach can reduce the operating cost and the number of voltage collapses. Thus, it can improve the performance of the electric utilities.

A novel LVSI as a criterion for voltage stability detection

This thesis proposes a LVSI which can detect precisely the voltage collapse in comparison with other LVSIs, especially after the occurrence of a given contingency due to the dynamic elements of the system. This index is based on the impedance theory which is a proper way to estimate the maximum power transferred to a load bus. The impedance seen at two buses of a transmission line can provide important information for the operation and control of the power system.

A multi-objective SOPF approach with the presence of uncertain wind power generations

The thesis also implements a multi-objective SOPF approach which consists of the operating cost, voltage stability and emission effects as the objective functions. The wind uncertainty is formulated as a scenario-based technique. DR program is considered in this study, which is one of the most efficient control ways to reduce the risk of voltage instability after a contingency occurrence or a stressed loading condition. In addition, the proposed approach uses the technique of fuzzification to normalize all objective functions and to find the optimal solution. A comprehensive comparison between different LVSIs as the objective function is given in the multi-objective SOPF. Also, the multi-objective SOPF with proposed LVSI is investigated under different scenarios. It can reduce the operating cost and increase the minimum voltage magnitude. Thus, it can improve the performance of the electric utilities.

Frequency and Voltage Constrained SOPF Considering Wind Power and Demand Response Resources

An approach for frequency and voltage control in SOPF with the presence of uncertain wind power generations and energy storage systems (ESSs) is proposed in this thesis. The proposed scenario-based SOPF utilizes a combined DR, ESS, LS and reserve to increase

reliability under various contingency occurrences. The objective function is the minimization of total operating cost and it considers costs for DR, LS, wind spillage and reserve resources. To solve frequency instability issue, it uses the reduced-order system frequency response (SFR) model and creates some extra constraints to be added to the SOPF. The frequency restoration scheme is defined in three levels. To keep a system safe from the viewpoint of voltage stability issue, it uses extended L-index (EL-index).

Thesis Outline

This thesis is organized as follows. Chapter 1 contains a literature review on the impact of different elements on voltage stability analysis and it also presents different VSIs, VSC-OPF and SOPF approaches. Chapter 2 describes a new VSC-OPF approach with proposed improved IB index. The index can model the great changes during a voltage collapse process such as line tripping, load tap changing and reactive power limits of DFIG and conventional generator. This index can also monitor online voltage stability. The proposed IB index can model the DFIG reactive power capability characteristics as a variable virtual impedance which is adaptable in the dynamic studies.

An OLTC model is also added to this index. The OLTC can affect both TEI and load impedance. Thus, the IB index equation is modified by considering those impedance variations on the OLTC model. A new VSC-OPF is also carried out with the proposed IB index. The proposed VSC-OPF can reduce the operating cost and the number of voltage collapses. Thus, it can improve the performance of the electric utilities.

In Chapter 3, a multi-objective SOPF approach with the presence of uncertain wind power generations is investigated. This chapter proposes a multi-objective SOPF problem considering wind uncertainty and DR. This multi-objective SOPF consists of the operating cost, voltage stability and emission effects as the objective functions. Furthermore, a new LVSI is presented that can detect precisely the voltage collapse in comparison with other LVSIs. Finally, a comprehensive comparison between different LVSIs as the objective

function is given in the multi-objective SOPF. Also, the multi-objective SOPF with proposed LVSI is investigated under different scenarios. It can reduce the operating cost and increase the minimum voltage magnitude. Thus, it can improve the performance of the electric utilities.

Chapter 4 includes a frequency and voltage constrained SOPF considering wind power and demand response resources. The proposed scenario-based SOPF utilizes a combined DR, ESS, load shedding (LS) and reserve to increase reliability under various contingency occurrences. In the proposed frequency and voltage stability assessment, the objective function is the minimization of total operating costs and it considers costs for DR, LS, wind spillage and reserve resources. To solve frequency instability issues, this chapter uses the reduced-order system frequency response (SFR) model and creates some constraints to be added to the SOPF. To keep a system safe from the viewpoint of voltage stability issues, it uses the EL-index. The EL-index is one of the voltage stability indices that can predict voltage collapse accurately. Finally, a conclusion and future works are presented at the end of this document.

CHAPTER 1

LITERATURE REVIEW

1.1 Basic principles of voltage stability

This section contains a summary in subjects such as different types of stability, voltage stability evaluation methods, important operating points and QSS time domain simulation.

1.1.1 Different types of stability and voltage stability

The behavior of power system stability changes dynamically and all dynamic systems are based on complicated mathematical equations. From an economical viewpoint, a power system cannot be stable for any perturbations. When a perturbation appears, power system variables such as bus voltages, and machine rotor speeds, active and reactive power will change greatly. These variations activate all governors and voltage regulators to restore a power system to the equilibrium point. Even some elements may be disconnected from network to preserve the main system from cascading instability (Kundur et al., 2004).

Power system stability can be categorized in several forms based on: 1) main variables of the power system; 2) extent of the perturbations; 3) time scales of simulation. Figure 1.1 shows the main types of the power system stability (Canizares, 2002). Long-term voltage stability includes slow dynamic elements such as OLTC, OXL, and some controlled loads. The time scale of this voltage stability is until several minutes. Different forms of instability may change from one form to another in the power system dynamically. To realize the instability forms, it needs to be familiar with dynamic operation behavior of power systems (Kundur et al., 2004). Long-term voltage stability can be divided into large-disturbance and small-disturbance voltage stability. The small-disturbance voltage stability problem can be modeled with linearized power system equations with acceptable error. But it cannot disregard nonlinear behavior of some elements such as OLTC. Increasing the active and reactive power

in the inductive elements has a major effect on voltage reduction. Over excitation and under excitation limits of generators or synchronous compensators may intensify this process of voltage reduction when a fault causes and also when the reactive power is not sufficient. In addition, transferring the reactive power for long distance is improper. It has a negative effect on active and reactive power losses and it increases the risk of voltage collapse (Taylor, Balu et Maratukulam, 1994).

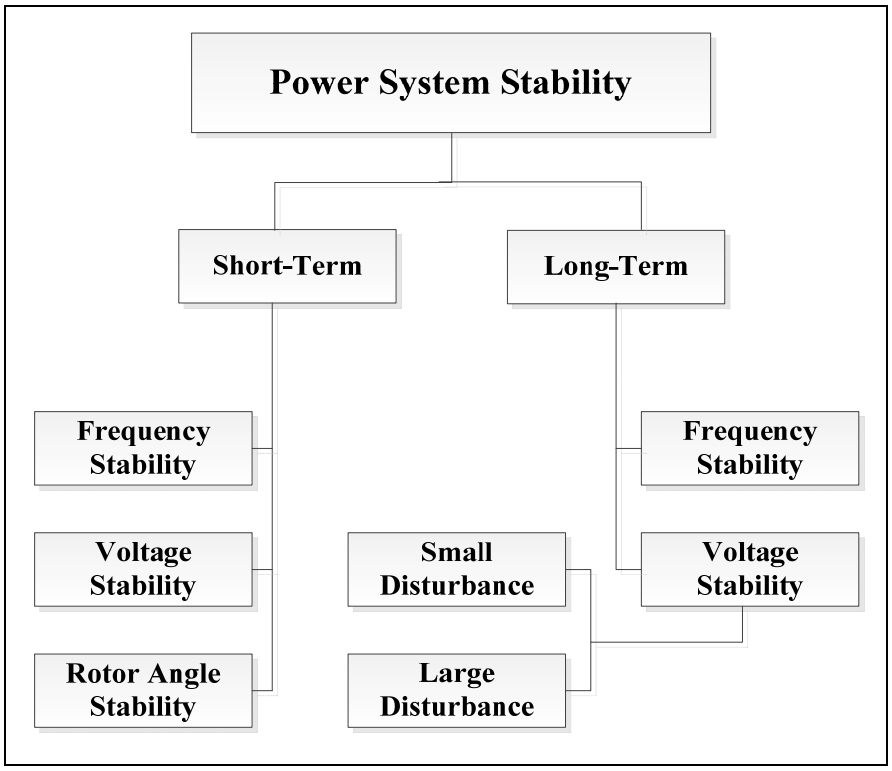

Figure 1.1 Different types of power system stability

When the short-term dynamics have diminished, the long-term dynamics (slow dynamics) will remaines and it should be considered. Long-term (LT) voltage instability is classified into three types of instability (Canizares, 2002; Cutsem et Vournas, 1998). LT1 is loss of equilibrium. This instability is the most common instability procedures; load restoration and OLTCs affect on this instability. LT2 is a lack of attraction towards a stable equilibrium. For instance, first LT1 occurs and then corrective actions are performed with a delay. Therefore, there is not enough time to restore the operating point. LT3 is a slow growth of the voltage

oscillation. This instability is less common; one example can be produced by the cascaded load restoration or incorrectly tuned OLTCs.

1.1.2 Operating points and zones

One of the methods for evaluation of voltage stability is continuation power flow (CPF) which produces some curves such as PV, PQ and QV curves. Different types of operating zones represented in Figure 1.2 are divided into the controllable zone and uncontrollable zone in the PV curve. Controllable zone (stable operating zone) is the upper part of the curve. All points of this zone have negative sensitivities. It can be defined as two sub-zones for better evaluation (optimal and critical zones). Uncontrollable zone (unstable operating zone) is the lower part of the curve. All points of this zone have positive sensitivities (Eremia et Shahidehpour, 2013).

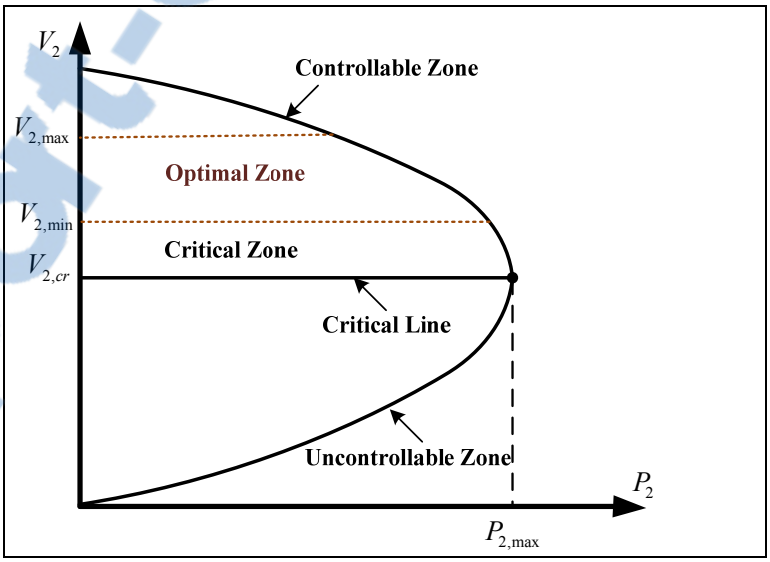

Figure 1.2 Operating zones in a PV curve

The range of these zones is dependent on different system topology and ISO regulations. For example, as reported by Western Electricity and Coordinating Council (WECC), a safety margin in case 1 (N-0, N-1 contingencies) and case 2 (N-2, N-3 contingencies) are 5% and 2.5%, respectively (Al Dessi, Osman et Ibrahim, 2013).

1.1.3 Voltage stability evaluation methods

Voltage stability evaluation methods are divided into two fundamental methods which are named static and dynamic methods. Static methods are based on PF equations and linearized differential-algebraic equations (DAEs); also they are considerably quicker than the dynamic methods. Some indices (local or global) are introduced in these methods which will be described in detail. The dynamic methods based on DAEs are divided into the integration and global methods.

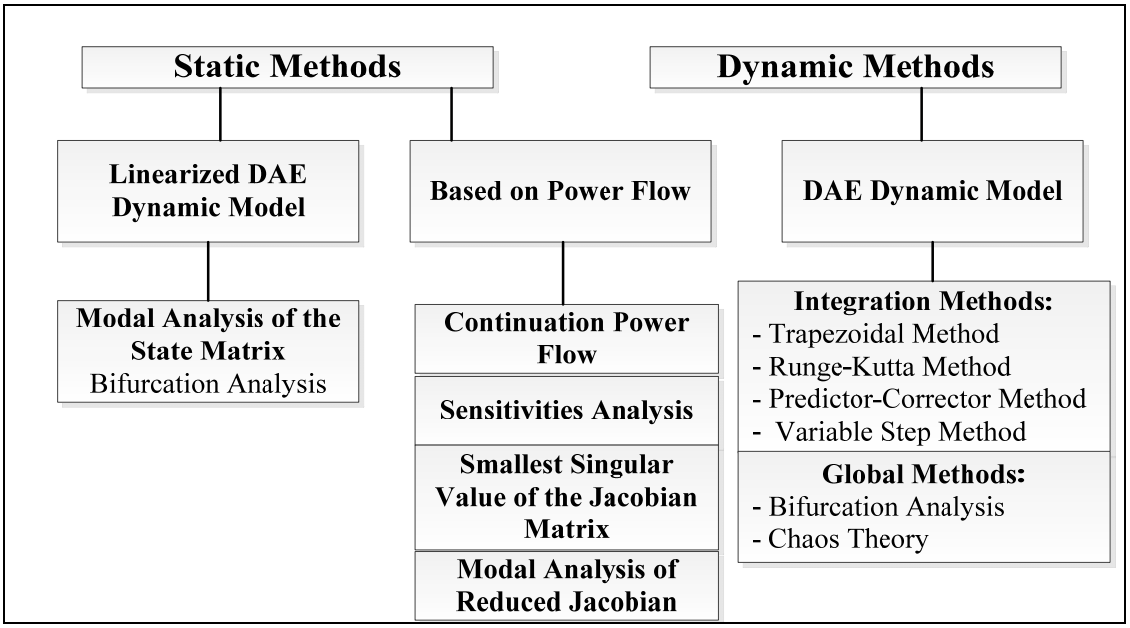

Figure 1.3 Voltage stability evaluation methods
Adapted from Eremia and Shahidehpour (2013)

The bifurcation theory assumes that variations of system parameters are slow and also it can evaluate the behavior of a system until reaching instability. The power system equations in the bifurcation analysis are defined as states and parameters. The states such as magnitudes and angles of bus voltage, and machine angles change very fast. The parameter changes slowly in the power system equations such as active power demands. How to choose states and parameters are significant in the power system modeling (Canizares, 2002).

Saddle node bifurcation is defined when PF solutions will change until vanishing the convergence. Therefore, there are no PF solutions at this point. Singularity induced bifurcations is defined when the singularity appears in the DAEs of a power system because of changing a state parameter gradually, and then the system immediately falls into instability by an infinite behavior. Voltage instability due to the reactive power limit of generator can be caused the singularity induced bifurcation (Gomez-Exposito, Conejo et Canizares, 2008; Ilić et Zaborszky, 2000).

1.1.4 QSS time-domain simulation

The QSS approach relies on the time-scale decomposition in the long-term dynamics. This approach is a well-known technique which can increase the computational efficiency and also it can be used in the real time voltage assessment. The QSS simulation analyses the long-term instability dynamics and ignores the short-term dynamics. In addition, it can change the value of step size for reaching the optimum time and accuracy (Van Cutsem et Vournas, 1996). The power system dynamics can be divided into continuous and discrete-time parameters because the components (controllers and protecting devices) can be operated based on both continuous and discrete-time state vectors. Based on the above considerations, equations of Full Time Scale (FTS) simulation and QSS simulation are provided in Figure 1.4.

The algebraic function g represents the network equations. The differential function f relates to some components which can be divided into two sub-functions where x_s is the "slow" state vector, x_f is the "fast" state vector. The algebraic function h shows the discrete events like as capacitor switching, OLTC and OXL operation. As seen in Figure 1.5, parameter h is defined as the time step size of the algorithm (about 1s to 10s) and each dot shows a short-term equilibrium point.

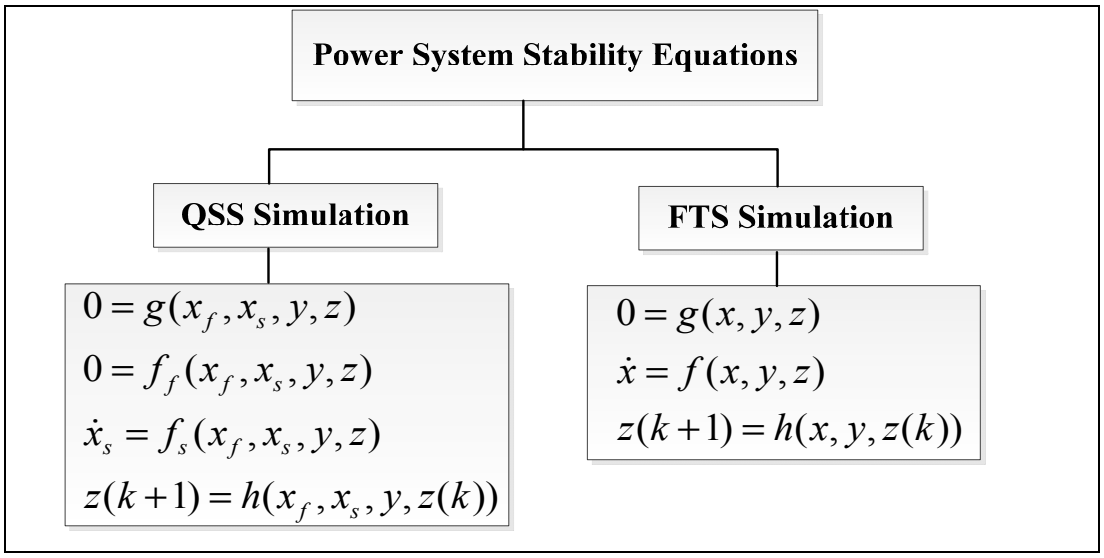

Figure 1.4 Equations of FTS and QSS simulations

Some components like as OXLs, OLTCs and switched shunt elements can act as discrete dynamics, so vertical jumps (A to A', B to B') show this behavior. Horizontal jumps (A' to B, B' to C) can be obtained from the differential equations and the load self-restoration (Van Cutsem et Mailhot, 1997). The comparison between QSS and FTS simulations is presented in (Gear, 1971) that shows two curves are approximately same and cannot simply be distinguished. The extended QSS model presented in (Grenier, Lefebvre et Van Cutsem, 2005) considers the long-term frequency dynamics. It is useful for the frequency analysis due to large disturbances and also it shows the interaction between frequency and voltage.

1.2 Evaluation of main effects on voltage stability

The voltage stability can be affected by several elements and control ways which operate on different time scales. In particular the role of OLTCs, loads and reactive power limits are significant.

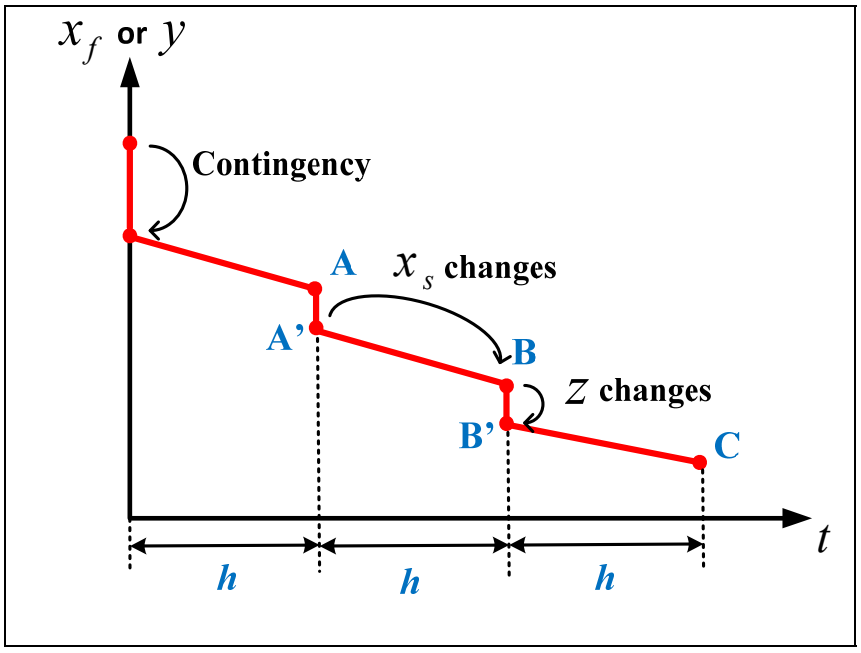

Figure 1.5 QSS simulation mechanism

1.2.1 Effect of reactive power limits on voltage stability

One of the major impacts on voltage instability is the reactive power limits which are produced by the generators excitation limiters. The system will lose voltage control of generators when the reactive power limits become active (Canizares, 2002). Two examples of PV curves are provided in Figure 1.6(a), when these limits are on or off. In the case I, the reactive power limit decreases the stability margin because the distance between point B and the critical point is decreased. If the load increases in this situation, the point B will reach to the critical point and the voltage instability can be triggered easily. In the case II, the operating point becomes instantly unstable after considering the reactive power limit. As seen in Figure 1.6(b), when the limit is considered, the equilibrium point becomes in the lower part of the constrained PV curve which is unstable. A generator with no reactive power limit is considered as a PV bus, and then a PV bus will change into a PQ bus after involving to the reactive power limit.

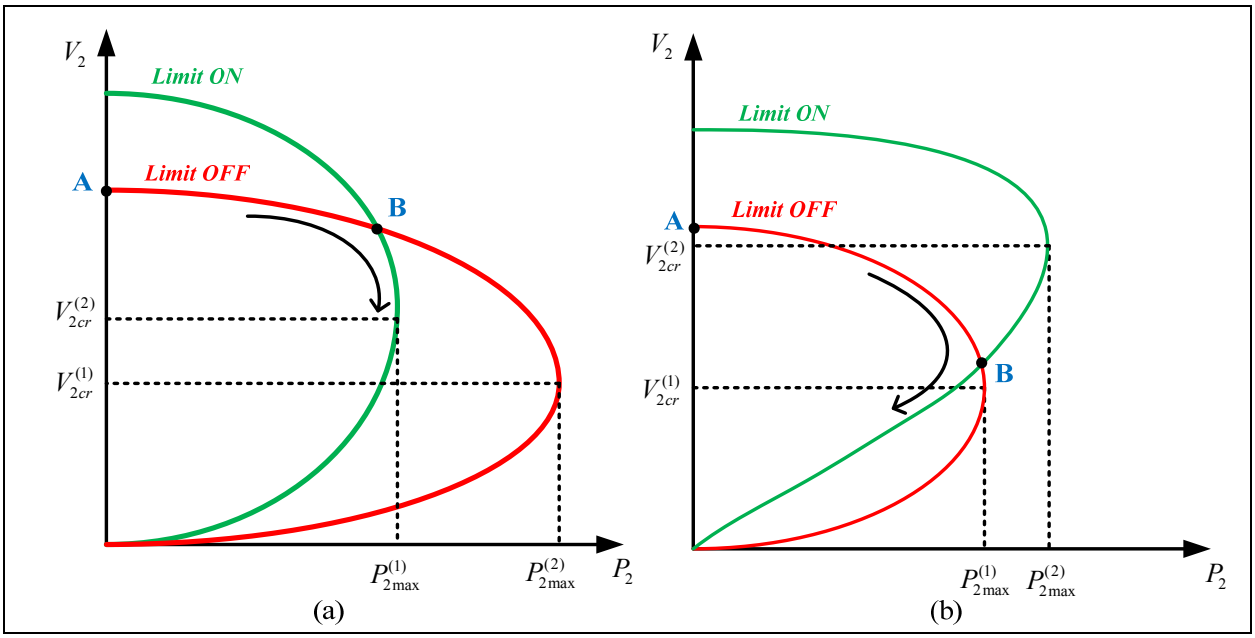

Figure 1.6 Effect of reactive power limit (a) Case I, (b) Case II

There are different models for the representation of reactive power limits of generators in the voltage stability and electricity market studies. One of the most common models is the consideration of the reactive power limits as a fixed value in an OPF approach, but this model is not very accurate due to the nonlinear characteristics of the constraints. Another model can be improved by applying a complete model of generator capability limits. This model considers the maximum currents of field and the maximum currents of stator in its formula. The following represents this model of maximum reactive power limits:

$$Q_{G1max} = \sqrt{\left(\frac{V_{to}E_{fmax}}{X_S}\right)^2 - {P_S}^2} - \frac{{V_{to}}^2}{X_S} \tag{1.1}$$

$$Q_{G2max} = \sqrt{(V_{to}I_{amax})^2 - {P_S}^2} \tag{1.2}$$

$$Q_{Gmax} = \begin{cases} Q_{G1max} & if\ P_S < P_{S_M} \\ Q_{G2max} & if\ P_S > P_{S_M} \end{cases} \tag{1.3}$$

where Q_{G1max} and Q_{G2max} represent the reactive power limits for maximum field currents and maximum stator currents, respectively.

Results in (Tamimi, Canizares et Vaez-Zadeh, 2010) show that the model in (1.1)-(1.3) acts better than fixed values of reactive power limit due to providing a improved voltage profile and less power losses. If we want to use other models, it is very important to understand, whether the improvement of voltage profile is more valuable rather than the increase of computational burden or not. Moreover, this model is appropriate model for cylindrical rotor and it can be used for salient pole rotor due to conservative consideration.

1.2.2 Effect of OLTCs on voltage stability

The OLTCs have an important role on voltage stability and they may trigger the instability process. The tap ratio can be changed via manual or automatic procedure. Some OLTCs operate accompany with an automatic voltage regulator (AVR) in power systems, so this action worsen the procedure of voltage instability. The behavior of OLTC equipped with AVR can be presented by two models (discrete or continuous). OLTCs generally operate after a pre-specified delay, and then the tap ratio keeps constant the load side voltage (Weedy et al., 2012).

There are some ways to control the voltage stability by OLTCs which is known as corrective actions. These corrective actions used to control the restoration schemes after a contingency which have negative impacts on voltage stability problem. These are classified into groups below (Vournas et Karystianos, 2004): 1) Tap blocking behavior of an OLTC. One of the easiest methods is the tap blocking of an OLTC which ends to the continuation of the voltage instability. It has some disadvantages such as decreasing the voltage level in both the transmission and distribution system and producing the negative effect on other load restoration processes. Also, it is hard to prevent unnecessary tap blocking and it has a problem in finding which tap needs to be blocked. 2) Specific tap or voltage switching of an

OLTC. This method avoids the continuation of voltage reduction from a specific value. It can be limited by a specific tap ratio or a reference value of the voltage. These values can obtain from the highest probability of contingency or the operator experiences. 3) Tap reversing behavior of an OLTC. This way operates to control the voltage level in both the distribution and transmission sides. An OLTC wants to keep the voltage magnitude at an acceptable level. It causes to prevent the voltage collapse.

The tap reversing behavior avoids the voltage reduction and operates more profitable than other corrective actions. Tap reversing behavior of an OLTC provides enough time for a system to employ other corrective actions. There are some methods to optimize an OLTC setting such as the gradient projection method which is based on maximizing the stability margin (Polak, 1971; Vournas et Karystianos, 2002). In (El-Sadek et al., 1999), a case study is analyzed as a Thevenin's equivalent system which E is an equivalent Thevenin's emf and V is the load node voltage. Then a $\frac{\mathrm{dE}}{\mathrm{dV}}$ criterion (El-Sadek et al., 1997) is introduced as an analytical factor to evaluate the behavior of OLTCs. Note that tap ratio does not change the maximum active and reactive power of a load.

Furthermore, finding the critical OLTCs can help to improve the voltage stability problem. In (Thukaram et Parthasarathy, 1996; Thukaram et al., 2004), the linear programming method has been applied to solve two objective functions which are the minimization of the voltage deviations from desired values and the minimization of the sum square of L-indices. Thus, these methods can show the critical OLTCs which may lead to the voltage instability under the peak load conditions.

1.2.3 Effect of load models on voltage stability

Some elements can intensify the effects of load on voltage stability, such as OLTCs, voltage regulators, thermostats and motor slip adjustments. Restored loads consume more and more reactive power which it cuts down the voltage magnitudes. Moreover, different types of load models have impacts on the voltage stability problem (Lee et Lee, 1993; Pal, 1992; Zeng,

Berizzi et Marannino, 1997). It is beneficial for the electricity industry to develop dynamic load models instead of conventional load models. Note that only dynamic systems have the unstable behavior (Hatipoglu, 2014). (Pal, 1992) proposes an accurate load model with a constant MVA characteristic. The dynamic behavior of this model is indicated by a first-order delay term. (Chowdhury et Taylor, 2000) compares between two methods of stability evaluation (QV curve obtained from the conventional PF approach and the dynamic simulation). This paper evaluates three worst outages which are stable in the dynamic simulation, but they are unstable by the PF approach and there is no operating point in the QV curve. Thus, the results of the PF approach are not reliable. Well-known curves such as PV and QV curves cannot consider the dynamic load characteristics, because they are not time-dependent. In (Lian et al., 2010), the authors propose a method to consider the dynamic load characteristics. It first converts a power system into an equivalent two-node system and then an approximated method is used to model the dynamic load with a polynomial form. Figure 1.7 represents that different types of load models have distinct operating points. It shows that constant impedance (Z), constant current (I) and constant power (P) load models have significant impacts on the voltage stability problem due to different intersections in the PV curve.

(Regulski, 2012) investigates a voltage stability evaluation in different load characteristics. When a contingency occurs, some loads act quickly and reach to new operating points, while others act with delay. In the case of a constant power load, an operating point may be vanished; when it passes maximum active power limit. Thus, consideration of fixed value for the load model creates many errors in the voltage stability results.

1.3 Methods of solving reactive power dispatch problem

The reactive power dispatch (RPD) problem tries to keep the voltages in acceptable values. There are some control variables which are needed to optimize such as generator parameters, switchable VAR sources and OLTCs. As discussed in (Thukaram et Parthasarathy, 1996;

Thukaram et al., 2004), the authors use the linear programming method to solve this problem. The RPD problem can be solved by Genetic Algorithm (GA) which the RDP objective function is the minimization of the maximum of L-indices for all buses (Devaraj et Roselyn, 2010). The hybrid differential evolution (HDE) is another heuristic method which solves the RDP optimization (Yang et al., 2012). This technique can obviously enhance the voltage stability of a system and reduce the line losses. Also, it can determine the optimal tap settings of OLTCs, the excitation settings of generators and the locations of the SVCs.

In (Wang et al., 2011), a new enhanced particle swarm optimization (EPSO) is presented for solving a preventive control. The new EPSO has a difference with PSO in the selection of inertia weight. Moreover, a gravitational search algorithm (GSA) is introduced to solve the RPD problem in (Duman et al., 2012a). GSA is a new metaheuristic search algorithm and motivated by Newtonian gravitational law and law of motion (Rashedi, Nezamabadi-pour et Saryazdi, 2009). In this algorithm, a heavier mass has a higher pull and moves slower.

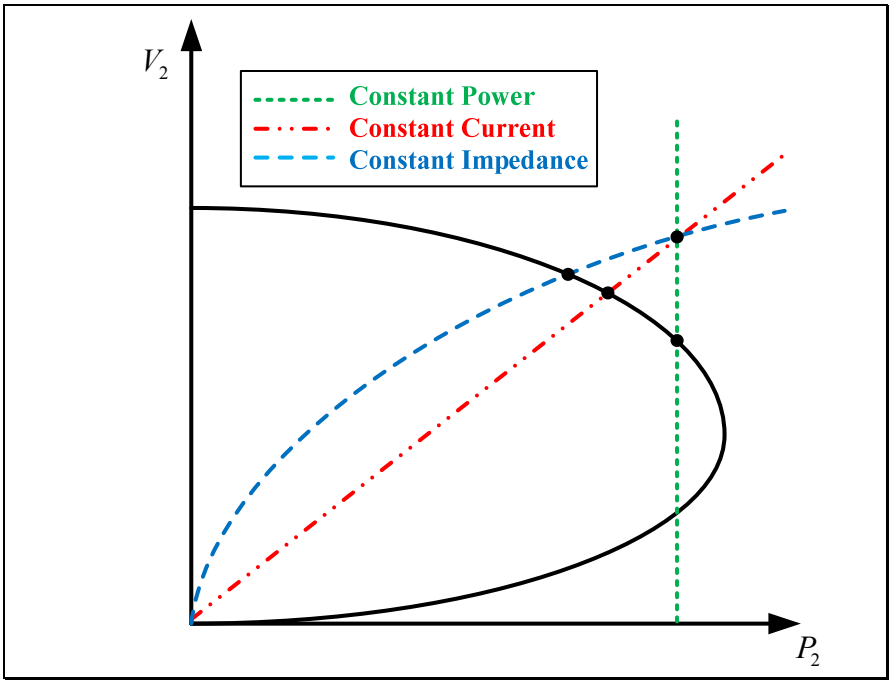

Figure 1.7 Different operating points with various load types in a PV curve

1.4 Analysis of main voltage stability indices

One of the useful methods to evaluate the voltage instability risk is the calculations of voltage stability indices (VSIs). These indices usually calculate the stable operating point which is obtained from load flow feasibility (LFF). They are also identified as performance indices (PI) which are an interesting topic for the researchers in the power system operation. A threshold value (TH) as a measurement criteria is defined for each VSI (Chow, Fischl et Yan, 1990). When $VSI(z, z^c) \leq TH$, the voltage profile is adequate and when $VSI(z, z^c) > TH$, the voltage profile is inadequate. Where z^c is a reference value of z, and $VSI(z, z^c)$ is obtained from a group of variables that produces the operating point z. Some of these VSIs are introduced in Table 1.1.

Table 1.1 Different types of VSIs
Adapted from Fischi (1989) and, Eremia and Shahidehpour (2013)

Criterion of Index	Formulation	Explanation
Maximum power transfer (Barbier et Barret, 1980)	$max_{i\in L} \frac{\lvert \underline{V}_{Li}^{critical} \rvert}{\lvert \underline{V}_{Li}(u) \rvert} \leq TH$ where $\lvert \underline{V}_{Li} \rvert$ is the voltage magnitude at load bus i; $\lvert \underline{V}_{Li}^{critical} \rvert$ is the critical voltage magnitude at bus i	Critical voltages of load bus calculated based on maximum power transfer limit, $TH = 1.0$
Maximum power transfer from OPF (Carpentier, 1984)	$max_{i\in L} \left\{ \frac{\partial Q_G^{tot}}{\partial Q_L(u)} \Big\rvert_* \right\} \leq TH$(Selected by operators) where Q_G^{tot} is the total reactive power generation, Q_{Li} is defined from optimal power flow $(*)$	A voltage collapse sensitivity index based on maximum power transfer criteria and computed from an optimal power flow
Load flow feasibility (Jarjis et Galiana, 1981)	$\frac{1}{\{\sin([u_a], [u_1])\}^k} \leq TH$ $u_a = au_1 + (1-a)u_0$ where u_0 is the base case input vector; u_1 is the closest input vector boundary of load flow region from u_0; k is a positive integer;	At boundary of load flow feasibility region $TH = \infty$

Load flow (L-Index) (Kessel et Glavitsch, 1986)	$max_{i\in L}\left\|1-\frac{\sum_{i\in G}F_{ij}\underline{V_{Gi}}}{\underline{V_{Li}}}\right\|\leq TH$ where $\left\|\underline{V_{Li}}\right\|$ is the load bus voltage magnitude of bus i; and F_{ij} is the elements of the matrix, $[F]=-\underline{Y_{LL}}^{-1}\underline{Y_{LG}}$	At boundary of load flow feasibility region $TH=1.0$
Multiple Load flow (Tamura, Mori et Iwamoto, 1983)	$\frac{1}{2}\sum_{i,j}\gamma_{ij}$ where $\gamma_{ij}=sign\{[J(x^a)]\}-sign\{J(x^{BC})\|_{ij}\}$ $J(x^a)\|_{ij}=ij$th element of the $[J]$ matrix, Maximum between a and b load flow solutions is selected	Necessary condition of sensitivity matrix for voltage stability of multiple load flow solutions
Singular Value of Jacobian (Tiranuchit et Thomas, 1988)	$\frac{1}{\sigma(J)}\leq TH$(Selected by operators) where σ is a singular value of Jacobian matrix	A index for characterizing proximity to instability
Singular Value of Reduced Jacobian (Lof, Andersson et Hill, 1993)	$\sigma_{min}(J_R)\leq TH$(Selected by operators) where $\sigma_{min}(J_R)$ is minimum singular value of reduced matrix	A suitable index for a large power system and it can detect voltage instability during increasing the load

(continue the previous Table)

Criterion of Index	Formulation	Explanation
Ratio of smallest singular value for no-load and operating points (Eremia et Shahidehpour, 2013)	$\frac{\sigma_{min}(J_R)}{\sigma_{0min}(J_R)}\leq TH$ where $\sigma_{0min}(J_R)$ is minimum singular value of reduced matrix for no-load operating points	A global index for determining exact initial operating point, $TH=1.0$
Maximum power transfer (VCPI) (Moghavvemi et Faruque, 1998)	$\frac{P_r}{P_{r(max)}}\leq TH$, $\frac{P_l}{P_{l(max)}}\leq TH$ where $P_r(P_l)$ is real power (loss) transferred to the receiving end and $P_{r(max)}$ $(P_{l(max)})$ is maximum real power (loss)	Indices with several advantages such as great accuracy, easy calculation, and recognition of weak lines, $TH=1.0$
Load flow (Extended L-Index) (Yang et al., 2013)	$\left\|1-\frac{\sum_{i\in\alpha_G}F'_{ji}E_{Gi}}{V_j}\right\|\leq TH$ where modeling adds an equivalent internal impedance Z_{gi} in front of a voltage phasor E_{Gi}, so it uses complete generator equivalent model (GEM)	A suitable index for involving DG in power system and uses complete generator equivalent model (GEM), $TH=1.0$
Maximum power transfer (LQP) (Mohamed, Jasmon et Yusoff, 1989)	$4\left(\frac{X}{{V_s}^2}\right)\left(\frac{X}{{V_s}^2}{P_s}^2+Q_r\right)\leq TH$ where subscripts of s and r shows sending	Based on the single transmission line calculation , $TH=1.0$

	and receiving buses in the considered transmission line	
Maximum power transfer (L_{mn}) (Moghavvemi et Omar, 1998)	$\frac{4XQ_r}{[V_s \sin(\theta - \delta)]^2} \leq TH$ X is line reactance; θ is line series impedance angle and δ is angle difference between sending and receiving buses	The calculation of this index is based on one single line between two buses , $TH = 1.0$
Maximum power transfer (FVSI) (Musirin et Rahman, 2002)	$\frac{4Z^2Q_r}{{V_s}^2X} \leq TH$ where subscripts of s and r shows sending and receiving buses in the considered transmission line	Based on the single transmission line calculation and it is more compatible with the contingency ranking, $TH = 1.0$
Maximum power transfer (Nath et Pal, 2010)	$-\frac{\partial S}{\partial Y} \leq TH$ (Selected by operators) where S is the apparent power generation, Y is defined the admittance matrix	Based on sensitivity method (the derivative of apparent power against the admittance).

1.4.1 Evaluation of loading margin as global index

The loading margin provides the global information, thus this margin can be considered as a global index. it can be calculated easily and does not need a specific system model (Canizares, 2002). Also, this margin has two disadvantages, first heavy computational burden. Because the critical point is usually far from the operating points. Second the initial condition is commonly hard to be defined for load increase. The loading margins can be classified into three types: 1) Reactive power loading margin (the active power is constant). 2) Active power loading margin (the reactive power is constant). 3) Apparent loading margin (the power factor is constant).

Increasing the load from the operating point to the critical point defines as the loading margin. There are two methods which can calculate the loading margin (Canizares, 2002). First direct methods calculate the singular bifurcation from a set of nonlinear system equations. It also has a high computational burden on the large power systems. Therefore, there are several drawbacks in the direct methods. Another method which is continuation

method is used for determining the closeness to the voltage collapse. The method is based on calculating the consecutive power flow solutions.

1.4.2 Indices based on singular value method

Indices based on the smallest singular value of the Jacobian and Reduced Jacobian matrices can be considered as global index. The concepts below are obtained from the smallest singular values $\sigma_{min}(J)$ of the Jacobian matrix (Lof, Andersson et Hill, 1993):

- $\sigma_{min}(J)$ is a criterion which calculates the closeness of the operating point to the critical point because of determining the singularity of the Jacobian matrix;
- Right singular vector shows the sensitivities of the voltage magnitudes and the angles for changes in the power flow solutions;
- Left singular vector shows the most sensitive directions of the power and the most serious perturbation for changes in the power flow solutions.

Figure 1.8 shows the comparison between different behaviors of $\sigma_{min}(J)$ and $\sigma_{min}(J_R)$. Both indices can determine the proximity to the voltage collapse. With the increasing reactive power loading, several jumps seen in the figure show the changes of the PV nodes into the PQ nodes due to reaching several generators to their maximum reactive power limits. It has an effect in increasing the risk of voltage instability. This is a desirable signal to know when the power system needs extra reactive power (Lof, Andersson et Hill, 1993).

Albeit, the smallest singular value $\sigma_{min}(J_R)$ provides the global information, it does not determine the exact initial operating point. Concluding, the index below is defined to detect better the voltage instability (Eremia et Shahidehpour, 2013):

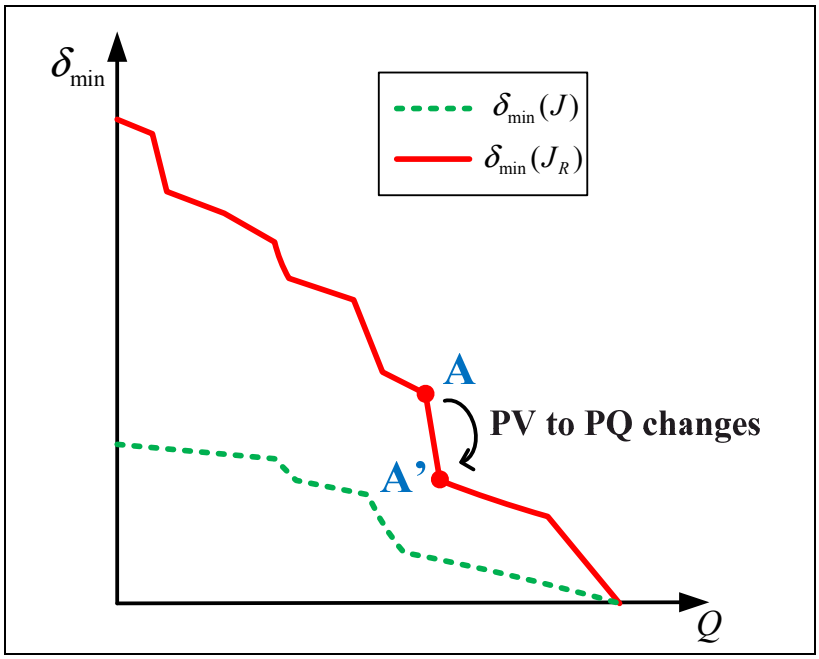

Figure 1.8 Comparison between $\sigma_{min}(J_R)$ and $\sigma_{min}(J)$ (reactive load increase) Adapted from Lof, Andersson et al (1993)

$$VSI = \frac{\sigma_{min}(J_R)}{\sigma_{0min}(J_R)} \tag{1.4}$$

where $\sigma_{0min}(J_R)$ is the smallest singular value of reduced Jacobian for no-load points. The values of this performance index change from zero to one. If the system is located on the closeness of the voltage collapse, the values are close to zero and if the system is located far from the voltage collapse, the values become one.

1.4.3 Line voltage stability indices (LVSIs)

Several indices are introduced in this section and they are well-known as line voltage stability indices (LVSIs). Line stability Index (Lmn), Fast Voltage Stability Index (FVSI), Voltage Collapse Point Indicators (VCPI), and Line Stability Index (LQP) are the most important indices of this group. Generally, the calculation of these voltage stability indices is based on one single line between two buses. Therefore, the voltage stability limit is based on the theory of maximum power transfer between two buses.

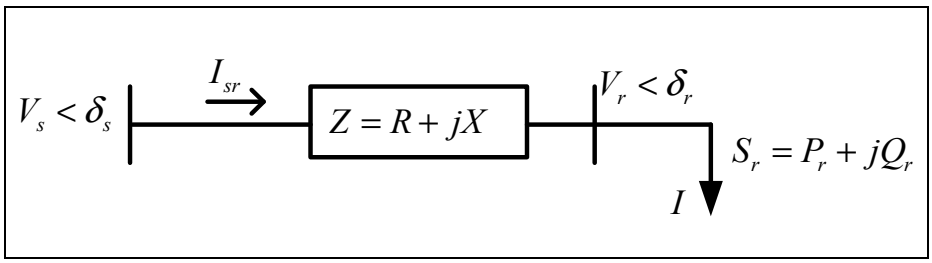

Figure 1.9 A two-bus power system

Voltage Collapse Proximity Indicator (VCPI)

Voltage collapse proximity indicators (VCPI) are based on the theory of maximum power transfer between two buses (Moghavvemi et Faruque, 1998):

$$VCPI_{(1)} = \frac{P_r}{P_{r(max)}} \tag{1.5}$$

$$VCPI_{(2)} = \frac{Q_r}{Q_{r(max)}} \tag{1.6}$$

where P_r and Q_r are active and reactive power transferred to the receiving end. $P_{r(max)}$ and $Q_{r(max)}$ are the maximum active and reactive power that can be transferred.

$$VCPI_{(3)} = \frac{P_l}{P_{l(max)}} \tag{1.7}$$

where P_l is active power losses in the line and $P_{l(max)}$ is the maximum possible active power losses. All values are calculated from the power flow calculations. The behavior of these indices is approximately linear in the cases with light loads. $VCPI_{(3)}$ is more sensitive at higher load than $VCPI_{(1)}$ in the proximity to the voltage collapse point (due to RI^2). The behavior of $VCPI_{(1)}$ and $VCPI_{(3)}$ is shown in Figure 1.10 when the power transfer through

the line increases gradually. These indices have several advantages such as greater accuracy, the easy calculation, and the recognition of weak lines.

Line Stability Factor

Line Stability Factor is defined as an index to monitor online the voltage evaluation based on the transmission line calculation. When the value of this factor reaches to 1.0, it shows that the system becomes unstable. This index is defined as (Mohamed, Jasmon et Yusoff, 1989):

$$LQP = 4\left(\frac{X}{V_s^{\,2}}\right)\left(\frac{X}{V_s^{\,2}}P_s^{\,2} + Q_r\right) \tag{1.8}$$

where subscripts of s and r shows sending and receiving buses in the considered transmission line, respectively; X is the line reactance.

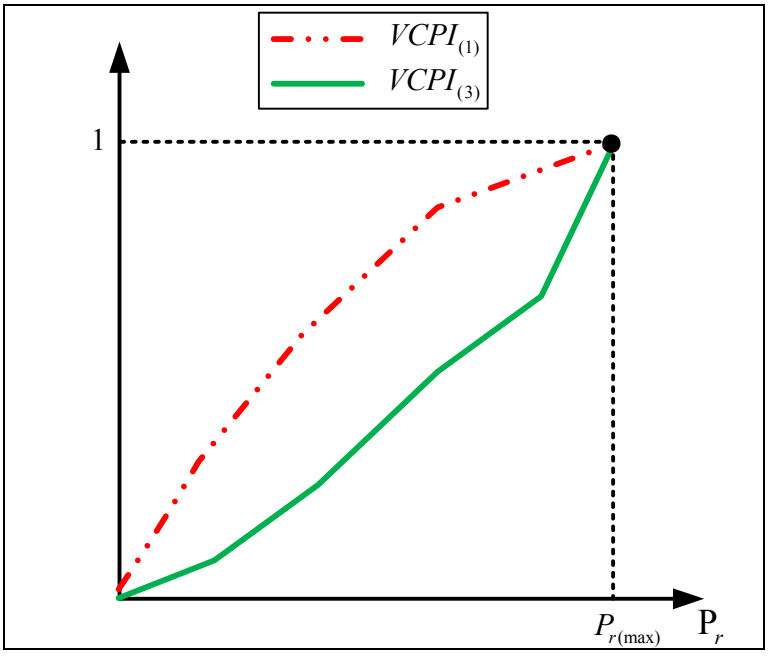

Figure 1.10 Comparison between voltage collapse proximity indicators
Adapted from Moghavvemi and Faruque (1998)

Line Stability Index

Line Stability index L_{mn} is used to evaluate the system stability and when the value of L_{mn} reaches to 1.0, it shows that the system becomes unstable. The index equation is given as follows:

$$L_{mn} = \frac{4XQ_r}{[V_s \, sin(\theta - \delta)]^2} \tag{1.9}$$

where $X\angle\theta$ is the line reactance and δ is the angle difference between two buses. An advantage of this index is that can distinguish between weak and strong transmission lines. It also helps the ISO to find the voltage collapse in the vicinity of bifurcation point. Moreover, the computational burden is relatively low which is proper for large power system (Moghavvemi et Omar, 1998).

Fast Voltage Stability Index (FVSI)

FVSI is a criterion that shows both voltage stability situation and contingency ranking. This index is used to predict the system instability when the value of FVSI reaches to 1.0. The FVSI is defined as (Musirin et Rahman, 2002):

$$FVSI = \frac{4Z^2Q_r}{{V_s}^2X} \tag{1.10}$$

The calculation process of this index like other LVSIs is based on the single transmission line calculation. Thus, they are more compatible with the contingency ranking. A disadvantage of these methods is that they cannot give any idea about the weak buses and only show the weak lines.

(Cupelli, Doig Cardet et Monti, 2012) shows a comparison between these four indices based on accuracy, control adequacy and robustness to the load increase. Generally, all indices represent the linear behavior before reach to the voltage collapse. But they show a nonlinear

behavior during the voltage collapse. The values of Lmn and LQP indices increase more than one and they detect wrongly the voltage instability. Otherwise, the results show that the VCPI is the best index from the mentioned criteria and it is less dependent on the load dispatch.

1.4.4 Indices based on L-Index

An indicator L (L-Index) is introduced as a quantitative value to calculate the distance from the operating points to the stability limit (Kessel et Glavitsch, 1986). The system admittance matrix is defined by the load and generator buses as follows:

$$\begin{bmatrix} I_L \\ I_G \end{bmatrix} = \begin{bmatrix} Y_{LL} & Y_{LG} \\ Y_{GL} & Y_{GG} \end{bmatrix} \begin{bmatrix} V_L \\ V_G \end{bmatrix} \tag{1.11}$$

The voltages at the load buses can be shown as:

$$V_L = Z_{LL} I_L - Z_{LL} Y_{LG} V_G = Z_{LL} I_L + F_{LG} V_G \tag{1.12}$$

where $Z_{LL} = (Y_{LL})^{-1}$ and $F_{LG} = -Z_{LL} Y_{LG}$.

For a particular load bus j, we have

$$V_j = \sum_{i \in \alpha_L} Z_{ji} I_i + \sum_{i \in \alpha_G} F_{ji} V_i \tag{1.13}$$

where α_L and α_G indicate the sets of load buses and generator buses.

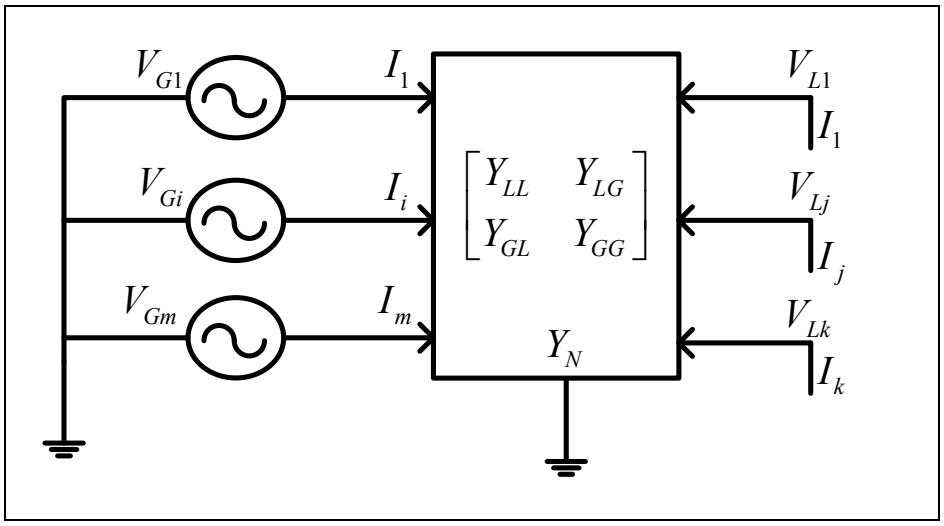

Figure 1.11 Power system model with m PV bus and k Loads (L Index)
Adapted from Yang, Caisheng et al. (2013)

L index is defined as:

$$L_j = \left| 1 - \frac{\sum_{i \in \alpha_G} F_{ji} V_i}{V_j} \right| \tag{1.14}$$

When the value of L_j becomes 1.0 or close to 1.0, it shows that the voltage at bus j is near to its voltage stability limit. The contingencies affect on the L-Index due to changing the system state like new voltage profile. Calculation of the L-Index is simple, time-saving and it can be changed easily. The L-index has an accurate result when the loads gradually increase.

(Salama, Saied et Abdel-Maksoud, 1999) describes a simplification method for calculation of L-Index, which reduces the computational burden. It suggests using the imaginary parts of the admittance matrix in the L-index formula. Thus, instead of using $F_{LG} = -(Y_{LL})^{-1} Y_{LG}$, it is changed as follows:

$$F_{LG} = -(B_{LL})^{-1} B_{LG} \tag{1.15}$$

where B_{LL} and B_{LG} are the imaginary parts of sub-matrices of the admittance matrix. This simplification is useful for large power systems and it can increase the calculation speed, because the matrices with only imaginary part can be inverted quickly. The comparison between with/without simplification shows that the results are very close and acceptable.

When the distance of generators and loads become closer or/and the PV generators have converted to the PQ nodes in case of the reactive power limits, the L-Index is not very accurate. (Yang et al., 2013) has proposed an extended L-Index that uses a complete generator equivalent model (GEM). This model adds an equivalent internal impedance Z_{gi} in front of a voltage phasor E_{Gi}. The extended L-index is obtained as follows:

$$L_j = \left| 1 - \frac{\sum_{i \in \alpha_G} F'_{ji} E_{Gi}}{V_j} \right| \tag{1.16}$$

In conclusion, the results shows that extended L-Index can predict better the voltage collapse than the L-Index.

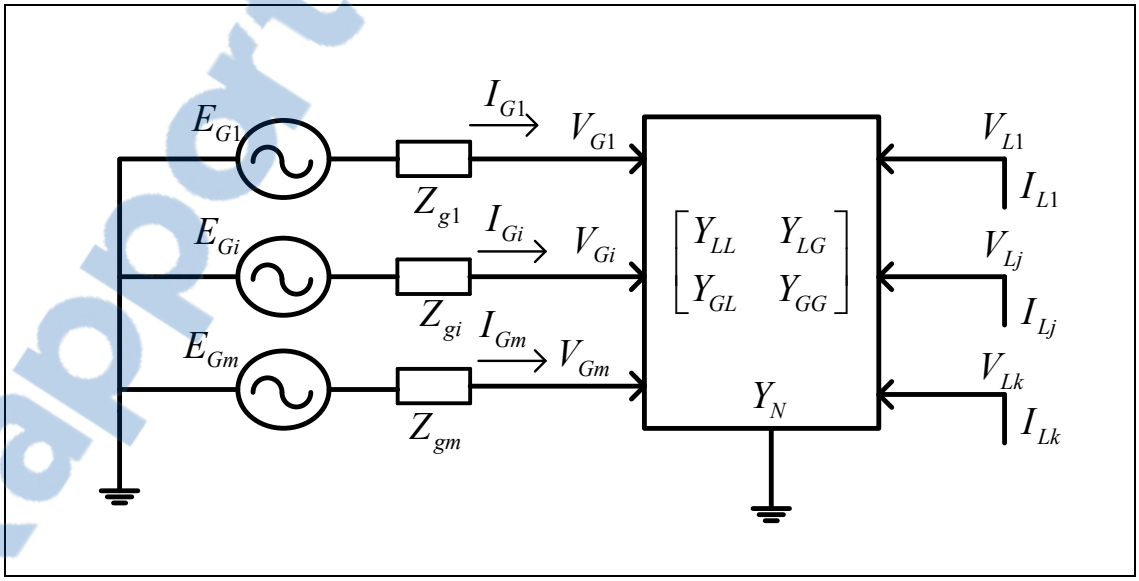

Figure 1.12 Power system model with m PV bus and k Loads (Extended L Index)
Adapted from Yang, Caisheng et al. (2013)

1.5 Different types of VSC-OPF approach

In recent years, the computational tools have been expanded to simulate on-line dynamic stability problems by modifying the equivalent algebraic equations. Stability problems generally is solved with nonlinear programming methods (Gan, Thomas et Zimmerman, 1998). The VSC-OPF solution should satisfy both technical and economic issues which can be the minimization of total costs (or the maximization of social welfare) and the consideration of voltage stability limits, respectively (Mo et al., 2007). Nowadays, ISOs have a noticeable problem with the voltage stability based on two reasons: (1) lack of detail regulations in the power flow analysis; (2) high use of stressed elements and transmission line in the restructured power system (Wu et al., 2007). A proper VSC-OPF approach has a strategy that model both pre- and post-contingencies. In order to solve VSC-OPF, at least one extra constraint should be included in the standard OPF model. Therefore, this inequality constraint can be allocated as a cost into the model. There is another model for the consideration of the voltage stability with OPF which is well known as a *linear combination* model. This model uses weighting factors to combine two or more objective functions. The *linear combination* model has some drawbacks. For example, assigning the proper values of these weighting factors is very hard.

1.5.1 Power transfer constraint

The power transfer constraint can be calculated offline based on $N-1$ contingency and it represents the transmission lines security limits. The security formula is obtained as below, and it adds an extra inequality constraint to the OPF approach.

$$P_{ij}(\delta, V) \leq P_{ijmax} \tag{1.17}$$

where $P_{ij}(\delta, V)$ indicates the active power in each transmission line between buses i and j $(i \neq j)$.

This constraint which indicates the system security limits in the auction model is not a beneficial model due to providing improper price signals and reducing available power system transmission capacity (Milano, Canizares et Invernizzi, 2005).

1.5.2 Loading margin constraint

In general, loading margin is defined as a criterion of the distance between the operating points to the critical point. The voltage stability formula can be generically written as:

$$\lambda_c - \lambda_p \geq \Delta\lambda_{min} \tag{1.18}$$

where the subscripts c and p represent the critical and current operating points, respectively; $\Delta\lambda_{min}$ indicates the minimum acceptable load margin and it is defined by the ISO. This voltage stability inequality constraint operates as a cost. This method has some disadvantages, for example the process of calculation λ_c needs some computations and extra constraints. All constraints should be considered in both critical and current operating points. This model considers one value of loading margin for all buses, so there is no distinction between vulnerable and secure buses (Milano, Canizares et Invernizzi, 2005; Rosehart, Canizares et Quintana, 2003a; 2003b).

1.5.3 Singular value constraint

Minimum Singular Value (MSV) can estimate the closeness of the operating point to the critical point due to determining the singularity of the Jacobian matrix. The MSV can be considered as a constraint which be added to the OPF (Avalos, Canizares et Anjos, 2008; Canizares et al., 2001; Lage, da Costa et Canizares, 2012; Venkatesh, Arunagiri et Gooi, 2003). The MSV constraint is defined as follows:

$$\sigma_{min}\{J_{PF}(\delta, V, Q_G, P_G)\} \geq \sigma_c \tag{1.19}$$

where J_{PF} is the Jacobian of the power flow; and σ_c is the critical singular value obtained from off-line voltage stability studies. For example, σ_c can be obtained from the worst contingency. Generally, setting the value of σ_c is very significant; an improper setting may produce an unfeasible OPF solution. The MSV operates nonlinearly and implicitly in the optimization process.

The VSC-OPF with MSV constraint has a considerable computational burden that may make their applicability unsolvable. Moreover, MSV obtained from Tangent Vector (TV) can be used as a voltage stability criterion and it can be demonstrated explicitly in the main problem. Assigning a critical value for the voltage stability indices is very important and the results shows that these two indices are very conservative (Lage, da Costa et Canizares, 2012). Due to changing PV buses to PQ buses, Jacobian matrix varies during the optimization process.

Although, Jacobian matrix should be considered constant in this model (Avalos, 2008). (Venkatesh, Arunagiri et Gooi, 2003) presents a new VSC-OPF approach, which increases the voltage stability margin (VSM) based on maximizing the MSV. The main objective function is to minimize the total cost which uses the linearized OPF approach with the fuzzy algorithm. The fuzzy algorithm is flexible in adding and changing the constraints, but the linearized OPF reduces the accuracy and it increases the gap between the real operating point and the calculated operating point.

1.5.4 L-Index constraint

Another VSC-OPF approach is L-Based VSC-OPF that uses the L-Index as a constraint for voltage stability evaluation. The formula of the additional L-index constraint can be generically restated as:

$$L_{max}(\delta, V, Q_G, P_G) \leq L_c \tag{1.20}$$

where L_{max} represents the maximum value of L-Index; L_c represents the critical value of the L-Index which can be obtained from the worst contingency or different load dispatches. The method has some advantages such as easy calculation, the distinction between vulnerable and secure buses. The range of L index value is between 0 to 1 that provides a better understanding of the VSM.

1.5.5 LVSI constraint

A LVSI can be used as an extra constraint to define a VSC-OPF approach. These types of indices are based on the theory of maximum power transfer between two buses. For instance, (Zabaiou, Dessaint et Kamwa, 2014) is implemented VCPI as a constraint. The extra constraint is formulated as:

$$LVSI_{max}(\delta, V, Q_G, P_G) \leq LVSI_{limit} \tag{1.21}$$

where $LVSI_{limit}$ is a desired limit value for stability limit and $LVSI_{max}$ is the maximum value of LVSI in all transmission lines. Using the LVSI has less computational burden than using the L-Index.

1.6 Stochastic Optimal Power Flow (SOPF)

One of the crucial issues in the optimal power flow (OPF) is the consideration of an applicable model for uncertainties in the system. When variations of unpredicted resource create a high amount of uncertainties, a power system may result in outage or even collapse. In this situation, stochastic OPF (SOPF) can reduce the risk of outages (Bienstock, Chertkov et Harnett, 2014). The types of wind power control are investigated in (Roald et al., 2016).

Another study (Condren, Gedra et Damrongkulkamjorn, 2006) considers uncertain security costs, interrupting consumption costs and generator ramping during a contingency event. A novel probabilistic DC OPF approach has been proposed in (Vrakopoulou et al., 2013) considering $N-1$ contingencies criterion.

One of the famous techniques in uncertainty modeling is scenario-based technique that provides less operating cost for ISOs (Bouffard, Galiana et Conejo, 2005). Dupacova et al. first proposed the scenario selection and reduction algorithms based on scenario's probability (Dupačová, Gröwe-Kuska et Römisch, 2003). Also Papavasiliou and Oren present a criterion to select scenarios based on the expected cost (Papavasiliou et Oren, 2013).
(Summers et al., 2014) proposes a scenario-based SOPF approach based on the convex approximations. This approach is a tradeoff between stable power systems while diminishing the conservative behavior. Stochastic formulations in OPF approach consist of a set of scenarios. Their probabilities of each scenario should be determined for uncertainty modeling of renewable energy sources (RESs). These scenarios can be obtained from statistical models like neural network (Kusiak et Zhang, 2010) and random forest (Breiman, 2001).

The authors in (Pand et al., 2016) represent that the scenario-based technique is the most profitable technique in comparison with the other techniques like robust, interval and improved interval techniques. One of the challenges in the scenario-based technique is the scenarios selection and their probabilities. (Gröwe-Kuska et al., 2002) presents an appropriate algorithm for the scenario selection. This study is the pioneer of scenario reduction algorithms in the stochastic programs.

As the number of scenarios is high, the scenario-reduction techniques have been demonstrated to reduce the computational burden. A comparison between these techniques has been presented in (Dvorkin et al., 2014). A fast forward scenario selection technique is presented in (Morales et al., 2009). (Papavasiliou et Oren, 2013) proposes an importance sampling approach based on operating cost variation. In (Papavasiliou, Oren et Neill, 2011), a two-stage weighted scenario-based technique considering reserves and wind power is

presented. Another model to consider uncertainties in the OPF formulation is robust optimization technique (Warrington et al., 2013). The results in robust optimization technique can be conservative.

1.6.1 Demand Response (DR) in SOPF

The DR is defined in (Lee et al., 2013) as follows:

"Changes in electric use by demand-side resources from their normal consumption patterns in response to changes in the price of electricity, or to incentive payments designed to induce lower electricity use at times of high wholesale market prices or when system reliability is jeopardized."

There are a lot of benefits to utilize DR, for instance DR can diminish the uncertainty of renewable energies. (Papavasiliou et Oren, 2012) claims some models for DR resources. In the central control model, DR dispatches will be managed by an ISO centrally. This model is impractical and its computational burden is heavy, especially for large systems. Several studies consider this model in the process of DR dispatches (Joskow et Tirole, 2006; 2007; Sioshansi, 2012; Sioshansi et Short, 2009).

Authors in (Vrakopoulou, Mathieu et Andersson, 2014) demonstrate a scenario-based SOPF with utilization of uncertain DR which has been modelled as a virtual energy storage unit. Aggregations of DR resources is studied with a model of uncertain flexibility in (Mathieu et al., 2013). Generally, aggregation of DR resources can be utilized in ancillary services, security and stability in power systems. The effect of DR on distribution systems has been presented in (Lu et al., 2011; Steen et al., 2011; Vrettos et Andersson, 2013). These studies examine different types of DR controls like the centralized and decentralized controls on the distribution systems. Their results show that DR can decrease the stresses on the distribution

systems. The authors in (Rabiee et al., 2014) investigate a VSC-OPF approach considering DR and stochastic wind resources. They consider the loading margin as a voltage stability index.

1.6.2 Energy Storage Systems (ESSs) in SOPF

Energy storage systems (ESSs) have a vital role in power systems. ESSs usage provides several benefits for ISOs. It causes to reduce the losses and transmission congestion and to increase voltage and frequency stability (Delille et al., 2009; Rastler, 2010). ESSs have some advantages for consumers like less load shedding, improvement in reliability and power quality. Also, they can decrease the risk of uncertainty of RESs (Chu et Majumdar, 2012).

Recently, several studies have been carried out to optimize the size of EESs in the system (Harsha et Dahleh, 2015; Kraning et al., 2011; Su et El Gamal, 2011). However, (Lin, Mathieu et Johnson, 2016) proposes a scheme to control ESSs and DR simultaneously. The authors in (Meyer-Huebner et al., 2016) consider an AC OPF approach with ESSs and a multi-terminal HVDC. (Chacra et al., 2005) presents the economic effects of ESS costs on a distribution substation. Another important issue on ESS is how to allocate them. (Atwa et El-Saadany, 2011; Atwa et al., 2010) claims techniques to allocate an ESS in a distribution system with a large number of wind farms.

ESSs first has been investigated in 1981 by (Yau et al., 1981). (Sjödin, Gayme et Topcu, 2012) studies a risk mitigated OPF considering ESSs with high penetration of wind farm. ESSs can decrease the amount of operating reserves. As mentioned before, ESSs can reduce the fluctuations of wind power and it can act like load and generator in different hours.

In (Pan et al., 2016), a new control scheme of ESSs is proposed that can minimize the operating costs. The OPF approach is solved with evolutionary programming (EP) algorithm. Atwa and El-Saadany (Atwa et El-Saadany, 2010) formulate an OPF approach to allocate ESSs in a distribution system. Gabash (Gabash et Li, 2012) investigates an OPF approach

with ESSs and wind farms. The simulations are carried out in two optimization horizons and they show that the longer horizon provides better economical and technical results.

ISO manages the SOC to increase the performance of ESSs. In (Lin, Mathieu et Johnson, 2016), a chance constraint DC-OPF is proposed that can dispatch ESSs in a power system. The SOC variation is considered via a redispatch reserve scheme in this approach. After the establishment of first pump storage power plant in Switzerland in 1882, many studies on ESSs have been done throughout the world. Peak-shaving is the most significant advantages of ESSs for ISOs (Wang et al., 2013).

1.7 Conclusion

A comprehensive SOPF approach is essential to formulate in modern power systems. A comprehensive SOPF consists of some extra constraints from voltage stability issues, DR program, OLTC, OXL, ESSs and wind power. For voltage stability issues, many voltage stability indices (VSIs) have been reviewed that have a role to evaluate the voltage instability risk and to predict the voltage collapse point. A comprehensive approach can help an ISO to reach its main goal which is to run the power system operation without any voltage stability collapse at low cost or high revenue. Furthermore DR program can help to reduce excessive load shedding. As the voltage stability can be affected by several elements which operate on different time scales, the role of OLTCs, OXL and ESSs were investigated in this section.

CHAPTER 2

A NOVEL APPROACH TO DYNAMIC VOLTAGE STABILITY ANALYSIS FOR DFIG WIND PARK INTEGRATION

Majid Bavafa and Louis-A. Dessaint

Department of Electrical Engineering, Ecole de technologie supérieure,
1100 Notre-Dame West, Montréal, Quebec, Canada H3C 1K3

Paper submitted to IET Renewable Power Generation, May, 2016

Abstract

In this chapter, an improved voltage stability index that can evaluate unstable behavior of the power system with doubly-fed induction generator (DFIG) wind parks integration is presented. Accordingly, voltage stability constrained optimal power flow (VSC-OPF) is studied including an improved impedance-based (IB) index. In particular, the chapter has two main contributions. First, it proposes an IB index with consideration of DFIG capability curve limits and on-load tap changer (OLTC) behavior. These factors have significant roles in the long-term voltage stability studies.

The proposed voltage stability index can detect precisely the voltage collapse, especially after the occurrence of a given contingency due to the dynamic elements of the system. In this chapter, a model is proposed for DFIG capability curve limits that can be integrated to the internal circuit of the generator. In particular, the proposed model can be appended to impedance matching theory. Furthermore, the OLTC model is added to this index. The index uses the concept of coupled single-port circuit.

The second contribution proposes a VSC-OPF with an improved IB index that is also compared with three existing VSC-OPF methods in stressed and single line outage conditions. These VSC-OPF methods are, namely, based on the L-index, the minimum singular value and the voltage collapse proximity indicator (VCPI). These approaches are

tested and validated on modified WECC test system, IEEE 39-bus, IEEE 57-bus and Polish 2746-bus systems.

2.1 Introduction

Nowadays, voltage stability assessment is an important issue in the power system due to blackouts in different countries (McLinn, 2009). The main goal of the power system operator is to run the power system without any voltage instability at the lowest cost. Voltage stability can be affected by several elements and controllers, which operate on different time scales (Canizares, 2002). In particular, the effects of wind generator (WG) are undeniable. The WG equipped with induction generator absorbs reactive power. As known, most reasons of voltage collapse are based on failing to provide reactive power demands. Therefore, the proper modelling of the WG and its reactive power limits should be adequately analyzed for voltage instability detection (Youssef, Azab et Amin, 2015).

Doubly fed induction generators (DFIGs) are employed in the most newly installed WG in a modern power system. The wind penetration level has been increased in recent times. Many studies had been carried on DFIG reactive power capability curve (Engelhardt et al., 2011; Kayikci et Milanovic, 2007; Konopinski, Vijayan et Ajjarapu, 2009; Lund, Sørensen et Eek, 2007; Meegahapola, Littler et Perera, 2013). The DFIG and converter systems can provide the reactive power capability curve. As an illustration, the authors in (Kayikci et Milanovic, 2007) have investigated the reactive capability curve of DFIG in rotor-side converter (RSC) and the grid-side converter (GSC). In (Londero, Affonso et Vieira, 2015), the authors show the different types of reactive capability curves in fully rated converter (FRC), DFIG with RSC support and DFIG with RSC and GSC support. Those papers disregarded to propose a method to detect voltage instability.

Most studies have investigated the WG on short-term voltage stability (Kayikci et Milanovic, 2007; Meegahapola, Littler et Flynn, 2010), steady-state voltage stability analysis (Vittal,

Malley et Keane, 2010), low voltage ride through (LVRT) control scheme (Xie et al., 2013). The studies still lack a detailed model considering the DFIG reactive power capability characteristics in the long-term voltage stability assessment. They also ignored to consider the dynamic behavior of over excitation limiter (OEL) and on-load tap changer (OLTC).

In order to detect voltage instability, different voltage stability indices have been proposed in the literature. The roles of these indices lie in the evaluation of voltage instability risk and the prediction of voltage collapse point. Some indices are minimum singular value (MSV) of the power flow Jacobian, MSV of the reduced Jacobian (Lof, Andersson et Hill, 1993) and L-index (Kessel et Glavitsch, 1986). Also, there are several line stability indices that have a close relation with active power, reactive power and the voltage stability (Guo-yun, Luo-nan et Aihara, 2015). Such indices are namely: voltage collapse proximity indicator (VCPI) (Moghavvemi et Faruque, 1998; Zabaiou, Dessaint et Kamwa, 2014) and equivalent node voltage collapse index (ENVCI) (Wang, Li et Lu, 2009). The above-mentioned indices cannot consider the dynamic behavior of power system, especially in post-contingency conditions.

One of the important indices in voltage stability studies is an index based on the impedance matching theorem. Different approaches were presented to calculate Thevenin equivalent impedance (TEI) such as least-squares technique (Vu et al., 1999), Tellegen's theorem (Smon, Verbic et Gubina, 2006), adaptive algorithm (Corsi et Taranto, 2008) and recursive least-squares technique (V, Gutiérrez et Ramirez, 2014). The above-mentioned methods use two successive phasor measurements to compute TEI, (Abdelkader et Morrow, 2012) and (Abdelkader et Morrow, 2015) have implemented respectively three and five successive phasor measurements. The impedance calculation has been simplified in (Lee, 2015) by changing the impedance matrix of power system into two-bus equivalent system.

A new concept called coupled single-port model was reported in (Yunfei et al., 2011). This concept helps calculating Thevenin parameters by decoupling the load and generator buses. However, this model suffers from several major drawbacks. Specifically, if the load

scenarios increase suddenly or randomly, this model behaves inaccurately. This drawback can be overcome by modified coupled single-port model (Jian-Hong et Chia-Chi, 2014). This method still cannot detect the voltage instability after the occurrence of a contingency. The comparison of different approaches for the calculation of Thevenin equivalent impedance has been carried out based on accuracy and number of phasor measurement units (PMUs) in (Haoyu et Fangxing, 2014). It shows that coupled single-port model is one of the worst models for the voltage stability detection in dynamic studies. Furthermore, this model has not been developed with high penetration of wind parks.

Optimal Power Flow (OPF) with wind generation has become one of the most widely tools used in the power system planning, operation and electricity market (Jabr et Pal, 2009; Xie, Chiang et Li, 2011). However, these studies do not investigate voltage stability constrained optimal power flow (VSC-OPF) with consideration of wind generation. Also, traditional VSC-OPF methods have some disadvantages such as inaccuracy of the voltage instability detection (Avalos, Canizares et Anjos, 2008; Lage, da Costa et Canizares, 2012; Milano, Canizares et Invernizzi, 2005; Zabaiou, Dessaint et Kamwa, 2014). Due to dynamic behavior of the power system, VSC-OPF methods should use an appropriate index to properly predict the unstable operating point.

This section attempts to overcome these aforementioned limitations and presents a comprehensive model to identify proper criteria for voltage stability evaluation and then to combine it with an OPF while considering the contingency. The main contributions of this chapter could be summarized as follows.

1) This chapter proposes an impedance-based (IB) index that can model the great changes during a voltage collapse process such as line tripping, load tap changing and reactive power limits of DFIG and conventional generator. This index can also monitor online voltage stability.

2) The proposed IB index can model the DFIG reactive power capability characteristics as a variable virtual impedance which is adaptable in the dynamic studies. Therefore, the model of DFIG reactive limits can be integrated to the internal circuit of the generator and it can be appended to impedance matching theory.

3) An OLTC model is also added to this index. The OLTC can affect both TEI and load impedance. Thus, the IB index equation is modified by considering those impedance variations on the OLTC model. The robustness of the proposed method has been investigated by including SVC and different load types in the power systems.

4) A new VSC-OPF is carried out with the proposed IB index. The proposed VSC-OPF can reduce the operating cost and the number of voltage collapses. Thus, it can improve the performance of the electric utilities.

The rest of the chapter is organized as follows. The chapter presents a detailed statement of background in section 2.2. The new IB voltage stability index is introduced in section 2.3. The VSC-OPF method that combines both the OPF and the proposed index is provided in section 2.4. The case studies and simulation results are presented in section 2.5, whereas Section 2.6 draws the conclusion and future works.

2.2 Background

2.2.1 Impedance matching theory and its application

An impedance matching is a proper way to estimate the maximum power transferred to a load bus. As known, the TEI is a criterion for the voltage stability assessment. The impedance matching can be determined as equation (2.1):

$$|Z_L| = |Z_{eq}| \tag{2.1}$$

where Z_L and Z_{eq} are respectively the load impedance and the TEI.

The voltage of the Thevenin equivalent circuit can be defined as follows:

$$E_{eq} = V_L + I_L Z_{eq} \tag{2.2}$$

where V_L and I_L are the load voltage and load current, respectively.

As mentioned before, there are many methods to calculate Z_{eq}. One of these methods adopts coupled single-port model. In this model, the buses are first divided into generator buses, tie buses and load buses in the admittance matrix (Y), which is shown in equation (2.3):

$$\begin{bmatrix} I_L \\ 0 \\ I_G \end{bmatrix} = \begin{bmatrix} Y_{LL} & Y_{LT} & Y_{LG} \\ Y_{TL} & Y_{TT} & Y_{TG} \\ Y_{GL} & Y_{GT} & Y_{GG} \end{bmatrix} \begin{bmatrix} V_L \\ V_T \\ V_G \end{bmatrix} \tag{2.3}$$

Then, the system equivalent impedance matrix (Z_{LL}) can be expressed as (Yunfei et al., 2011):

$$V_L = KV_G - Z_{LL} I_L \tag{2.4}$$

$$Z_{LL} = (Y_{LL} - Y_{LT} Y_{TT}^{-1} Y_{TL})^{-1} \tag{2.5}$$

$$K = Z_{LL} (Y_{LT} Y_{TT}^{-1} Y_{TG} - Y_{LG}) \tag{2.6}$$

Equations (2.4)-(2.6) can be reformulated for load bus i as follows (Yunfei et al., 2011):

$$\mathrm{V_{Li}} = \mathrm{E_{eq,i}} - \mathrm{Z_{LLii}I_{Li}} - \sum_{\mathrm{j=1,i\neq j}}^{\mathrm{n}} \mathrm{Z_{LLij}I_{Lj}} = \mathrm{E_{eq,i}} - \mathrm{Z_{LLii}I_{Li}} - \mathrm{E_{coupled,i}} \tag{2.7}$$

where $E_{eq,i}$ represents the equivalent voltage on the ith bus and $E_{coupled,i}$ denotes the coupling effects of other loads on V_{Li}. Z_{LL} presents the system equivalent impedance and Z_{LLii} is created by the diagonal elements of Z_{LL}.

The coupled impedance has been presented via the concept of coupled single-port circuit. The coupled impedance is determined as follows (Yunfei et al., 2011):

$$\mathrm{Z_{coupled,i}} = \frac{\mathrm{E_{coupled,i}}}{\mathrm{I_{Li}}} = \sum_{\mathrm{j=1,i\neq j}}^{\mathrm{n}} \mathrm{Z_{LLij}} \left(\frac{\mathrm{I_{Lj}}}{\mathrm{I_{Li}}}\right) \tag{2.8}$$

2.2.2 DFIG capability curve limits

There are different models for the representation of the DFIG capability curve limit in the voltage stability studies. As mentioned before, it can be defined for the DFIG capability curve of the RSC and the GSC. The RSC capability is generally bound by the rotor current, rotor voltage and stator current limits. These constraints can change with the slip value of the generator. It is assumed GSC is a lossless converter and it has a unity power factor. Thus, the RSC capability curve is only considered in this chapter.

The equation below represents reactive power limit by rotor current (Londero, Affonso et Vieira, 2015):

$$Q_{Smax} = \sqrt{{S_{Ir_{max}}}^2 - {P_S}^2} - \frac{|V_s|^2}{X_m + X_S} \tag{2.9}$$

$$S_{Ir_{max}} = \left|I_{r_{max}}\right| . |V_s| . \left|\frac{X_m}{X_m + X_S}\right| \tag{2.10}$$

where Q_{Smax} represents the reactive power limit of the stator, $S_{Ir_{max}}$ is the maximum apparent power and $I_{r_{max}}$is the maximum rotor current. X_S and X_m are respectively the stator leakage and magnetizing reactance.

The maximum stator current can be constrained by thermal limit of stator coils. Thus, another limit of DFIG reactive power is as follows (Anaya-Lara et al., 2009):

$$Q_{Smax} = \sqrt{(\left|I_{s_{max}}\right| . |V_s|)^2 - {P_S}^2} \tag{2.11}$$

where $I_{s_{max}}$ represents the maximum stator current.

Since the rotor current limit is usually smaller than the rotor voltage limit, therefore the rotor voltage limit can be disregarded.

2.2.3 VSC-OPF model

The VSC-OPF solution should satisfy both technical and economic issues, which are the minimization of the total costs and the consideration of the voltage stability limits. In order to solve the VSC-OPF, at least one extra constraint should be included in the standard formalization of the OPF and also several supplementary constraints should be added for wind farm integration. The generated active power of wind farms are considered as a control variable. The limits in this case are related to the active power, reactive power, voltage, thermal, wind capacity and voltage stability. The costs are defined as linear and quadratic functions for wind and conventional generators, respectively. The first objective function and its limits are defined as follows:

$$Min \sum_{i \in \alpha_G} \left(C_{G_i} + C_{Q_i}\right) \tag{2.12}$$

$$\begin{aligned}
s.t. \quad & f(\delta, V, Q_G, P_G, Q_w, \mathrm{P}_w) = 0 && \rightarrow \text{PF equation} \\
& P_{G_{min}} \leq P_G \leq P_{G_{max}} && \rightarrow \text{Active power limit} \\
& Q_{G_{min}} \leq Q_G \leq Q_{G_{max}} && \rightarrow \text{Reactive power limit} \\
& \mathrm{V_{min}} \leq \mathrm{V} \leq \mathrm{V_{max}} && \rightarrow \text{Voltage limit} \\
& \mathrm{I_{ij}}(\delta, \mathrm{V}) \leq \mathrm{I_{ijmax}} && \rightarrow \text{Thermal limit} \\
& C_{w,min} \leq C_w \leq C_{w,max} && \rightarrow \text{Wind capacity limit} \\
& r_{w,min} C_{\mathrm{w}} \leq Q_w \leq r_{w,max} C_{\mathrm{w}} && \rightarrow \text{Wind reactive power limit} \\
& VSI_{min} \leq VSI \leq VSI_{max} && \rightarrow \text{Voltage stability limit}
\end{aligned}$$

where α_G represents the sets of generator buses; C_{G_i}, C_{Q_i} are the cost functions of the generator i for the generation of the active and the reactive power ($\$/h$). $P_{G_{min}}$ and $P_{G_{max}}$ are the minimum and maximum active power generation limits (MW), $Q_{G_{min}}$ and $Q_{G_{max}}$ are the minimum and maximum reactive power generation limits ($MVAR$), VSI_{min} and VSI_{max} are the minimum and maximum voltage stability index limits and $I_{ij}(\delta, V)$ indicates the current in the transmission line between buses i and j ($i \neq j$). $C_{w,min}$ and $C_{w,max}$ are the minimum and maximum capacity limit of wind farm (MW), $r_{w,min}$ and $r_{w,max}$ are the minimum and maximum limit in the ratio of reactive power to capacity of the wind farm, Q_w is the reactive power of wind farm ($MVAR$).

As known, generated active power of the wind farm (P_w) depends on wind speed. Hence, P_w can be calculated by multiplying the capacity limit by a generation coefficient between [0, 1]. For this chapter, there are other objective functions that will be introduced later like the minimization of the voltage stability index ($Min\ (VSI)$). where VSI is one of the voltage stability indices.

2.3 Proposed impedance-Based index

In this section, the IB voltage stability index is defined, which can precisely detect the voltage instability. The DFIG reactive power limit and OLTC behavior are chosen to modify the traditional IB index because of their effects on long-term voltage stability. The traditional IB index can be defined as follows:

$$IB_i = \frac{|Z_{eq,i}|}{|Z_{Li}|} \tag{2.13}$$

2.3.1 Model of DFIG reactive limit in improved IB index

In the impedance matching theory, the DFIG reactive limit affects both load impedance and TEI. In this section, the DFIG reactive limit is modelled using a variable virtual impedance in the impedance matching equation.
This constraint results in an increased TEI seen at the load bus. Hence, the additional impedance can be appended to this model. Note that due to DFIG and conventional generator reactive limits, it generally increases the risk of voltage instability.

This model is compatible with different operation modes of DFIG, for example, power factor controlled and voltage controlled mode. To operate in the voltage controlled mode, the DFIG can be modelled as a PV bus, and then it can be considered as a PQ bus when it reaches the reactive power limit. In the power factor controlled mode, DFIG is considered with unit or specific power factor in normal conditions. However, the DFIG will start to control the reactive power when the terminal voltage drops below a set value in the abnormal conditions. Figure 2.1 shows the model of the DFIG reactive limit. As shown in Figure 2.1a, the base case of DFIG circuit can become a PV bus (in a voltage controlled mode) and a PQ bus (in a power factor controlled mode) before reaching a reactive limit. The DFIG will be a PQ bus, when reaching a reactive power limit as shown in Figure 2.1b, and the DFIG terminal voltage

decreases from V_G to V_G'. In other words, an additional impedance Z_C is defined in Figure 2.1c to model the mentioned limit. Note that a new bus is added as a tie bus to the system.

The modified multi-port system is depicted in Figure 2.1d, when the reactive power limits are considered for all DFIG generators and Z_C is the virtual impedance of the model of the DFIG reactive limit.

The new equation of the admittance matrix after adding the proposed model is as follows:

$$\begin{bmatrix} I_L \\ 0 \\ 0 \\ I_G \end{bmatrix} = \begin{bmatrix} Y_{LL} & Y_{LT} & Y_{LG} & 0 \\ Y_{TL} & Y_{TT} & Y_{TG} & 0 \\ Y_{GL} & Y_{GT} & Y_{GG} + Y_C & -Y_C \\ 0 & 0 & -Y_C & Y_C \end{bmatrix} \begin{bmatrix} V_L \\ V_T \\ V_G' \\ V_G \end{bmatrix} \tag{2.14}$$

where Y_C is the diagonal matrix with $(\frac{1}{Z_{C1}}, \frac{1}{Z_{C2}}, \dots, \frac{1}{Z_{Cm}})$ values.

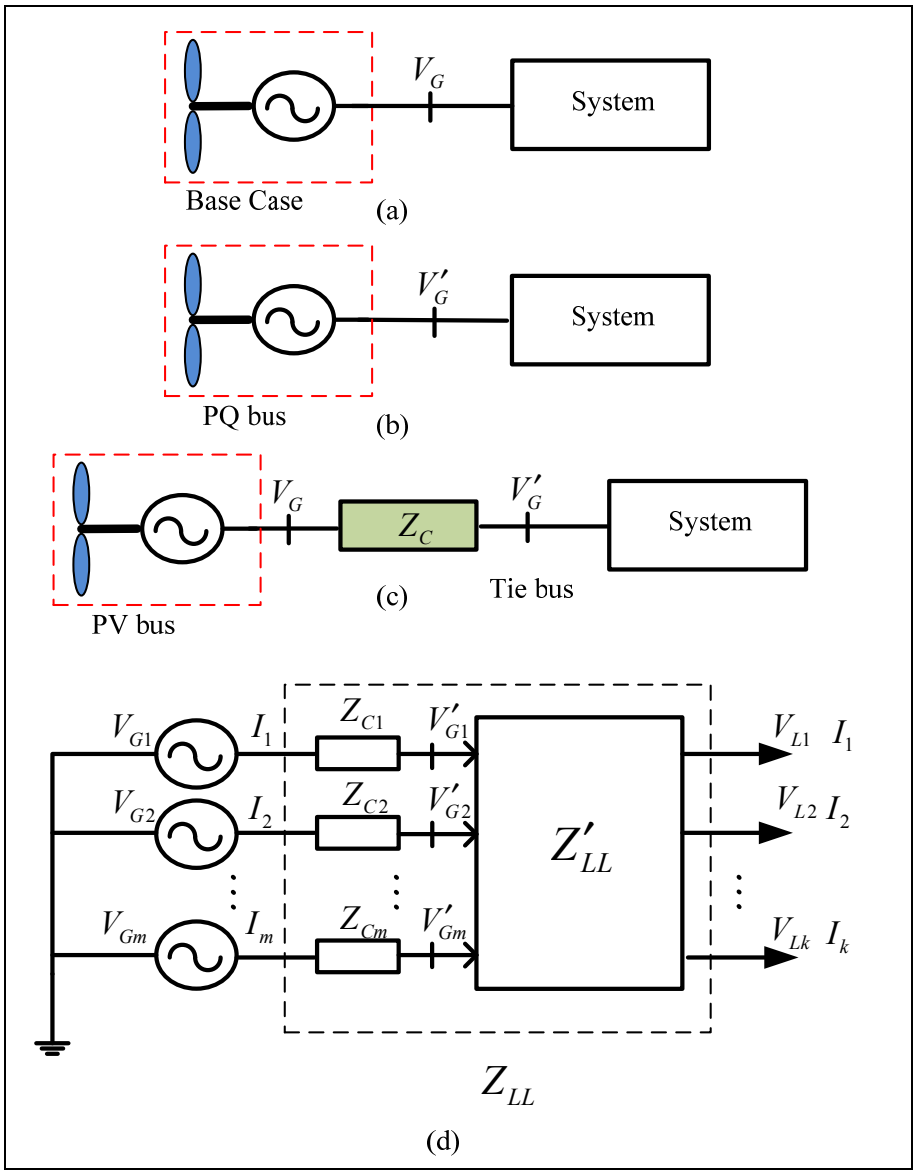

Figure 2.1 Modeling of the DFIG reactive limit (a) Base case (b) After DFIG reactive limit. (c) Modified system (d) Modified multi-port power system with considering proposed model

Since the added bus acts as a tie bus, Equation (2.14) is simplified as:

$$\begin{bmatrix} I_L \\ 0 \\ I_G \end{bmatrix} = \begin{bmatrix} Y_{LL} & Y'_{LT} & 0 \\ Y'_{TL} & Y'_{TT} & Y'_{TG} \\ 0 & Y'_{GT} & Y_C \end{bmatrix} \begin{bmatrix} V_L \\ V'_T \\ V_G \end{bmatrix} \tag{2.15}$$

The additional impedance can be detailed from the following equation:

$$Z_C = \frac{V_G - V_G'}{I_G} \tag{2.16}$$

where V_G and V_G' respectively are the generator voltage before and after DFIG reactive limit action.

The DFIG generator gives similar reactive power capability as a conventional generator. Thus, this model is applicable with the reactive power limit of conventional generators.

2.3.2 OLTC model in improved IB index

In order to present the effect of OLTC on the improved IB index, it is assumed that all LTCs have the same tap steps and time delay. As shown in Figure 2.2a and 2.2b, the effect of OLTC on element impedance is divided into two parts, namely, the OLTC impedance (Z_T) and load impedance (Z_L). Consequently, the IB index equation can be modified.

Figure 2.2c shows the multi-port system when the OLTC model is considered in the system. It is assumed that OLTC is installed on all loads. As shown, the TEI (Z_{eq}) and the load impedance (Z_L) are modified. The modeling of OLTC can enhance the voltage stability detection.

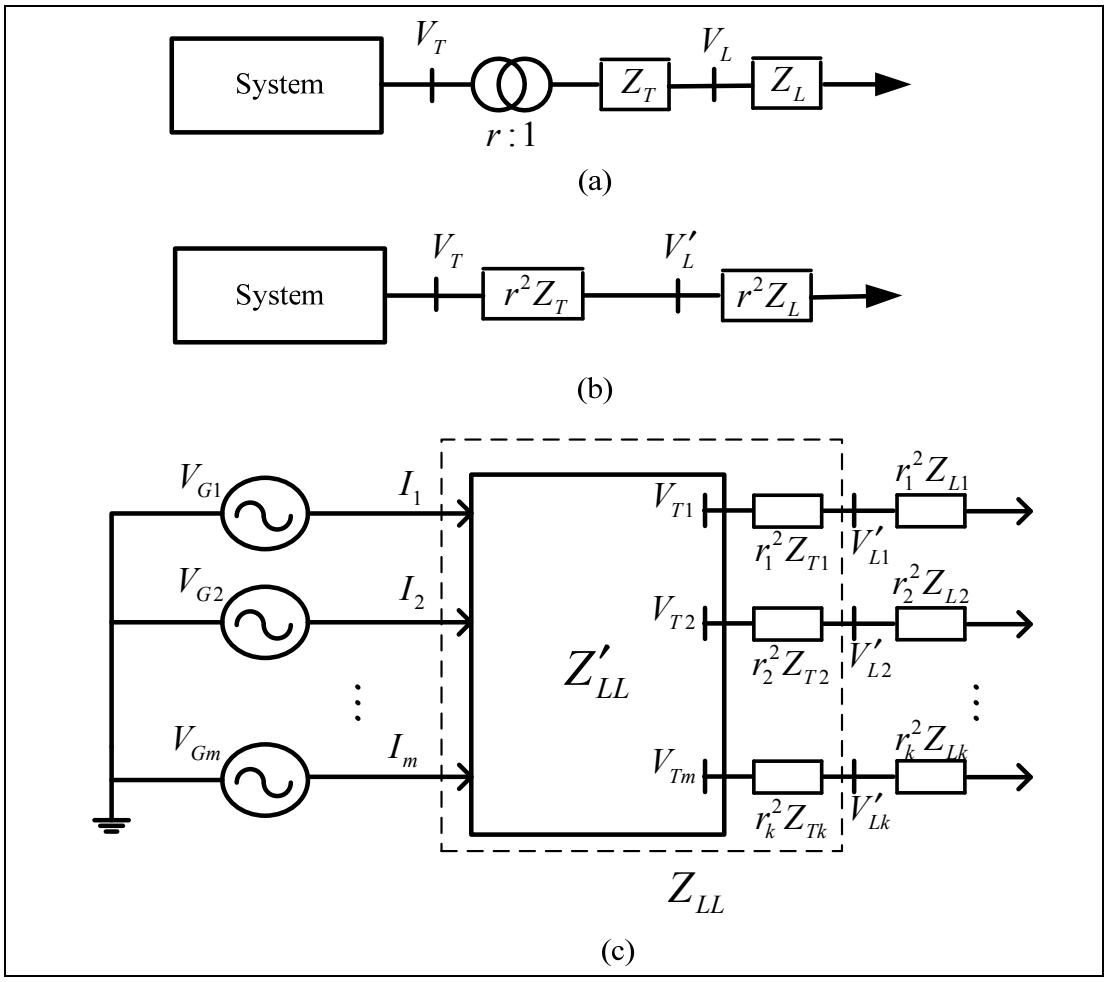

Figure 2.2 Modeling of the OLTC (a) System with OLTC (b) Modified system (c) Modified multi-port power system with considering OLTC model

2.4 Proposed VSC-OPF method

Due to the dynamic behavior of power systems, the traditional VSC-OPF methods cannot accurately perform in the voltage instability evaluation during OLTC actions and DFIG limits, especially in post-contingency conditions. This chapter proposes a new VSC-OPF method that is more practical and realistic. The approach includes a detailed modeling of the DFIG and OLTC. In the proposed voltage stability assessment, the first step is to define the IB voltage stability index. Then, the VSC-OPF is performed including the IB constraint as a voltage stability constraint. This IB constraint is defined as follows:

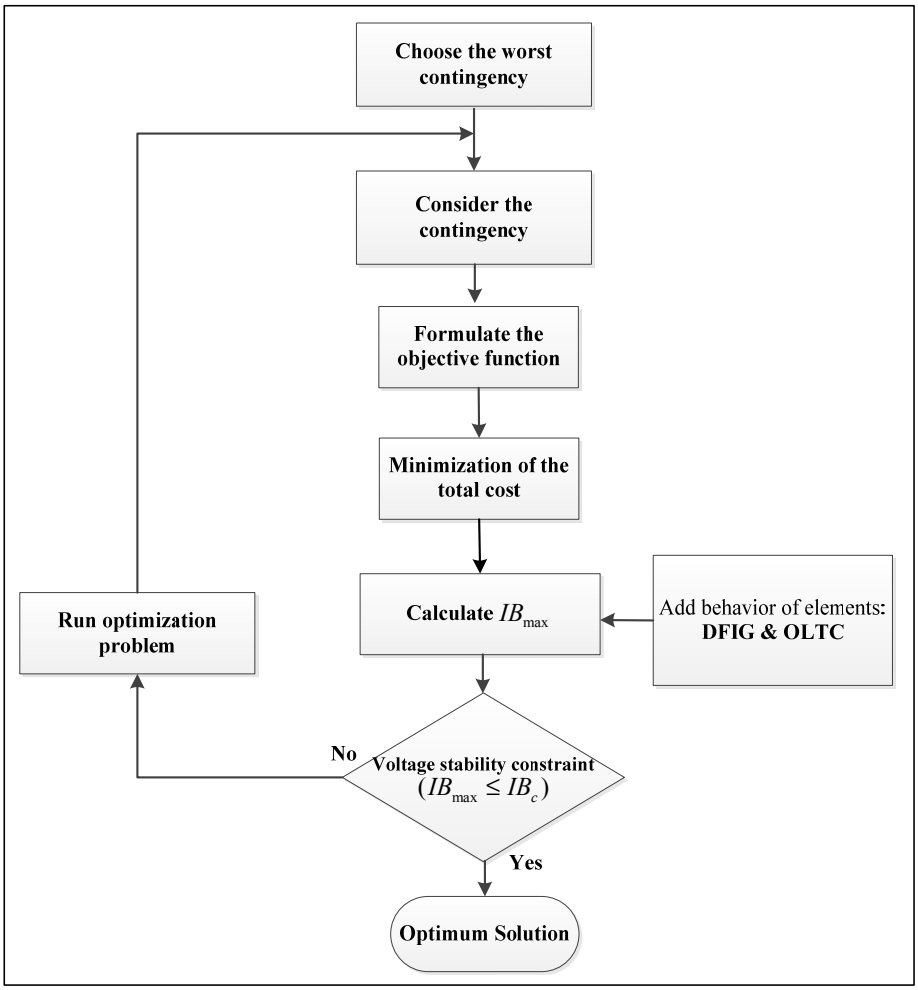

Figure 2.3 Flowchart of the proposed VSC-OPF method

$$IB_{max}(\delta, V, Q_G, P_G, Q_w, \mathrm{P}_w) \leq IB_c \tag{2.16}$$

where IB_{max} and IB_c represent the maximum and the critical value of the improved IB index, respectively. IB_{max} can show the weakest transmission bus. A flowchart of the proposed VSC-OPF based on the improved IB index is depicted in Figure 2.3.

2.5 Simulation result and discussion

In this section, both dynamic and static studies are performed to demonstrate the effectiveness of the proposed model. They are divided into two parts: voltage stability monitoring and VSC-OPF. Several case studies are selected to verify the results which are detailed as below.

2.5.1 Voltage stability monitoring

By applying the proposed model, several case studies such as modified WECC test system and IEEE 39-bus system are tested in PSAT (Milano, 2005). In order to evaluate the performance of this index, no under-voltage protection or load shedding is considered in this work.

2.5.1.1 Modified WECC test system

To analyze the effect of the proposed model on the voltage stability, a modified WECC test system is used which is a looped network system. This system shown in Figure 2.4 has an added bus with an OLTC transformer and it contains a wind park with DFIGs. The bus number is rearranged respectively as load buses, tie buses and generator buses, because of the coupled single-port model calculation. An automatic voltage regulator (AVR) and an OEL are installed on the conventional generator and loads will be increased until finding a voltage collapse in dynamic simulation. Note that a line transmission tripping is assumed between buses 4 and 7 (at $t = 5s$).

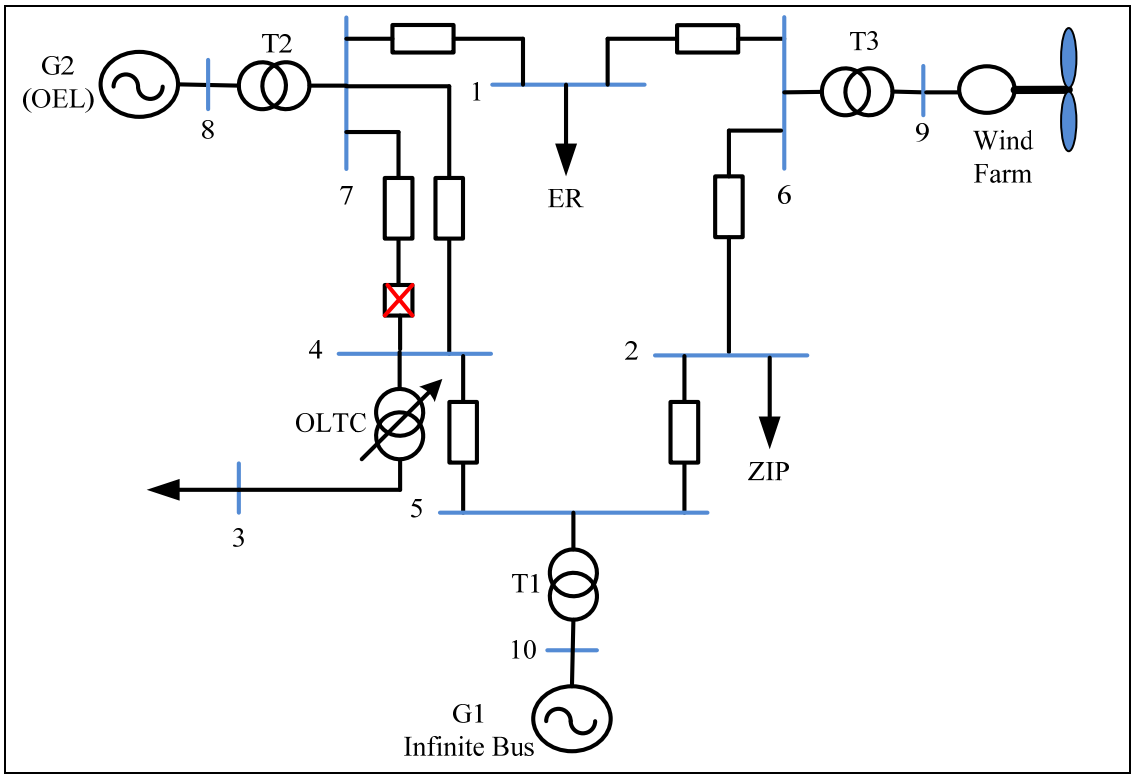

Figure 2.4 Modified WECC test system

Tap ratio step (0.02), minimum and maximum tap ratio (between 0.8 to 1.2) and reference voltage (0.9 p.u.) are the parameters of the OLTC. The nominal wind speed is considered 15 (m/s) and the Weibull distribution used to model the wind speed. The DFIG operates in the voltage controlled mode. The voltage magnitudes, tap changing, proposed IB index and virtual impedance are depicted in Figure 2.5a–d, respectively.

Figure 2.5a shows the voltage variations after the occurrence of the contingency, where the system reaches the voltage instability point at 36.4 s. It is assumed that the short-term voltage stability evaluation is ignored. The process of restoration by the OLTC is represented in Figure 2.5b, which has a negative effect on voltage stability.

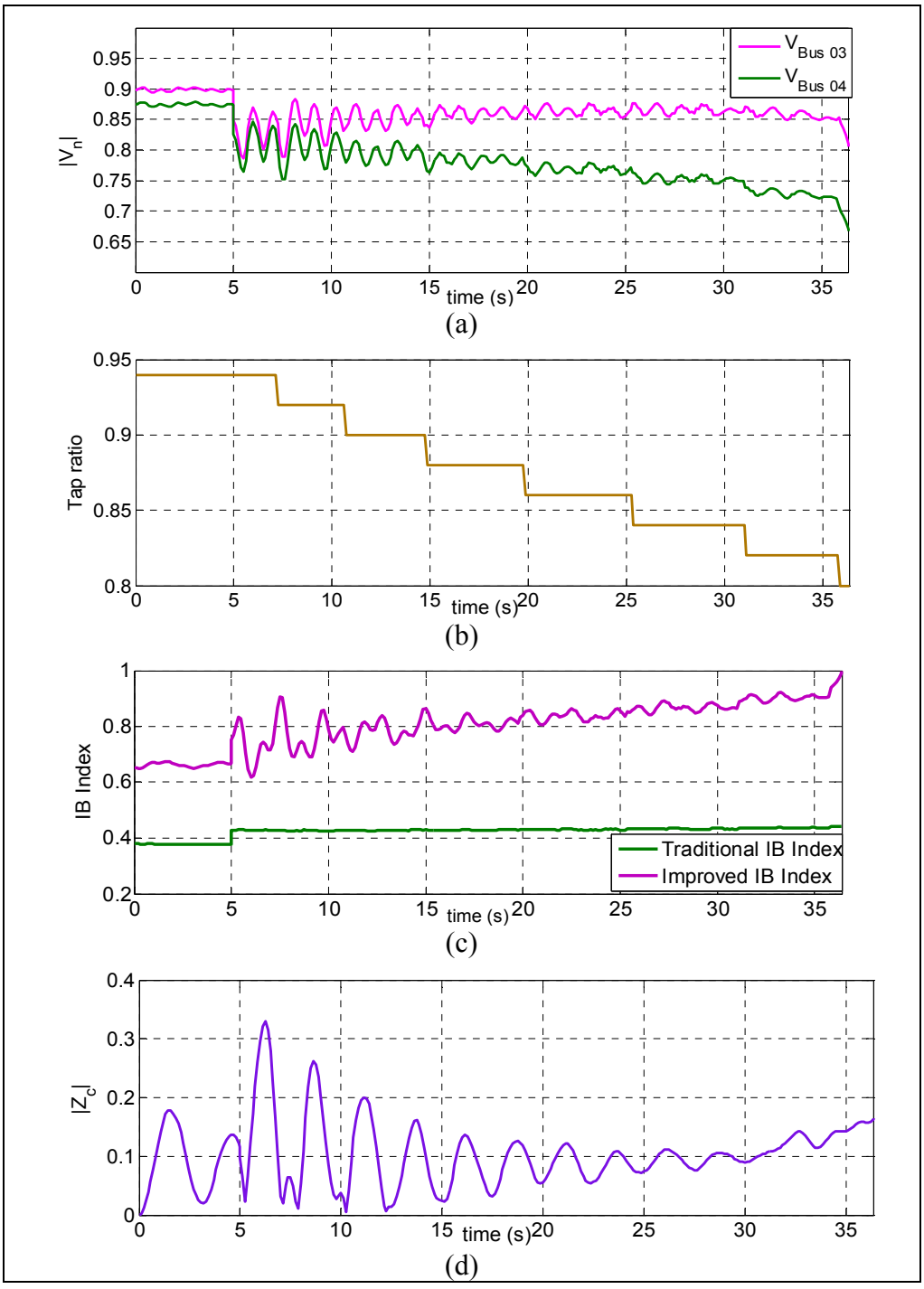

Figure 2.5 Voltage instability in modified WECC system (a) Voltage magnitude at buses 3 and 4 (b) Tap changing in the OLTC (c) Comparison of IB indices at the load (d) Virtual impedance of proposed model

The comparison between traditional and improved IB indices is evaluated in Figure 2.5c. The improved IB index with the modified coupled single-port model can predict the voltage

instability accurately, because the index value reaches 0.999 based on the impedance matching theory. As expected, when the improved IB index reaches 1, this operating point will be the collapse point. Otherwise, Figure 2.5c demonstrates that the traditional IB index (with coupled single-port model) reaches a value of 0.442 and it cannot detect the voltage collapse point. Therefore, the proposed IB index will improve by 55.7% the voltage instability detection in this case. The DFIG changes from PV bus to PQ bus; therefore, Z_c has large variation because of the DFIG reactive limit (see Figure 2.5d). To show the robustness of the proposed method with different load models, ZIP and exponential recovery load model are used in this case.

2.5.1.2 Modified IEEE 39-bus system

The IEEE 39-bus system that is well known as New-England power system (Athay, Podmore et Virmani, 1979) is evaluated in this part. To investigate the performance of the proposed model, a bus with OLTC is added at bus 8 that is called bus number 40 and two wind parks with DFIGs has been added at buses 34 and 37. The nominal wind speed is considered 15 (m/s) and the Weibull distribution used to model the wind speed. AVR and an OEL are also installed on the conventional generators.

The loading factor of additional bus and other buses has been increased up to 1.3 p.u. and 1.6 p.u., respectively. A contingency is considered as a line transmission tripping between buses 8 and 9 ($t = 5s$). The voltage magnitudes, tap changing, the impedances of the proposed IB index and comparison between traditional and proposed model are presented in Figure 2.6a–d, respectively. The results show that extra bus connected to the OLTC (bus 40) is the weakest bus in this case. Because it has higher index value than other buses. Figure 2.6c shows that the system is collapsing at 61.5 s. As observed, the proposed model can follow unstable behavior in this case study.

By applying the proposed model, Figure 2.6c represents the load impedance and the TEI at bus 40. The curves of these two impedances cross each other at the collapse point. Thus, the results are accurate. The impact of the proposed model is presented in Figure 2.6d that

compares the curves of traditional and improved IB index. The traditional IB index reaches a value of 0.708 at the collapse point that shows an optimistic prediction of the voltage instability. Thus, the proposed IB index will improve by 29.1% the voltage instability detection in this case.

To show the robustness of the proposed model, the application of a static var compensator (SVC) has been investigated in this part which is installed in bus 6. As known, SVC increases the voltage stability margin of power systems. Thus, the previous system is stable. To produce a collapse point, the active power of loads and generators will be increased by 15%.

The voltage magnitudes and comparison between traditional and improved index are presented in Figure 2.7a–b, respectively. Where the system reaches the voltage instability point at 39.6 s. As shown in Figure 2.7b, the proposed model can predict the voltage instability accurately.

2.5.2 VSC-OPF

By applying the proposed model for DFIG wind parks integration, the VSC-OPF is performed in these case studies: IEEE 39-bus, IEEE 57-bus and Polish 2746-bus systems. All results in this section are carried out in MATPOWER (Zimmerman et C. Murillo-Sánchez). The comparison has been done between IB-index, L-index, VCPI and MSV. The VSC-OPF can be carried out with different objective functions as follows:

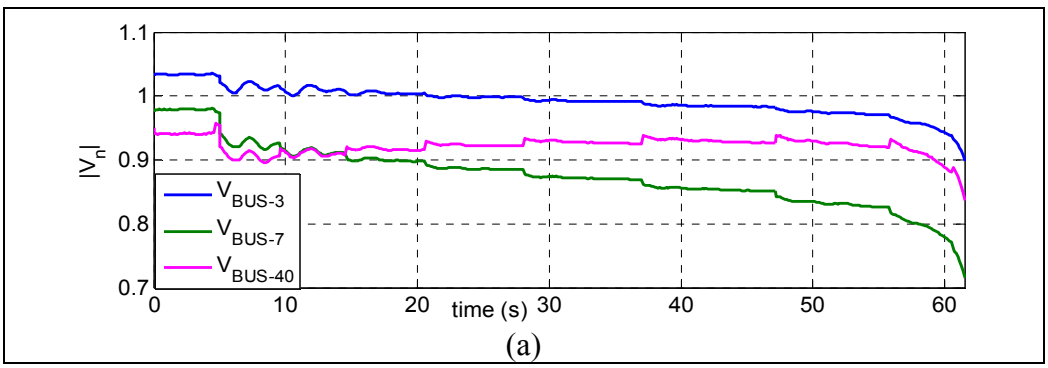

(a)

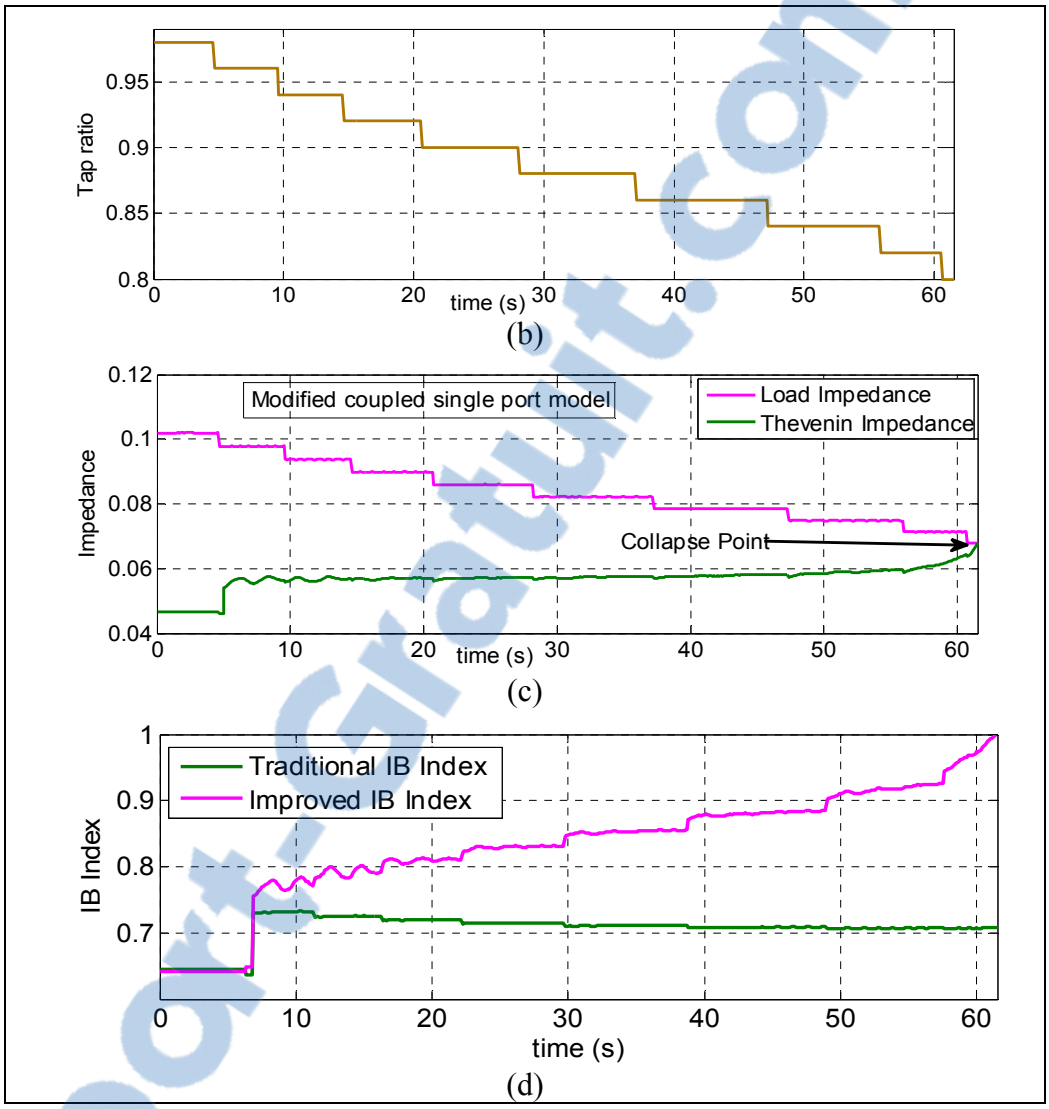

Figure 2.6 Voltage instability in modified IEEE 39-bus (a) Voltage magnitude at buses 3, 7 and 40 (b) Tap changing in the OLTC (c) System and load impedances at bus 40 (d) Comparison between traditional and proposed IB index

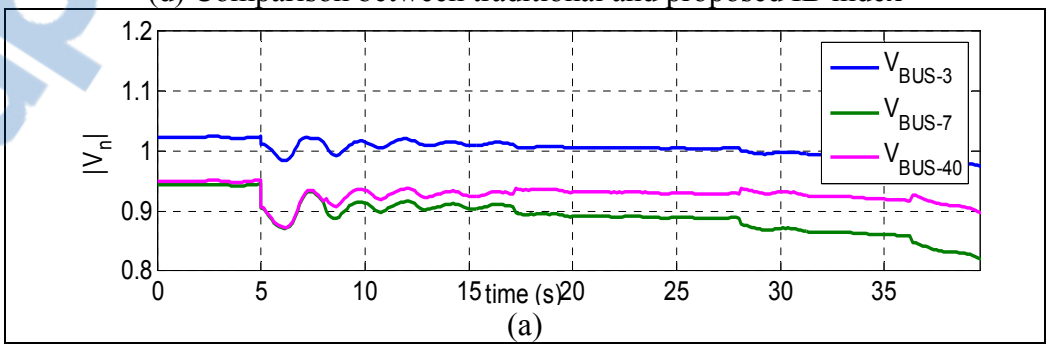

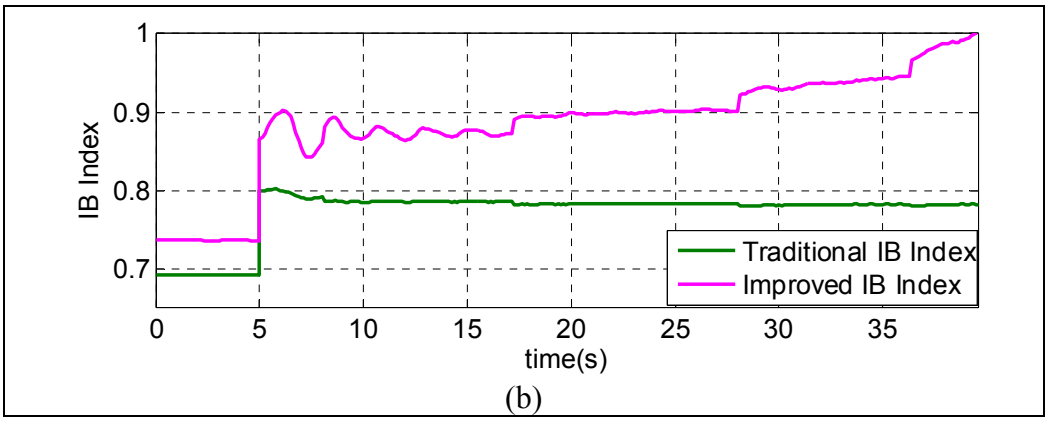

Figure 2.7 Voltage instability in modified IEEE 39-bus with SVC (a) Voltage magnitude at buses 3, 7 and 40 (b) Comparison between proposed and traditional index

CASE 1: minimize the cost function.

CASE 2: minimize the cost function with the extra voltage stability constraint.

CASE 3: minimize the index or maximize it, which depends on the type of index.

2.5.2.1 IEEE 39-bus system

The proposed VSC-OPF method that is OPF combined with improved IB index is presented in Table 2.1 in the stressed conditions. Loading factor of bus 8 and other buses has been increased to 1.3 p.u. and 1.6 p.u., respectively. A line transmission outage is assumed between buses 8 and 9 for single line outage conditions. Also, two wind parks with DFIGs have been added at buses 34 and 37. In case 2, the value of voltage stability constraint should be defined by independent system operator (ISO). This value is assumed equal to 0.56 for stressed conditions. Table 2.1 can also produce different scenarios with several objective functions and load profiles. Hence, ISO can identify the best strategy in these different scenarios. Where IB_T and IB_{max} are total and maximum voltage stability index between all load buses, respectively, and FC is the fuel cost function. P_w is generated active power of the wind farms. Based on different objective functions, generated wind active power can change in buses 34 and 37.

Table 2.1 Proposed VSC-OPF results for stressed condition (IEEE 39-bus)

	Objective functions		
	Case 1	**Case 2**	**Case 3**
P_w, MW	1393.6	1394.0	1386.2
IB_{max}	0.572	0.56	0.558
IB_T	4.09	4.07	3.48
FC,$/h	108897.48	109562.30	124462.73

In order to minimize the objective function in case 3, improved IB index should be obtained for all load buses. As illustrated in Figure 2.8, bus 8 has the maximum value of the index; therefore, it is the weakest bus. Thus, the improved IB index value of bus 8 was selected to be minimized.

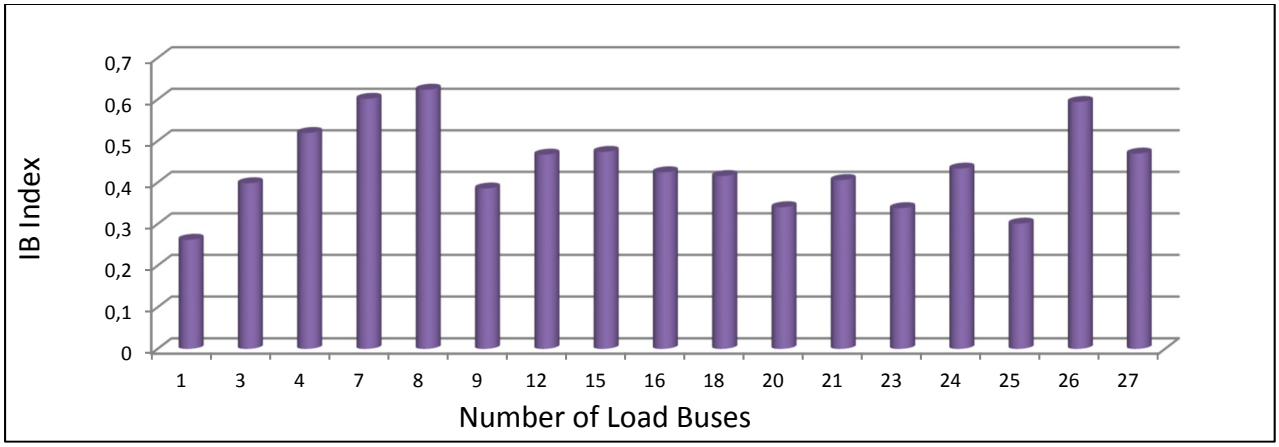

Figure 2.8 Improved IB index values in the IEEE 39-bus system

2.5.2.2 IEEE 57-bus system

To compare the proposed VSC-OPF method with other methods, the IEEE 57-bus system is selected to demonstrate the performance of the method. A line transmission outage is considered between buses 8 and 9 for the single line outage conditions. One wind park with DFIGs has been added at bus 12. Figure 2.9 shows a comparison between different variables in the cases 1, 2 and 3. The fuel cost is the highest in case 3 and it is approximately same in cases 1 and 2. However, case 2 has the lowest generated reactive power and active power

losses. This case can satisfy the economic and security issues. It is also seen from Figure 2.9 that ISO can find the proper optimal solution from the three objective functions.

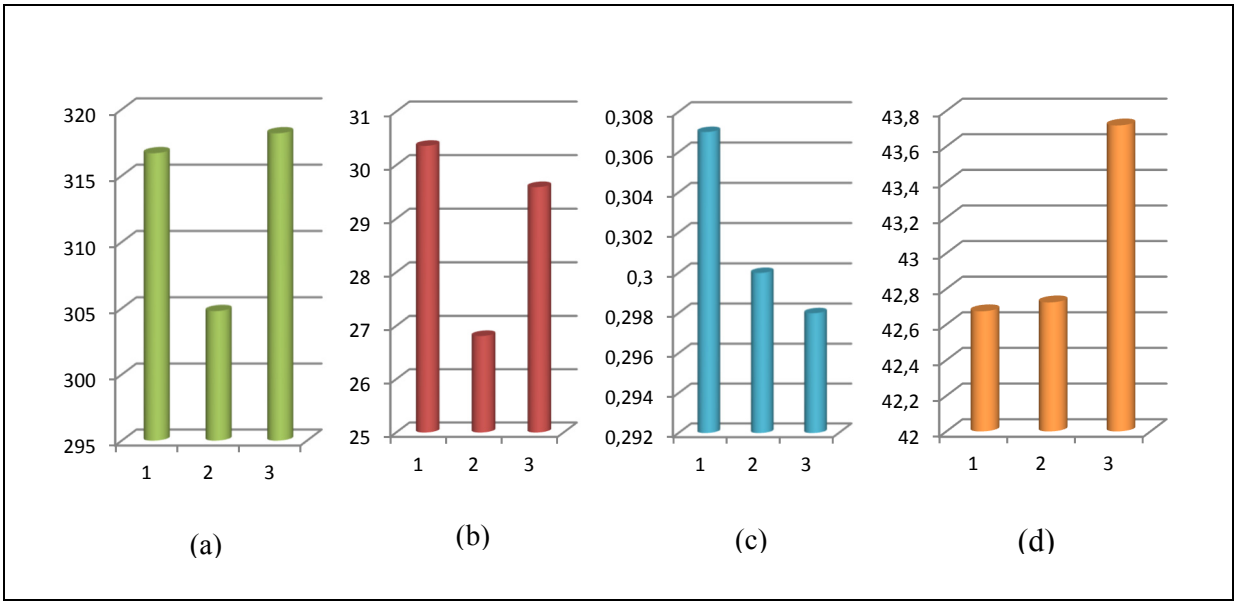

Figure 2.9 Comparison between Different variables in IEEE 57-bus system (a) Generated reactive power (MVAR) (b) Active power losses (MW) (c) Maximum values of improved IB index (d) Fuel cost function (K$/h)

The comparison between different VSC-OPF methods is presented in Table 2.2. The objective functions are as follows: minimize the maximum L-index value (min L_{max}), maximize the minimum singular value (max MSV), minimize total values of VCPI (min $VCPI_T$) and minimize the maximum IB-index value (min IB_{max}). As listed in Table 2.2, the proposed VSC-OPF (min IB_{max}) has the lowest fuel cost. However, min $VCPI_T$ achieves the lowest generated reactive power and active power losses. This result is due to the fact that VCPI is based on the theory of maximum power transfer between two buses. On the other hand, min $VCPI_T$ has the highest fuel cost. Accordingly, the proposed VSC-OPF has the highest performance between other methods.

Table 2.2 Comparison between different VSC-OPF results for IEEE 57-bus system (single line outage condition)

	Objective functions

	min L_{max}	max MSV	min $VCPI_T$	min IB_{max}
P_{loss}, MW	37.02	36.97	15.99	29.59
Q_{gen}, MVAR	341.4	342.6	269.2	318.2
IB_{max}	0.304	0.310	0.298	0.298
IB_T	5.398	5.497	5.252	5.3347
FC,$/h	43793.96	43832.90	47265.84	43718.50

2.5.2.3 Polish 2746-bus system

To validate the proposed VSC-OPF method in the larger system, the Polish 2746-bus system is selected. Forty wind parks with specific reactive power limits have been added into this system. Figure 2.10 shows sorted values of IB indices for all load buses where bus 506 has the maximum value of the index (0.2512); therefore, it is the weakest bus. The improved IB index value of bus 506 is selected to be minimized.

Table 2.3 shows the comparison between two scenarios with two critical values of the improved IB index. When VSC-OPF is applied, the generated power system is re-dispatched. The process of voltage stability improvement represents that the fuel cost increases, however the power system has a better voltage stability margin. The ISO can manage the active and reactive generated power.

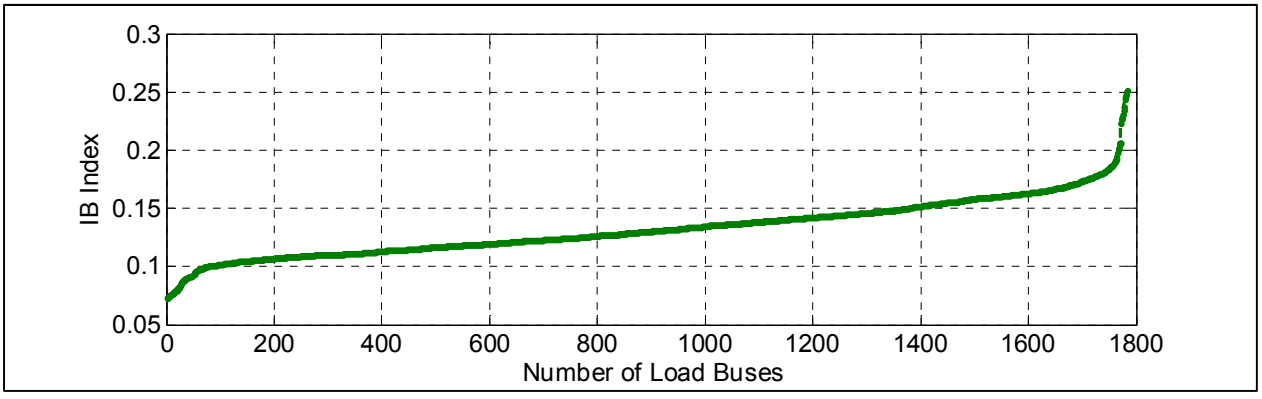

Figure 2.10 Sorted improved IB index values in the Polish 2746-bus system

Table 2.3 Proposed VSC-OPF for Polish 2746-bus system

Scenarios	Base Case (IB=0.2512)	IB VSC-OPF (IB=0.2510)
Objective Function [K$/h]	1307.88	1308.84

2.6 Conclusion

In this chapter, we propose the improved IB voltage stability index, which can detect precisely the voltage instability with high penetration of wind turbine. This index can model the DFIG reactive power limit and it uses the concept of coupled single-port circuit. A VSC-OPF is carried out with the proposed index. The improved model is based on a variable virtual impedance and it is adaptable with DFIG reactive behavior. The chapter proposes also the modeling of the OLTC in the IB index, if it is available in the system.

Several dynamic and static studies are proposed to demonstrate the effectiveness of the proposed model. They have been divided into two parts that are voltage stability monitoring and VSC-OPF. By applying the proposed model to voltage stability monitoring, the accurate voltage instability detection has been depicted in three case studies. In particular, the comparison between improved and traditional IB index represents the method performance. The proposed VSC-OPF also has been compared between improved IB-index, L-index, VCPI and MSV. The results reveal that the improved IB index has the lowest operating cost. The results can also produce different scenarios with several objective functions and load profiles. Hence, ISO can identify the proper strategy in these different scenarios. In future works, this VSC-OPF could consider the characteristics of an electricity market such as reactive power market. Therefore, it would be compatible with the electricity market regulations.

CHAPTER 3

MULTI-OBJECTIVE STOCHASTIC OPTIMAL POWER FLOW CONSIDERING VOLTAGE STABILITY AND DEMAND RESPONSE WITH SIGNIFICANT WIND PENETRATION

Majid Bavafa and Louis-A. Dessaint,

Department of Electrical Engineering, Ecole de technologie supérieure,
1100 Notre-Dame West, Montréal, Quebec, Canada H3C 1K3

Paper accepted in IET Generation, Transmission & Distribution, March 2017

Abstract

In this chapter, a multi-objective stochastic optimal power flow (SOPF) problem with the presence of uncertain wind power generations is introduced. In particular, the chapter has two main contributions. First, it proposes a multi-objective SOPF which consists of the operating cost, voltage stability and emission effects as the objective functions. The wind uncertainty is formulated as a scenario-based technique. Demand response (DR) program is considered in this chapter, which is one of the most efficient control ways to reduce the risk of voltage instability after a contingency occurrence or a stressed loading condition. In addition, the proposed approach uses the technique of fuzzification to normalize all objective functions and to find the optimal solution. The second contribution proposes a line voltage stability index (LVSI). The proposed LVSI can detect precisely the voltage collapse in comparison with other LVSIs, especially after the occurrence of a given contingency due to the dynamic elements of the system. The proposed multi-objective SOPF is also carried out with different existing LVSIs as the objective functions. These approaches are tested and validated by the modified WECC test system, the IEEE 39-bus.

Nomenclature

A. Sets

Ω_B	Set of buses, indexed by b.
$\Omega_{B_{DR}}$	Set of buses cooperated in the DR program, indexed by b_{DR}.
Ω_I	Set of generating units, indexed by i.
Ω_L	Set of transmission lines, indexed by l.
Ω_U	Set of scenarios, indexed by u.
Ω_w	Set of wind farms, indexed by w.

B. Variables

${p^C}_{w,u}$	Active power curtailment of wind farm w under scenario u (MW).
${p^{DR}}_{b,u}/{q^{DR}}_{b,u}$	Active/reactive power cooperated in the DR program at bus b_{DR} under scenario u (MW/MVAR).
$p_{i,u}/q_{i,u}$	Active/reactive power output of generator i under scenario u (MW/MVAR).
${q^W}_{w,u}$	Reactive power of wind farm w under scenario u (MVAR).
$S_{l,u}$	Apparent power of line l under scenario u (VA).
$V_{b,u}/\theta_{b,u}$	Voltage magnitude/angle at bus b under scenario u (V/rad).
$LVSI_{l,u}$	Line voltage stability index of line l under scenario u.

C. Parameters

C_G	Cost function of power output of generator ($/MW).
C_W	Penalty function of wind power spillage ($/MW).
C_{DR}	Cost function of DR program ($/MW).
E_G	Emissions function of generator (ton/h).
${P^D}_b/{Q^D}_b$	Active/reactive power of load at bus b (MW).

$P^{W}{}_{w,u}$	Available active power of wind farm w under scenario u (MW).
$\bar{P}_i/\bar{Q}_i$	Maximum active/reactive power output of generator i (MW/MVAR).
$\underline{P_i}/\underline{Q_i}$	Minimum active/reactive power output of generator i (MW/MVAR).
$\underline{Q_w^W}/\overline{Q_w^W}$	Min/maximum reactive power of wind farm w (MVAR).
$\overline{P}^{DR}{}_{b,u}/\overline{Q}^{DR}{}_{b,u}$	Maximum active/reactive power cooperated in the DR program at bus b_{DR} under scenario u (MW/MVAR).
$\bar{S}_l$	Maximum capacity of line l (VA).
$\bar{V}_b/\underline{V_b}$	Maximum/min voltage magnitude at bus b (V).
Y_{bm}/ϕ_{bm}	Admittance magnitude/angle of line connecting nodes b and m (S/rad).
ω_{1-3}	Weighting factors of objective functions.
π_u	Probability of scenario u.
α_i	Emission coefficient of generator i (ton/h).
β_i	Emission coefficient of generator i (ton/MWh).
γ_i	Emission coefficient of generator i (ton/M^2W^2h).
ξ_i	Emission coefficient of generator i (ton/h).
λ_i	Emission coefficient of generator i (1/MW).

3.1 Introduction

Optimal power flow (OPF) has become one of the most widely tools used in the power system planning, operation and electricity market. There are different linear and nonlinear solution methods for the OPF. In spite of the introduction of the OPF more than a half-century ago, the OPF encounters inaccurate and fragile solutions which may enforce an extra cost in billions of dollars per year to an independent system operator (ISO) (Cain, O'Neill et Castillo, December, 2012). Generally, OPF shows the behavior of elements in steady state conditions (Andersson, 2004). In recent years, several multi-objective OPF methods have been presented which are useful for an ISO (Duman et al., 2012b; Rezaei Adaryani et Karami, 2013).

One type of multi-objective OPF methods considers voltage stability issues as the objective function. These methods employ voltage stability indices to detect voltage instability (Avalos, Canizares et Anjos, 2008; Canizares et al., 2001; Lage, da Costa et Canizares, 2012; Milano, Canizares et Invernizzi, 2005; Rosehart, Canizares et Quintana, 2003a; 2003b; Venkatesh, Arunagiri et Gooi, 2003; Zabaiou, Dessaint et Kamwa, 2014). The roles of these indices lie in the evaluation of voltage instability risk and the prediction of voltage collapse point. There are several papers on OPF including wind farm (WF) integration (Jabr et Pal, 2009; Xie, Chiang et Li, 2011). Due to the increased number of WF, the effects of WF on voltage stability issues are undeniable. The WF equipped with an induction generator absorbs reactive power. As is known, most reasons of voltage collapse are based on failing to provide reactive power demands. Therefore, the consideration of the WF should be adequately analyzed for voltage instability detection (Youssef, Azab et Amin, 2015). Due to wind uncertainties, SOPF (Roald et al., 2016; Summers et al., 2014) was created to provide an appropriate model for wind uncertainties in the system so that it can reduce the risk of outages (Bienstock, Chertkov et Harnett, 2014). One of the famous techniques in uncertainty modeling is a scenario-based technique that provides less operating costs for ISOs (Bouffard, Galiana et Conejo, 2005). The authors in (Pand et al., 2016) also note that the scenario-based technique is one of the most profitable techniques. The scenario-based technique is applied in this section.

Demand response (DR) is defined as demand variations of several voluntary customers due to increasing their profits or enhancing the system reliability by directions from an independent system operator (ISO) (*Assessment of demand response and advanced metering*, 2012; Rabiee et al., 2014). Therefor DR is profitable due to increasing the stability limit and assessing the benefits of the unpredictable nature of renewable energies.

Another type of multi-objective OPF methods regards the emission issues as the objective function. Due to increasing energy demands, the power plants release more emissions. Thus, more international attention has been given to control this pollution. To manage the effects of emissions on the electricity industry, some emission directives have been presented such as the Kyoto Protocol (Kyoto Protocol to the United Nations Framework Convention on

Climate Change, 1992), and the National Emissions Ceilings Directive (National Emission Ceilings for Certain Atmospheric Pollutants, Directive 2001/81/EC of the European Parliament and of the Council, 2001). There are several ways to reduce the emissions. In (Niknam et al., 2012), the authors propose an environmental dispatch which is one of the economical solutions to reach that objective. Carbon capture plants (CCPs) can be used to reduce the emissions, for example an economic dispatch (ED) has been performed with CCPs with the minimization of the total cost and emissions in (Lu et al., 2013).

Since WF does not itself increase any emission levels, major emission reductions are found with high penetration of WF. Therefore, multi-objective SOPF considering operating cost, emission and voltage stability impacts with WF integration and DR is very beneficial for the ISOs. In order to change a multi-objective function into a single-objective function, fuzzification (Chandrasekaran et Simon, 2012; Esmaili, 2013) is employed in this chapter to avoid the scaling problem which will be described in detail. This chapter also uses line voltage stability indices (LVSIs) to investigate voltage stability assessment, because they have an advantage in terms of their computational efficiency. Such indices are namely: fast voltage stability index (FVSI) (Musirin et Rahman, 2002), voltage collapse proximity indicator (VCPI) (Moghavvemi et Faruque, 1998), line stability index (Lmn) (Moghavvemi et Omar, 1998), LSZ (Jalboub et al., 2012) and line stability factor (LQP) (Mohamed, Jasmon et Yusoff, 1989). Generally, the calculation of these LVSIs is based on one single line between two buses. Therefore, the voltage stability limit is based on a theory of maximum power transfer between two buses. The studies still lack a multi-objective OPF with comparison of line voltage stability indices.

This chapter attempts to overcome these aforementioned limitations and proposes a LVSI. It also carries out a multi-objective SOPF with WF integration and DR. The main contributions of this chapter could be summarized as follows. This chapter proposes a multi-objective SOPF problem considering wind uncertainty and DR. This multi-objective SOPF consists of the operating cost, voltage stability and emission effects as the objective functions. Furthermore, a new LVSI is presented that can detect precisely the voltage collapse in

comparison with other LVSIs, especially after the occurrence of a given contingency due to the dynamic elements of the system. Finally, a comprehensive comparison between different LVSIs as the objective function is given in the multi-objective SOPF. Also, the multi-objective SOPF with proposed LVSI is investigated under different scenarios. It can reduce the operating cost and increase the minimum voltage magnitude. Thus, it can improve the performance of the electric utilities.

The rest of the chapter is organized as follows. The chapter introduces a detailed formulation and constraints of multi-objective SOPF in section 3.2. A statement of background which consists of operating points and fuzzification in multi-objective SOPF is given in section 3.3 and 3.4. The new LVSI is introduced in section 3.5. The case studies and simulation results are presented in section 3.6, whereas section 3.7 draws the conclusion.

3.2 Multi-objective SOPF formulation and constraints

Multi-objective SOPF satisfies technical, economic and environmental issues with high penetration of WF and DR. These issues are defined as the total costs, the voltage stability index and the emission as the objective functions. In order to solve multi-objective SOPF, all three objective functions are considered and several supplementary constraints should be added by WF uncertainty and DR. The multi-objective function and its constraints are defined as follows:

$$Min \sum_{u\in\Omega_U} \pi_u \left[\omega_1 \left(\sum_{i\in\Omega_I} C_G(p_{i,u}) + \sum_{i\in\Omega_W} C_W\left(p^C{}_{w,u}\right) + \sum_{b\in\Omega_B} C_{DR}\left(p^{DR}{}_{b,u}\right) \right) + \omega_2 \sum_{i\in\Omega_I} E_G(p_{i,u}) + \omega_3 \sum_{i\in\Omega_L} LVSI_{l,u} \right] \tag{3.1}$$

$$\underline{P_i} \le p_{i,u} \le \bar{P}_i, \quad \forall u \in \Omega_U, i \in \Omega_I \tag{3.2}$$

$$\underline{Q_i} \le q_{i,u} \le \bar{Q}_i, \quad \forall u \in \Omega_U, i \in \Omega_I \tag{3.3}$$

$$\sum_{i\in\Omega_B} p_{i,u} + \sum_{w\in\Omega_B} (P^W{}_{w,u} - p^C{}_{w,u}) - V_{b,u} \sum_{\{b,m\}\in\Omega_L} V_{m,u}\, Y_{bm} \cos(\theta_{b,u} - \theta_{m,u} - \phi_{bm}) = P^D{}_b + p^{DR}{}_{b,u}, \quad \forall u \in \Omega_U, b \in \Omega_B \tag{3.4}$$

$$\sum_{i\in\Omega_B} q_{i,u} + \sum_{w\in\Omega_B} (q^W{}_{w,u}) - V_{b,u} \sum_{\{b,m\}\in\Omega_L} V_{m,u}\, Y_{bm} \sin(\theta_{b,u} - \theta_{m,u} - \phi_{bm}) = Q^D{}_b + q^{DR}{}_{b,u}, \quad \forall u \in \Omega_U, b \in \Omega_B \tag{3.5}$$

$$0 \le p^C{}_{w,u} \le P^W{}_{w,u}, \quad \forall u \in \Omega_U, w \in \Omega_W \tag{3.6}$$

$$\underline{Q_w^W} \le q^W{}_{w,u} \le \overline{Q_w^W}, \quad \forall u \in \Omega_U, w \in \Omega_W \tag{3.7}$$

$$-\bar{S}_l \le S_{l,u} \le \bar{S}_l, \quad \forall u \in \Omega_U, l \in \Omega_L \tag{3.8}$$

$$\underline{V_b} \le V_{b,u} \le \bar{V}_b, \quad \forall u \in \Omega_U, b \in \Omega_B \tag{3.9}$$

$$0 \le p^{DR}{}_{b,u} \le \overline{P}^{DR}{}_{b,u} \le P^D{}_b, \quad \forall u \in \Omega_U, b \in \Omega_B \tag{3.10}$$

$$0 \le q^{DR}{}_{b,u} \le \overline{Q}^{DR}{}_{b,u} \le Q^D{}_b, \quad \forall u \in \Omega_U, b \in \Omega_B \tag{3.11}$$

Constraints (3.2)-(3.3) show the limits of minimum and maximum active/reactive power output of the generator and (3.4)-(3.5) show the power balance of active/reactive power. Constraints (3.6)-(3.7) are the active/reactive power curtailment limits of the wind farm. Constraints (3.8)-(3.9) enforce the power flow and voltage angle limits, respectively. Constraints (3.10)-(3.11) enforce the limits of active/reactive power cooperated in the DR program. $\mathrm{C_G(p_{i,u})}$ is defined as quadratic functions for conventional generators and $\mathrm{C_W\left(p^C{}_{w,u}\right)}$ and $\mathrm{C_{DR}\left(p^{DR}{}_{b,u}\right)}$ are considered as linear functions. $LVSI_{l,u}$ is one of the line voltage stability indices. In this chapter, several line voltage stability indices and a proposed index are investigated. Such indices are namely: FVSI (Musirin et Rahman, 2002), VCPI

(Moghavvemi et Faruque, 1998), Lmn (Moghavvemi et Omar, 1998), LSZ (Jalboub et al., 2012) and LQP (Mohamed, Jasmon et Yusoff, 1989).

As mentioned in the literature review, due to increasing the emission, it is essential to manage the effects of emission on the electricity industry. An environmental dispatch is investigated in this chapter. There are different types of emission such as thermal emission, NO_x and SO_x. To model the emissions as a function, two considerable emissions (NO_x and SO_x) are looked at in this chapter. This function depends on the generated active power of conventional generators and it can be modeled as a quadratic and exponential function. Note that the emission of WF is assumed to be zero. The objective function is the minimization of the sum of emissions as follows (Niknam et al., 2012):

$$E_G(p_{i,u}) = \alpha_i + \beta_i p_{i,u} + \gamma_i p_{i,u}^2 + \xi_i \exp(\lambda_i p_{i,u}) \qquad \forall u \in \Omega_U, i \in \Omega_I \tag{3.12}$$

3.3 Operating points and zones

Multi-objective SOPF can provide several operating curves depending on the active power output of the generators and demands for all scenarios. These curves present operating points limits in cost, voltage stability and emission. As shown in Figure 3.1a, PV curve consists of the controllable zone (stable operating zone) and the uncontrollable zone (unstable operating zone). The voltages of the power system should be controlled in the stable operating zones (Eremia et Shahidehpour, 2013). The controllable zone can be divided into two sub-zones which are the optimal zone and the critical zone. Note that the minimum boundary of the critical zone is the critical line, and so the boundaries of the optimal zone can be selected by an ISO. Voltage stability studies tend to maintain the voltage in the optimal zone, which is obtained from an optimum result of multi-objective SOPF. Figure 3.1b shows the emission limit for a generator which depends on the power output of the generators and it is modeled as a quadratic and exponential function. Figure 3.1c presents variations in cost by the power output of the generators and variations in the penalty cost by active power curtailment of the wind farm and it shows the optimal and critical zones from an ISO viewpoint.

3.4 Fuzzification of multi-objective SOPF

In the fuzzy domain, multi-objective SOPF can be changed to single-objective SOPF. The scales in objective functions are different, so fuzzification can be essential to normalize the objective functions. In the first step, the membership functions for each objective should be defined. There are different forms of membership functions such as linear, triangular, Gaussian and so on. Among those forms, a linear membership function is appropriate for this study due to some reasons. A linear membership function is able to normalize the objective functions and bring them to the range [0,1]. Furthermore a linear membership function needs less computational burden. As the objective functions in (3.1) are continuous functions and they can change monotonically, this membership function can be rational. A linear membership function to fuzzify three objective functions is shown in Figure 3.2. The values of F_{ideal} and F_{nadir} are ideal and nadir values of each objective function. Note that these values can be obtained from the best and worst values of the single-objective function. The payoff table which is an organized way for finding ideal and nadir values is used in this study (see (Cohon, 2013) for details). In the fuzzy domain, μ_i as a fuzzy membership function is used to linearize the objective functions. Fuzzy membership in Figure 3.2a and Figure 3.2b is used for the objective function that should be maximized and minimized, respectively.

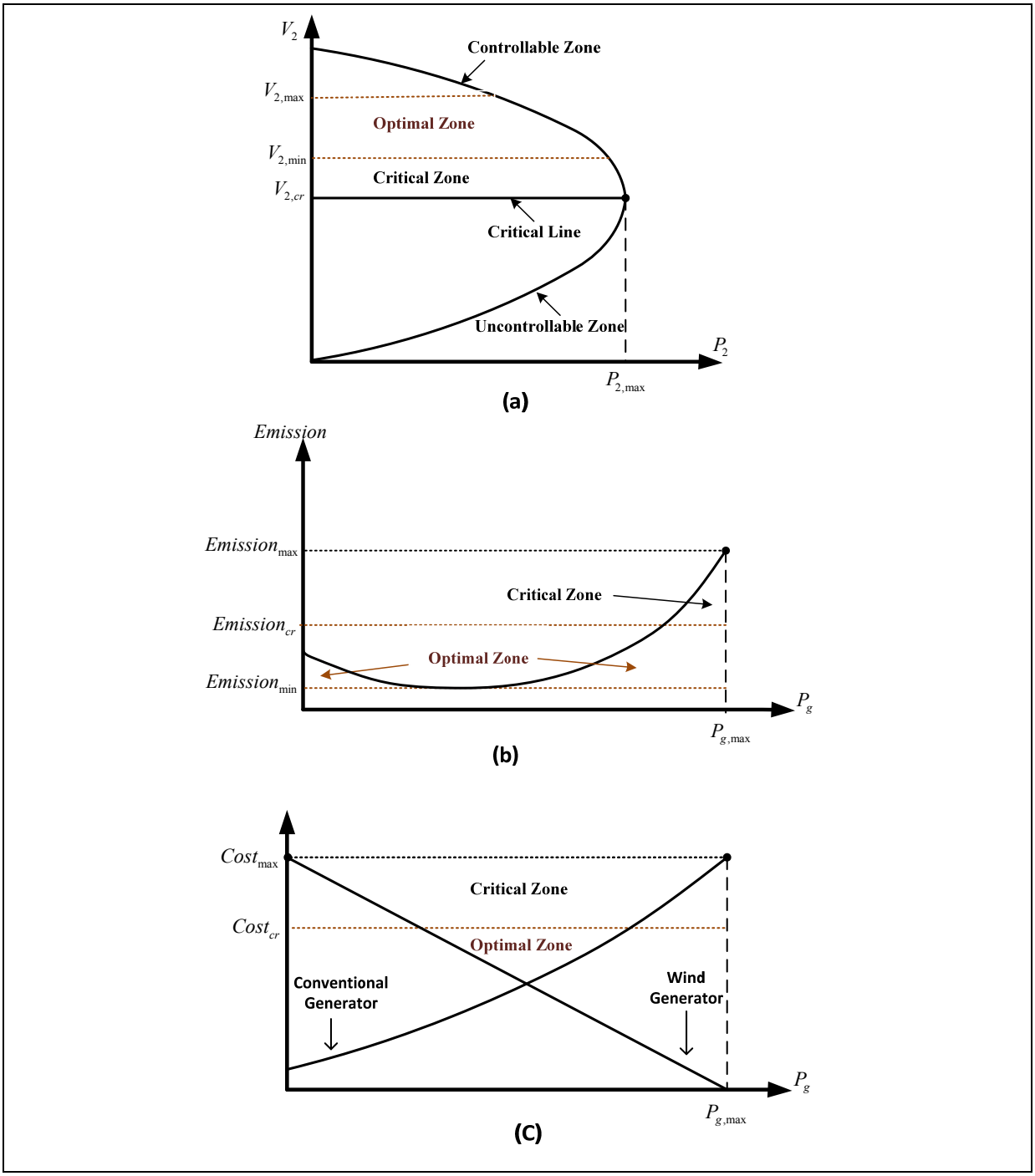

Figure 3.1 Operating zones (a) PV curve for a load bus (b) Emission curve for a conventional generator (c) Cost curve for a conventional and wind generator

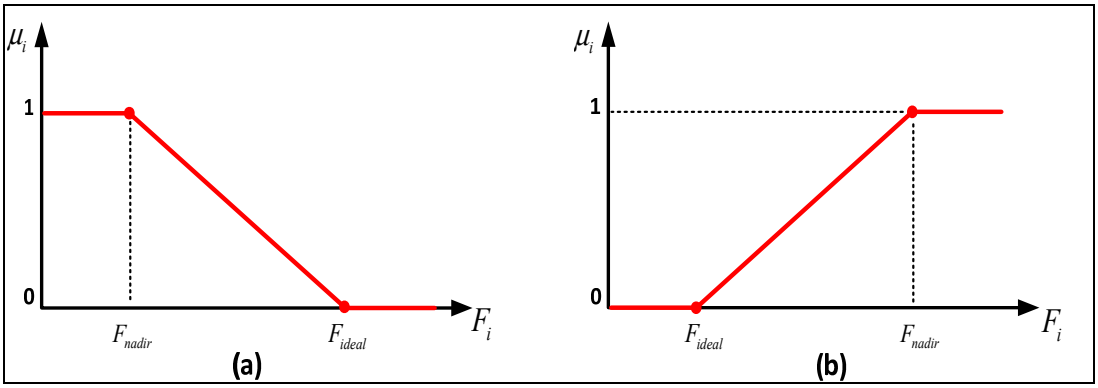

Figure 3.2 Fuzzy membership functions (a) Using for a SOPF objective function that should be maximized (b) Using for a SOPF objective function that should be minimized

The linear membership function for Figure 3.2a can be obtained as follows:

$$\mu_i = \begin{cases} 1 & \text{for } F_i \le F_{nadir} \\ \dfrac{(F_i - F_{nadir})}{(F_{ideal} - F_{nadir})} & \text{for } F_{nadir} < F_i < F_{ideal} \\ 0 & \text{for } F_i \ge F_{ideal} \end{cases} \tag{3.13}$$

When the objective function value is less than F_{nadir}, the value of fuzzy membership functions is considered one. If the objective function value is more than F_{ideal}, the value of fuzzy membership functions is considered zero in (3.13). Finally, the objective function is linearized and its values become between zero and one. The linear membership function for Figure 3.2b can be obtained as follows:

$$\mu_i = \begin{cases} 0 & \text{for } F_i \le F_{ideal} \\ \dfrac{(F_i - F_{ideal})}{(F_{nadir} - F_{ideal})} & \text{for } F_{ideal} < F_i < F_{nadir} \\ 1 & \text{for } F_i \ge F_{nadir} \end{cases} \tag{3.14}$$

A lower value of a membership function indicates a more favorable value. After the membership function calculation, the three-objective function in (3.1) can change into the single-objective function. It is clearly seen that choosing the weighting factors will be easy in

the fuzzy domain and they can be defined by ISO. The presented linear fuzzification method has a lesser computational burden than the Pareto-based methods (Cohon, 2013; Esmaili, 2013).

3.5 Line voltage stability index (LVSI)

An impedance theory is a proper way to estimate the maximum power transferred to a load bus. It can be useful in voltage stability assessment. The impedance theory is also adopted in power system protection such as distance relay (Chilvers, Jenkins et Crossley, 2005). Thus, the impedance seen at two buses of a transmission line can provide important information for the operation and control of the power system. A transmission line in a sample power system is shown in Figure 3.3a.

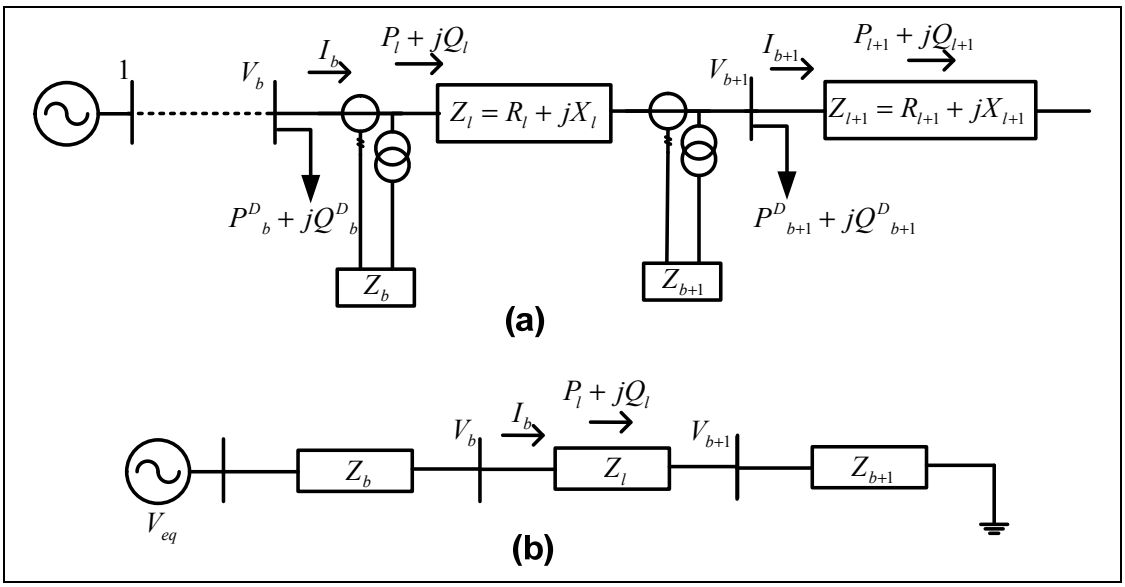

Figure 3.3 IBLVSI model in a sample power system (a) Two buses of transmission line (b) Impedances are seen in the equivalent circuit

First the impedances at the sending end and receiving end of the line are calculated in (17) and (18), respectively. Let us consider the simplified system shown in Figure 3.3b. Based on a theory of maximum power transfer between two buses, source impedance should be

matched with an impedance of the rest of the system. In this study, a line stability index is introduced which is based on impedance matching theory and it is named an impedance-based line voltage stability index (IBLVSI).

The impedance seen at bus b can be calculated as follows:

$$I_b = \left(\frac{S_l}{V_b}\right)^* = \left(\frac{P_l + jQ_l}{V_b}\right)^* \tag{3.15}$$

$$Z_b = \frac{V_b}{I_b} = \frac{V_b}{\left(\frac{P_l + jQ_l}{V_b}\right)^*} \tag{3.16}$$

$$Z_b = \left(\frac{P_l + jQ_l}{{P_l}^2 + {Q_l}^2}\right) \times |V_b|^2 \tag{3.17}$$

The impedance seen at bus $b + 1$ is defined in (3.18):

$$Z_{b+1} = \left(\frac{P_l + jQ_l}{{P_l}^2 + {Q_l}^2}\right) \times |V_{b+1}|^2 \tag{3.18}$$

Finally, IBLVSI is proposed as follows:

$$IBLVSI = \big||Z_b| - |Z_{b+1} + Z_l|\big| \tag{3.19}$$

Equation (3.19) can find the operating point with the voltage instability based on the maximum power transferred theorem. In Figure 3.3b, Z_b is considered as the impedance of the voltage source and $Z_{b+1} + Z_l$ is considered as a load impedance. In the maximum power transferred theorem, when the source impedance is matched with an impedance of the rest of the system; the system will be unstable.

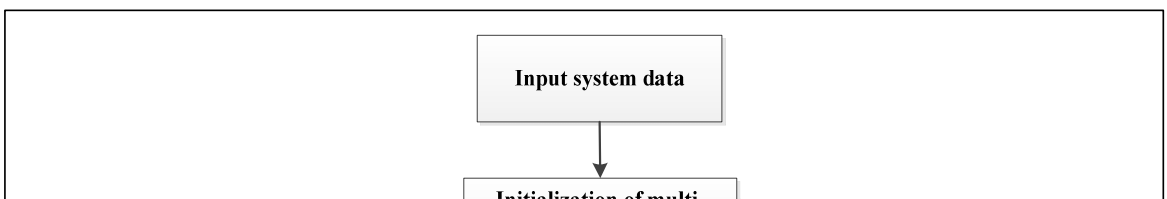

Figure 3.4 Flowchart of the proposed multi-objective SOPF approach

Therefore, $|Z_b|$ should be equal to $|Z_{b+1} + Z_l|$ in voltage instability conditions. It can be conquered that when the value of IBLVSI reaches zero, the system will be in a critical mode and it will be unstable. The application of the IBLVSI in voltage stability monitoring and multi-objective SOPF will be described in the results section. The step-by-step procedure for the proposed multi-objective SOPF is shown in Figure 3.4.

3.6 Simulation result and discussion

In this section, simulations are performed to demonstrate the effectiveness of the proposed multi-objective SOPF. They are divided into two parts: first the voltage stability detection of the proposed LVSI and traditional LVSIs is evaluated in the power system with WF and then the results of the multi-objective SOPF have been presented. Case studies are selected to verify the results which are detailed as below.

3.6.1 Voltage stability monitoring of LVSIs

By applying the proposed model, the modified WECC test system and the IEEE 39-bus system are tested in PSAT (Milano, 2005). In order to evaluate the performance of this index, no under-voltage protection or load shedding is considered in this work.

3.6.1.1 Modified WECC test system

This system shown in Figure 3.5 has an added bus with an OLTC transformer and it contains a WF. An automatic voltage regulator (AVR) and an over-excitation limiter (OEL) are installed on the conventional generator and loads will be increased until finding a voltage collapse in dynamic simulation. Note that a line transmission tripping is assumed between buses 4 and 7 (at $t = 5s$).

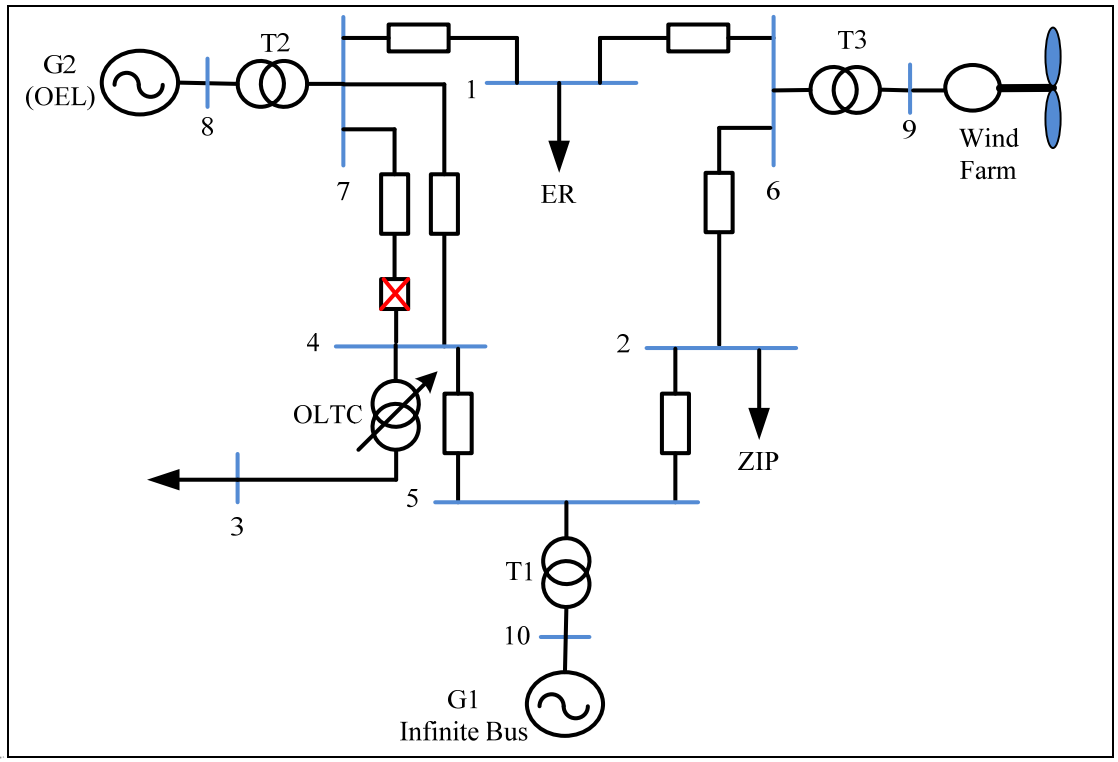

Figure 3.5 Modified WECC test system

Tap ratio step (0.02), minimum and maximum tap ratio (from 0.8 to 1.2) and reference voltage (0.9 p.u.) are the parameters of the OLTC. The nominal wind speed is considered to be 15 (m/s) and the Weibull distribution is used to model the wind speed. The WF uses DFIG which operates in the voltage controlled mode. The voltage magnitude, tap changing and LVSI index comparison are depicted in Figure 3.6a–c, respectively.

Figure 3.6a shows the voltage variations after the occurrence of the contingency where the system reaches the voltage instability point at 31.9 s. It is assumed that the short-term voltage stability evaluation is ignored. The process of restoration by the OLTC is represented in Figure 3.6b which has a negative effect on voltage stability. The comparison between different LVSIs is evaluated in Figure 3.6c. It shows that the IBLVSI can predict the voltage instability accurately because the index value reaches zero. Otherwise, Figure 3.6c demonstrates that the other LVSIs cannot detect the voltage collapse point. The values of Lmn, LQP, VCPI, FVSI and LSZ reach 0.28, 0.65, 0.718, 0.72 and 0.73 respectively. Note

that the values of these indices should reach one to detect voltage instability. To show the robustness of the index with different load models, ZIP and the exponential recovery load model are used in this case (see Figure 3.6).

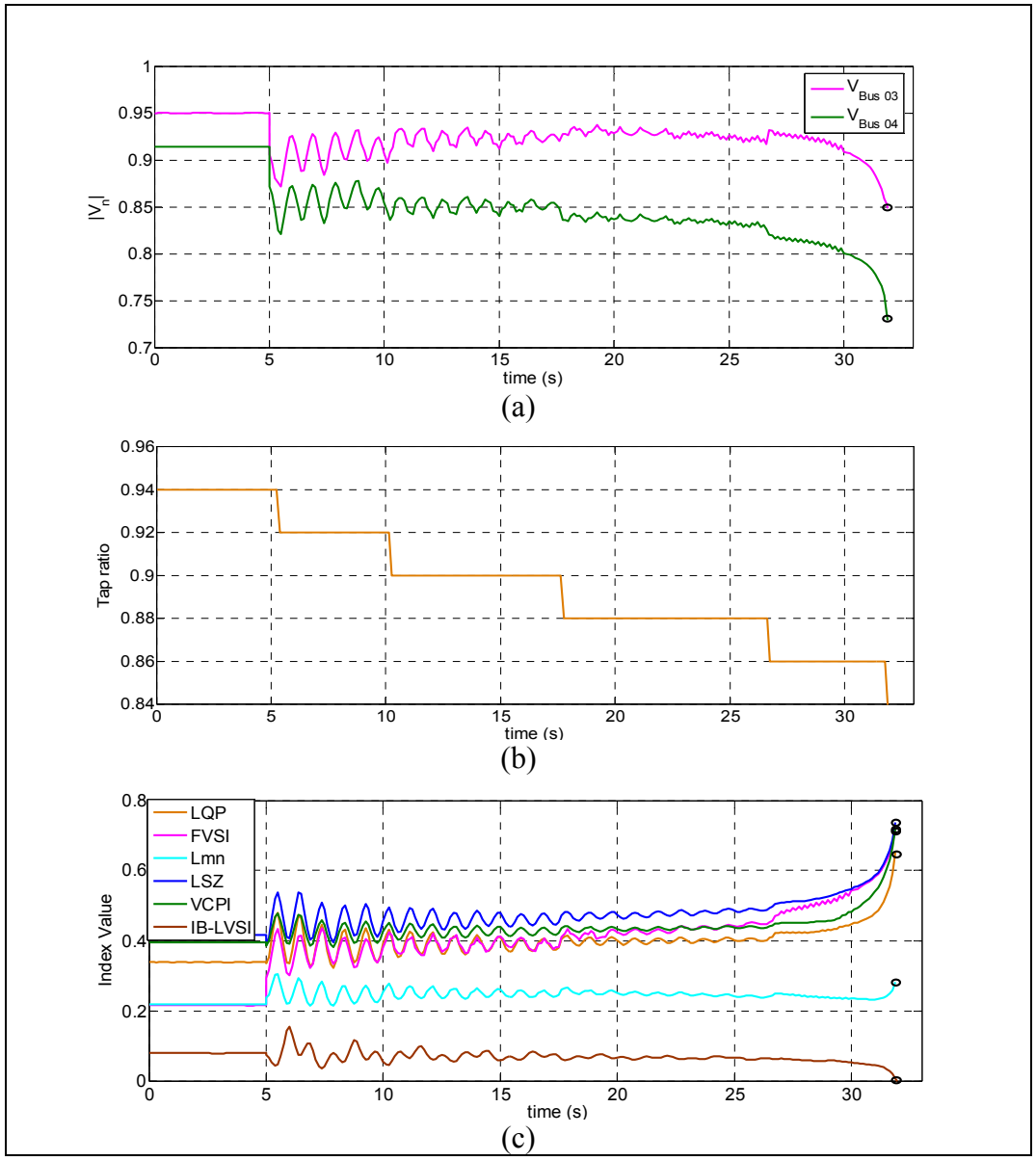

Figure 3.6 Modified WECC 9-Bus (a) Voltage magnitude at buses 3 and 4 (b) Tap changing in the OLTC (c) Comparison of LVSIs

The OLTC triggers the instability process in Figure 3.6b. The tap ratio keeps the voltage constant at load bus. The process of restoration by the OLTC continues until the voltage instability occurs. There are some methods to control the voltage stability by OLTC that is

well known as corrective actions, which are used to control the restoration actions after the occurrence of a contingency. They are 1) tap blocking behavior, 2) specific tap or voltage switching behavior and 3) tap reversing behavior. However, it assumes the worst possible condition where none of these corrective actions occur in Figure 3.6.

In another case study, tap blocking behavior is investigated to show the robustness of the index. Figure 3.7 shows this case study in which the OLTC is blocked. It shows that load at bus 3 is increased by 35% and a voltage collapse is found in dynamic simulation. As seen in Figure 3.7a, the system is collapsed at 10.05 s. The values of Lmn, LQP, VCPI, FVSI and LSZ reach 1.6, 1.62, 0.82, 1.57 and 4.22 which cannot predict voltage collapse accurately (see Figure 3.7b). Otherwise, the IBLVSI detects voltage instability accurately with and without the OLTC influence.

3.6.1.2 IEEE 39-bus system

The IEEE 39-bus system that is well known as the New-England power system (Athay, Podmore et Virmani, 1979) is evaluated in this part. To investigate the performance of the LVSIs, two WFs with DFIGs have been added to buses 36 and 37. The loading factor of an additional bus and other buses has been increased up to 1.35 p.u. and 1.65 p.u., respectively. A contingency is considered as a line transmission tripping between buses 8 and 9 ($t = 5s$). The voltage magnitudes, comparison between LVSIs and the behavior of IBLVSI are presented in Figure 3.8a–c, respectively.

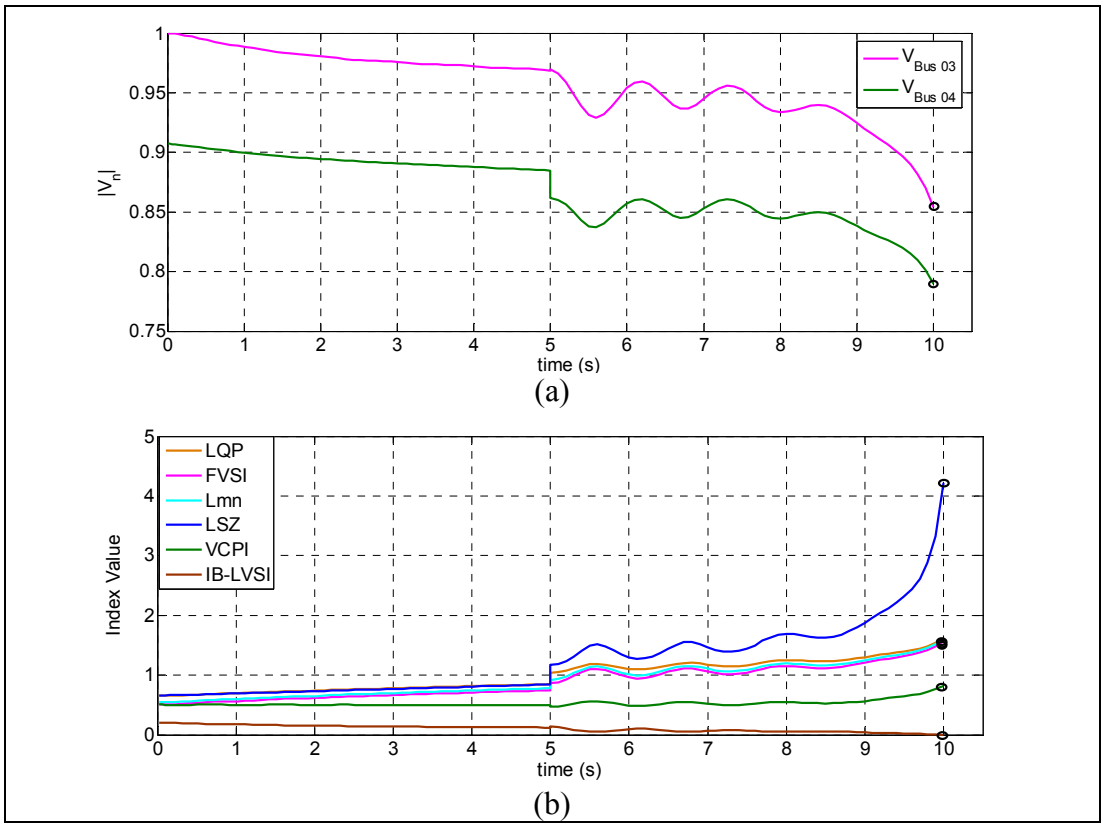

Figure 3.7 Modified WECC 9-Bus with blocked OLTC (a) Voltage magnitude at buses 3 and 4 (b) Comparison of LVSIs

Figure 3.8 shows that the system is collapsing at 50.4 s. As observed, the values of Lmn, LQP, VCPI, FVSI and LSZ reach 0.3, 0.3, 0.947, 0.24 and 0.63 at the collapse point in Figure 3.8b which shows an optimistic prediction of the voltage instability. However, the IBLVSI will improve the voltage instability detection in this case as shown in Figure 3.8c. It can be obtained from the results that the IBLVSI can be calculated easily and that it is compatible for modern power systems with high penetration of wind. Thus, it has an accurate result in post-contingency situations.

3.6.2 Multi-objective SOPF

Multi-objective SOPF considering WF integration and DR program is carried out in MATPOWER (Zimmerman et C. Murillo-Sánchez) using the IEEE 39-bus. All system data is given the IEEE 39-bus system that is provided from (Athay, Podmore et Virmani, 1979). It is assumed that two WFs are added at buses 36 and 37. The total wind generation capacity of each WF is considered to be 600 MW. The penalty factor of wind spillage and participation cost in the DR program are assumed to be 10 and 30, respectively. Wind power spillage is defined as the amount of wind power generation which is not utilized by power systems due to technical reasons. It is also assumed that loads at buses 7, 16, 18, 26 can participate in the DR program. To create congestion, the loading factor at bus 8 and other buses has been increased by 1.3 p.u. and 2.0 p.u., respectively. Note that 10 scenarios are selected to be considered in the optimization problem from (Pand et al., 2016) and these 10 scenarios can create a trade-off between calculation burden and cost accuracy. The wind data is given from NREL Western Wind dataset (Potter et al., 2008).

In order to investigate multi-objective SOPF from the viewpoint of voltage stability, several indices are considered as the objective functions. Table 3.1 shows the results of different multi-objective SOPF under scenario #1. Two objective functions are considered for each LVSI. First, the maximum or minimum value of index and, second, the sum index value for all transmission lines.

The proposed index considering $IBLVSI_{min}$ as the objective function provides better results than others. For instance, in comparison with $VCPI_{max}$; the proposed index improves total cost, emission and minimum voltage magnitude by 0.08%, 0.79% and 1.86%, respectively. Table 3.1 also shows the amount of active power cooperating in the DR program. The different objective functions can be compared from the aspect of appropriate deployment in the DR program. Note that the weighting factors of objective functions 1, 2 and 3 are assumed to be 0.1, 0.8 and 0.1, respectively.

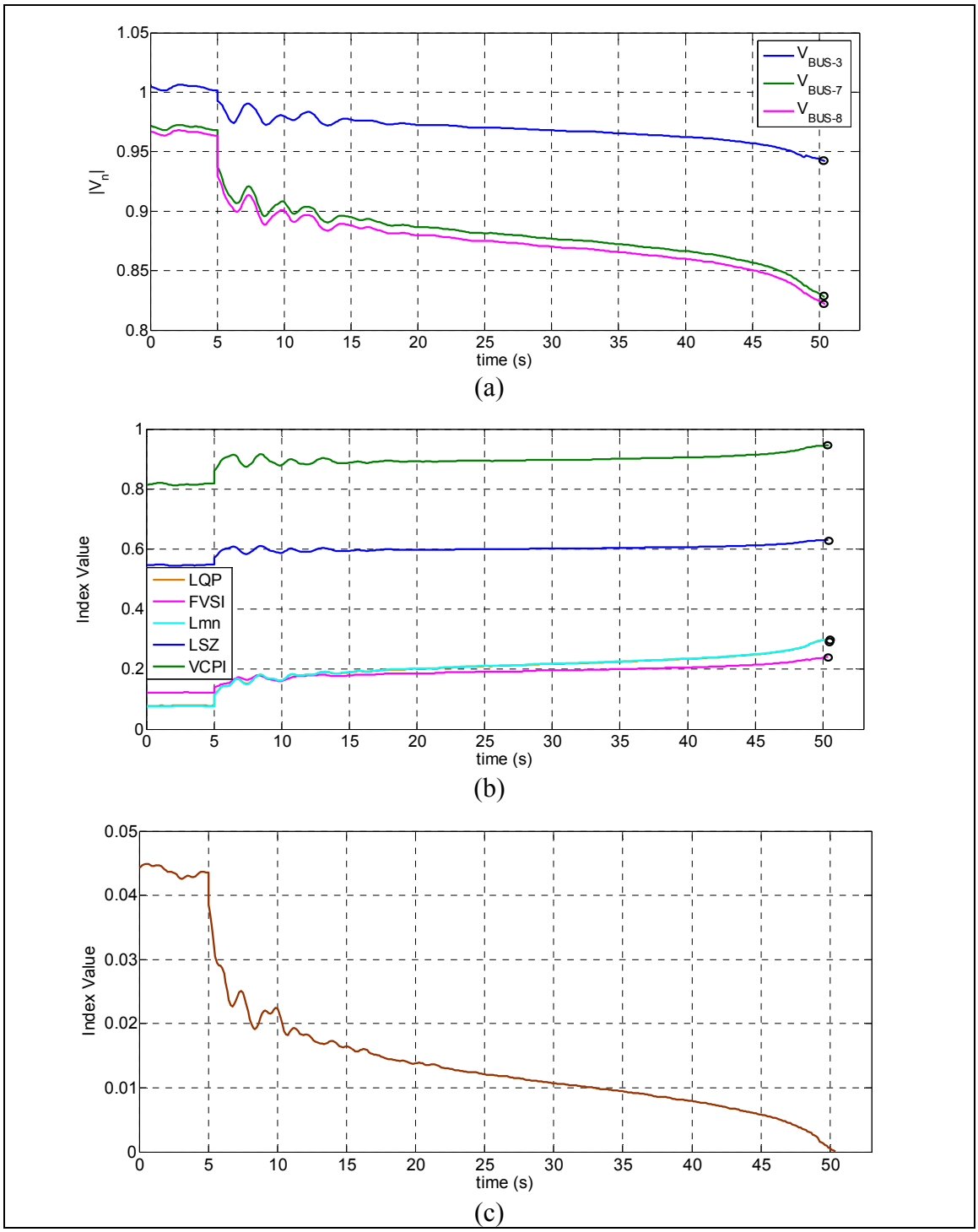

Figure 3.8 IEEE 39-bus system (a) Voltage magnitude at buses 3, 7 and 8 (b) Comparison of LVSIs (c) IBLVSI behavior

Table 3.1 Multi-objective SOPF for different LVSIs under scenario #1

	DR Program (MW)	Losses (MW)	Emission (Ton/hr)	Minimum voltage magnitude (pu)	Cost ($/hr)
$VCPI_{max}$	202.2	103.71	2.1530	0.861	101736
$\sum_{l\in\Omega_L} VCPI_l$	325	102.07	2.1047	0.857	102961
Lmn_{max}	325.2	101.97	2.1108	0.852	102993
$\sum_{l\in\Omega_L} Lmn_l$	323.1	101.98	2.1071	0.858	102949
$FVSI_{max}$	324.9	102.24	2.1063	0.854	102971
$\sum_{l\in\Omega_L} FVSI_l$	323.2	101.98	2.1071	0.858	102943
LSZ_{max}	208.1	103.63	2.1457	0.859	101794
$\sum_{l\in\Omega_L} LSZ_l$	324.8	101.32	2.1043	0.862	102956
LQP_{max}	325.3	101.97	2.1096	0.852	102987
$\sum_{l\in\Omega_L} LQP_l$	323.9	102.09	2.1073	0.856	102960
$IBLVSI_{min}$	193.3	103.75	2.1362	0.877	101641
$\sum_{l\in\Omega_L} IBLVSI_l$	192.7	103.71	2.1543	0.860	101658

Two cases are investigated in Figure 3.9. In case 1, only total cost is considered as the single-objective function. However, the multi-objective function is studied when $IBLVSI_{min}$ is given as the objective function of voltage issues in case 2.

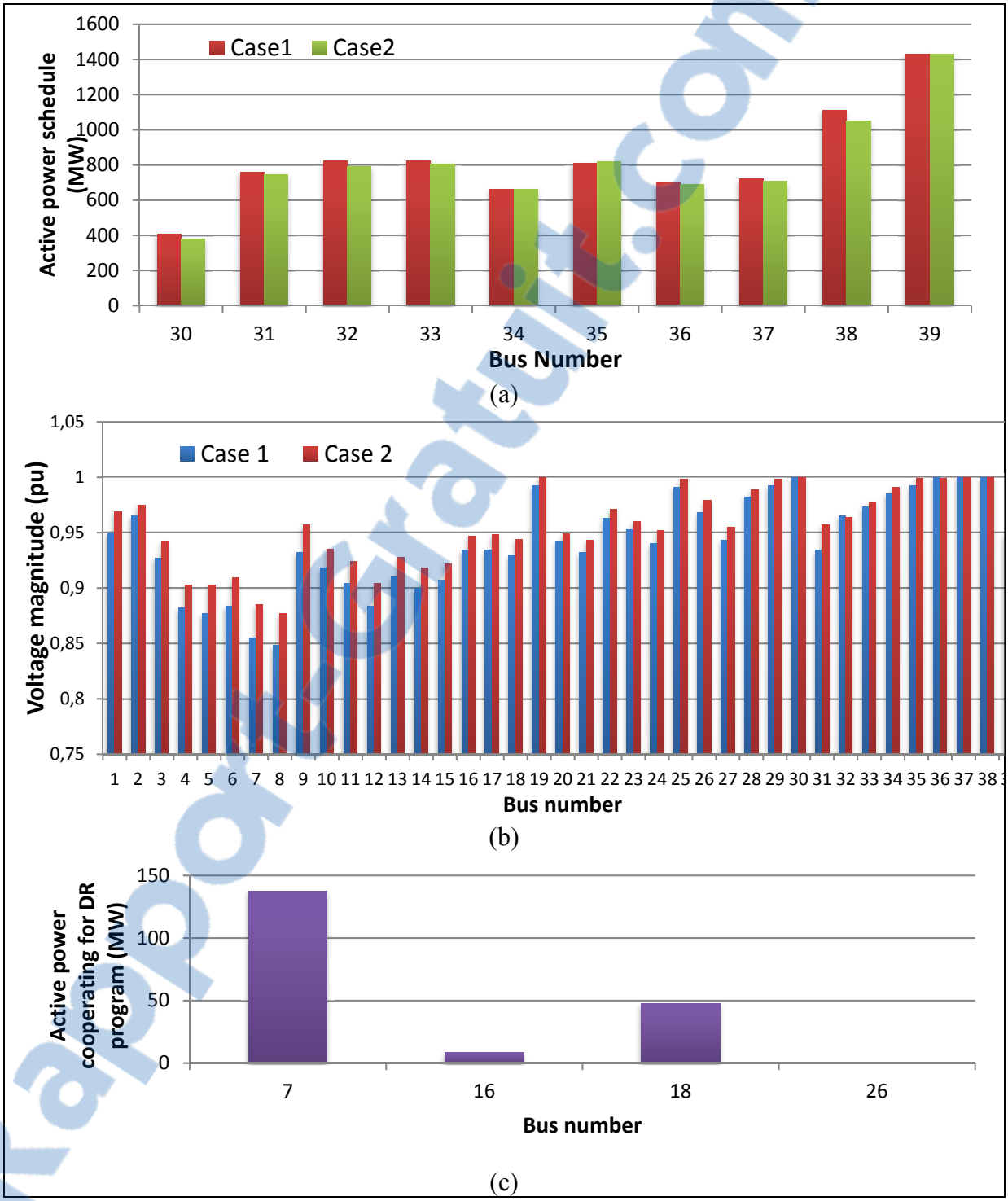

Figure 3.9 Single/multi-objective SOPF under scenario #1 (a) Comparison of active power schedule in case 1 & 2 (b) Comparison of voltage magnitude of buses in cases 1 & 2 (c) Active power cooperating in DR program case 2

Figure 3.9a presents a comparison of active power dispatches in case 1 and case 2. Figure 3.9b shows a comparison of the voltage magnitude of buses in cases 1 and 2. As seen in Figure 3.9b, the voltage magnitude of buses is increased in the multi-objective SOPF. To increase the voltage magnitude of buses and to decrease the total emission, selected loads participate in the DR program. Figure 3.9c shows the amount of active power cooperating in the DR program. Due to the topology of the system, maximum active power cooperated in the DR program is considered at bus 7. As seen in Figure 3.9b, bus 7 and buses near to this bus like buses 5, 6 and 8 are the weakest buses and they need to be improved from voltage stability issues.

Table 3.2 Active power output of wind farms (MW) under different scenarios

	Bus	u_1	u_2	u_3	u_4	u_5	u_6	u_7	u_8	u_9	u_{10}
${P^W}_{w,u} - {p^C}_{w,u}$	w_1	181.0	138.4	183.1	165.1	229.7	146.9	183.9	48.76	167.7	311.4
	w_2	193.1	151.9	200.9	132.6	186.8	81.08	196.08	178.01	107.21	297.02

Table 3.3 DR dispatches (MW) under different scenarios

	Bus	u_1	u_2	u_3	u_4	u_5	u_6	u_7	u_8	u_9	u_{10}
	B_7	137.24	154.96	139.01	155.06	138.72	158.48	139.22	156.93	156.34	141.75
${p^{DR}}_{b,u}$	B_{16}	8.37	55.83	17.84	54.93	15.31	60.23	18.14	61.55	56.57	30.40
	B_{18}	47.77	90.46	55.41	89.91	53.75	94.92	55.74	95.05	91.56	68.81
	B_{26}	0	50.25	7.30	50.01	5.59	57.01	7.77	55.12	52.48	20.18

Table 3.2 shows the active power output of two installed wind farms in the system. The active power output is changed based on 10 scenarios in the multi-objective SOPF. Table 3.3 shows the DR dispatches under different scenarios. As mentioned before, it is also assumed that loads at buses 7, 16, 18, 26 can participate in the DR program. The active power

cooperated for the DR program is different at those buses. It shows that all variables are dependent on the scenarios.

3.7 Conclusion

In this chapter, we propose a multi-objective SOPF problem with the presence of uncertain wind power generations and DR, in which this multi-objective SOPF consists of the operating cost, voltage stability and emission effects as the objective functions. The wind uncertainty is formulated as a scenario-based technique. The DR program is considered in this chapter and it improves voltage drop after a stressed loading condition. To normalize each objective function, the fuzzification technique is used to find the optimal solution. Furthermore, a new LVSI is presented that can detect precisely the voltage collapse in comparison with other LVSIs, especially after the occurrence of a given contingency due to the dynamic elements of the system. These comparisons, based on voltage stability monitoring, are tested by the modified WECC test system, the IEEE 39-bus. A comprehensive comparison between different LVSIs as the objective function is given in the multi-objective SOPF. These approaches are validated by the IEEE 39-bus. The results demonstrate that multi-objective SOPF with proposed LVSI decreases the operating cost and improves the voltage drop. The results also show that the proposed algorithm can be implemented easily, and it is compatible with the other technical constraints of the system.

CHAPTER 4

FREQUENCY AND VOLTAGE CONSTRAINED STOCHASTIC OPTIMAL POWER FLOW CONSIDERING WIND POWER AND DEMAND RESPONSE RESOURCES

Majid Bavafa [a], Louis-A. Dessaint [b] and Yury Dvorkin [c],

[a,b] Department of Electrical Engineering, Ecole de technologie supérieure,
1100 Notre-Dame West, Montréal, Quebec, Canada H3C 1K3

[c] Department of Electrical and Computer Engineering, Tandon School of Engineering,
New York University, New York, NY 11201 USA

Paper submitted to IEEE Transactions on Sustainable Energy, March 2017

Abstract

This chapter proposes an approach for frequency and voltage control in stochastic optimal power flow (SOPF) with the presence of uncertain wind power generations and energy storage systems (ESSs). The wind uncertainty is considered as a scenario-based model in SOPF approach. Demand response (DR) is one of the best efficient control ways to reduce operating costs. In particular, the proposed SOPF contains two main contributions. First, the frequency restoration scheme cooperates with DR and spinning reserve to stop frequency drop in contingency events. This scheme is defined in three levels. The second contribution utilizes an extended-L (EL) index to evaluate voltage stability analysis. A voltage constraint is defined from the EL-index in the SOPF approach. The EL-index considers a generator equivalent model (GEM). Active redispatch of generating units and DR deployment are employed to satisfy the frequency and voltage constraints in a new SOPF formulation with high penetration of wind energy. This method is analyzed in detail and it is tested on the IEEE RTS-96. The results show that the proposed approach operates successfully.

Nomenclature

A. Sets

α_B	Set of buses, indexed by b.
$\alpha_{B_{DR}}$	Set of buses cooperated in the DR program, indexed by b_{DR}.
$\alpha_{B_{ST}}$	Set of buses equipped with storage, indexed by b_{ST}.
α_{B_L}	Set of load buses, indexed by b_L.
α_{B_G}	Set of generator buses, indexed by b_G.
α_I	Set of generating units, indexed by i.
$\alpha_{I_{FR}}$	Set of generating units that can provide fast instantaneous reserve, indexed by i_{FR}.
α_L	Set of transmission lines, indexed by l.
α_T	Set of hours, indexed by t
α_U	Set of scenarios, indexed by u.
α_w	Set of wind farms, indexed by w.

B. Variables

$ch_{t,b,u}$	Charging rates of storage at bus b under scenario u during hour t (MW).
$dis_{t,b,u}$	Discharging rates of storage at bus b under scenario u during hour t (MW).
$el_{t,b,u}$	Voltage stability index at bus b under scenario u during hour t.
$p^C{}_{t,w,u}$	Active power curtailment of wind farm w under scenario u during hour t (MW).
$p^{DR}{}_{t,b,u}$ /$q^{DR}{}_{t,b,u}$	Active/reactive power cooperated in the DR program at bus b under scenario u during hour t (MW/MVAR).
$p^{LS}{}_{t,b,u}$ /$q^{LS}{}_{t,b,u}$	Active/reactive power cooperated in the LS program at the bus b under scenario u during hour t (MW/MVAR).

$p_{t,i,u}/q_{t,i,u}$ Active/reactive power output of generator i under scenario u during hour t (MW/MVAR).

$q^{W}{}_{t,w,u}$ Reactive power of wind farm w under scenario u during hour t (MVAR).

$r_{t,i,u}$ Spinning reserve of generator i under scenario u during hour t (MW).

$r^{f}{}_{t,i,u}$ Fast instantaneous reserve of generator i under scenario u during hour t (MW).

$S_{t,l,u}$ Apparent power of line l under scenario u during hour t (VA).

$soc_{t,b,u}$ Storage state of charge at bus b under scenario u during hour t (MWh).

$V_{t,b,u}/\theta_{t,b,u}$ Voltage magnitude/angle at bus b under scenario u during hour t (V/rad).

C. Parameters

C_G Cost function of power output of generator ($/MW).

C_R Cost function of spinning reserve ($/MW).

C_W Penalty function of wind power spillage ($/MW).

C_{DR} Cost function of DR program ($/MW).

C_{LS} Cost function of LS program ($/MW).

$\overline{ch}_b$ Maximum charging rates of storage at bus b (MW).

$\overline{dis}_b$ Maximum discharging rates of storage at bus b (MW).

D Damping factor.

EL_{des} Desired voltage stability index value.

$P^{D}{}_{t,b}/Q^{D}{}_{t,b}$ Active/reactive power of load at bus b during hour t (MW).

$P^{W}{}_{t,w,u}$ Available active power of wind farm w under scenario u during hour t (MW/MVAR).

$\bar{P}_i/\bar{Q}_i$ Maximum active/reactive power output of generator i (MW/MVAR).

$\underline{P}_i/\underline{Q}_i$ Minimum active/reactive power output of generator i (MW/MVAR).

$\overline{P}^{DR}{}_b/\overline{Q}^{DR}{}_b$ Maximum active/reactive power cooperated in the DR program at bus b (MW/MVAR).

$P^{FD1}{}_t$	Deficit power by frequency drop from 60 Hz to 59.2 Hz during hour t (pu).
$P^{FD2}{}_t$	Deficit power by frequency drop from 60 Hz to 59.5 Hz during hour t (pu).
$P^{FD3}{}_t$	Deficit power by frequency drop from 60 Hz to 59.7 Hz during hour t (pu).
$P^{GL}{}_t$	Magnitude of generation loss by the contingency during hour t (MW).
$\underline{Q_w^W}/\overline{Q_w^W}$	Min/maximum reactive power of wind farm w during hour t (MVAR).
R	Generator's speed-droop response.
RD_i	Ramp down limit of generator i (MW/h).
RU_i	Ramp up limit of generator i (MW/h).
$RD^{DR}{}_i$	Ramp down limit of demand cooperated in the DR program at bus b (MW/h).
$RU^{DR}{}_i$	Ramp up limit of demand cooperated in the DR program at bus b (MW/h).
$\bar{S}_l$	Maximum capacity of line l (VA).
$\overline{soc}_b$	Maximum state of charge (MWh).
$\bar{V}_b/\underline{V}_b$	Maximum/min voltage magnitude at bus b (V).
Y_{bm}/ϕ_{bm}	Admittance magnitude/angle of line connecting nodes b and m (S/rad).
π_u	Probability of scenario u.
η_{ch}	Charging efficiencies of storage.
η_{dis}	Discharging efficiencies of storage.

4.1 Introduction

Nowadays most power systems operate close to their stability limits to minimize the operating costs. To reduce closeness to the voltage and frequency stability limit, demand response (DR) is profitable due to assessing the benefits of the unpredictable nature of renewable energies. DR is defined as demand variations of several voluntary customers due to increasing their profits or enhancing the system reliability by directions from an independent system operator (ISO) (*Assessment of demand response and advanced metering*, 2012).

Power system frequency acts as an important signal to understand the safe and secure dynamic behavior of power systems. Frequency fluctuations could be very risky and even result in outages especially at low frequencies (Horta, Espinosa et Pati, 2015). To maintain the frequency in safe fluctuations, ISO needs to balance the load and generation. Primary frequency control has the important role to this balance by altering the power output of generating units and demand of flexible loads (Rebours et al., 2007). After occurrence of contingency, under-frequency load shedding (UFLS) is traditionally utilized to raise the frequency during shortages of spinning reserve. It causes excessive load shedding that produces several economic and technical problems for power systems. However, deployment of DR can reduce the load shedding and it can improve stability and reliability of power systems (Chang-Chien et al., 2012; Goel, Qiuwei et Peng, 2006).

One of the crucial issues in the optimal power flow (OPF) is the consideration of an applicable model for uncertainties in the system. When variations of unpredicted resource create a high amount of uncertainties a power system may result in outage or even collapse. In this situation stochastic OPF (SOPF) can reduce the risk of outages (Bienstock, Chertkov et Harnett, 2014). A SOPF with weighted-chance constraints is presented in (Roald et al., 2016; Summers et al., 2014) while considering the uncertainty of wind power. The types of wind power control are investigated in (Roald et al., 2016). Another study (Condren, Gedra et Damrongkulkamjorn, 2006) considers uncertain security costs, interrupting consumption costs and generator ramping during a contingency event. (Vrakopoulou et al., 2012) represents uncertain reserve costs, but reserve is considered as a linear function of the generation-load mismatch to model behavior of the secondary frequency controller. One of the famous techniques in uncertainty modeling is a scenario-based technique that provides less operating costs for ISOs (Bouffard, Galiana et Conejo, 2005). The authors in (Pand et al., 2016) also claim that the scenario-based technique is the most profitable technique in comparison with the other techniques like robust, interval and improved interval techniques.

One of the challenges in the scenario-based technique is the selection of scenarios and their probabilities. (Gröwe-Kuska et al., 2002) presents an appropriate algorithm for scenario selection. This study is a pioneer of scenario reduction algorithms in stochastic programs. In (Papavasiliou, Oren et Neill, 2011), a two-stage weighted scenario-based technique considering reserves and wind power is presented. Authors in (Vrakopoulou, Mathieu et Andersson, 2014) demonstrate a scenario-based SOPF with utilization of uncertain DR which has been modelled as a virtual energy storage unit. (Papavasiliou et Oren, 2012) presents a SOPF considering DR and wind power as certain and uncertain variables, respectively. Aggregations of DR resources are studied with a model of uncertain flexibility in (Mathieu et al., 2013). Generally, aggregation of DR resources can be utilized in ancillary services, security and stability in power systems. The effect of DR on distribution systems has been presented in (Lu et al., 2011; Steen et al., 2011; Vrettos et Andersson, 2013). These studies examine different types of DR controls like the centralized and decentralized controls on the distribution systems. Their results show that DR can decrease the stresses on the distribution systems.

Different types of OPF considering voltage stability issues called voltage stability constrained OPF (VSC-OPF) are reported in (Avalos, Canizares et Anjos, 2008; Lage, da Costa et Canizares, 2012; Milano, Canizares et Invernizzi, 2005; Zabaiou, Dessaint et Kamwa, 2014). The VSC-OPF approaches detect the closeness of the system to the voltage collapse. Several indices have been proposed in the literature in order to evaluate voltage stability. For instance, minimum singular value (MSV) of the power flow Jacobian (Tiranuchit et Thomas, 1988), MSV of the reduced Jacobian (Lof, Andersson et Hill, 1993), L-index (Kessel et Glavitsch, 1986) and extended-L (EL) index (Yang et al., 2013). The EL-index has been introduced recently and it has more advantages than other performance indices which have been presented with numerical results in (Yang et al., 2013). The authors in (Rabiee et al., 2014) investigate a VSC-OPF approach considering DR and stochastic wind resources. They consider the loading margin as a voltage stability index.

Due to the unpredictable nature of renewable energies, energy storage systems (ESSs) become more and more beneficial to decrease the energy variations. Atwa and El-Saadany (Atwa et El-Saadany, 2010) formulate an OPF approach to allocate ESSs in a distribution system. Gabash (Gabash et Li, 2012) investigates an OPF approach with ESSs and wind farms. The simulations are carried out in two optimization horizons and they show that the longer horizon provides better economical and technical results.

The studies reviewed in this section still lack a complete SOPF approach considering both voltage and frequency control. This chapter presents a frequency and voltage constrained SOPF with the presence of uncertain wind power generations. The proposed scenario-based SOPF utilizes a combined DR, ESS, load shedding (LS) and reserve to increase reliability under various contingency occurrences. In the proposed frequency and voltage stability assessment, the objective function is the minimization of total operating costs and it considers costs for DR, LS, wind spillage and reserve resources. To solve frequency instability issues, this chapter uses the reduced-order system frequency response (SFR) model and creates some constraints to be added to the SOPF. To keep a system safe from the viewpoint of voltage stability issues, it uses the EL-index. The EL-index is one of the voltage stability indices that can predict voltage collapse accurately.

The chapter is organized as follows: Section 4.2 presents a statement of background, whereas section 4.3 provides the formulation for proposed frequency and voltage constrained SOPF approach. In section 4.4, the simulation results are given to present the performance of the proposed approach with single and double contingencies. Finally, conclusions are presented in section 4.5.

4.2 Background review

4.2.1 System frequency response model

The reduced-order SFR model (Anderson et Mirheydar, 1990) has been used in this study for the estimation of frequency behavior of a large power system after a contingency occurrence. This SFR model disregards nonlinearities and it only considers crucial dynamics of the system. There are several effective factors in the frequency dynamics. For example, the inertia constant, damping factor and the generator's speed-droop response may decrease the frequency trend after a contingency occurrence. Based on the reduced-order SFR model, the frequency response is obtained as follows (Anderson et Mirheydar, 1990; Chang-Chien et al., 2012):

$$\Delta\omega = \left(\frac{R \times \omega_n^2}{D \times R + K_m}\right)\left(\frac{1 + T_R s}{s^2 + 2\zeta\omega_n s + \omega_n^2}\right)(P_d) \tag{4.1}$$

where

$$\omega_n^2 = \frac{D \times R + K_m}{2H \times R \times T_R} \tag{4.2}$$

$$\zeta = \left(\frac{2H \times R + (D \times R + K_m \times F_H) \times T_R}{2(D \times R + K_m)}\right)\omega_n \tag{4.3}$$

where K_m gain factor, H inertia constant, T_R reheat time constant, F_H fraction of generated power by high pressure turbine, D damping factor, R generator's speed-droop response, P_d system disturbance and $\Delta\omega$ incremental speed.

The contingency can be considered as the unit step function ($P_d = \frac{P_{step}}{s}$). After solving (4.1) in the time domain, the following equation is obtained.

$$\frac{d\Delta\omega(t)}{dt} = \frac{a\omega_n \times R \times P_{step}}{2 \times R + K_m}(e^{-\zeta\omega_n t}\sin(\omega_r t + \varphi)) \tag{4.4}$$

where

$$\omega_r = \omega_n\sqrt{1-\zeta^2} \tag{4.5}$$

$$a = \sqrt{\frac{1 - 2T_R\zeta\omega_n + \omega_n^2 T_R^2}{1-\zeta^2}} \tag{4.6}$$

$$\varphi = tan^{-1}\left(\frac{\omega_r T_R}{1 - T_R\zeta\omega_n}\right) - tan^{-1}\left(\frac{\sqrt{1-\zeta^2}}{-\zeta}\right) \tag{4.7}$$

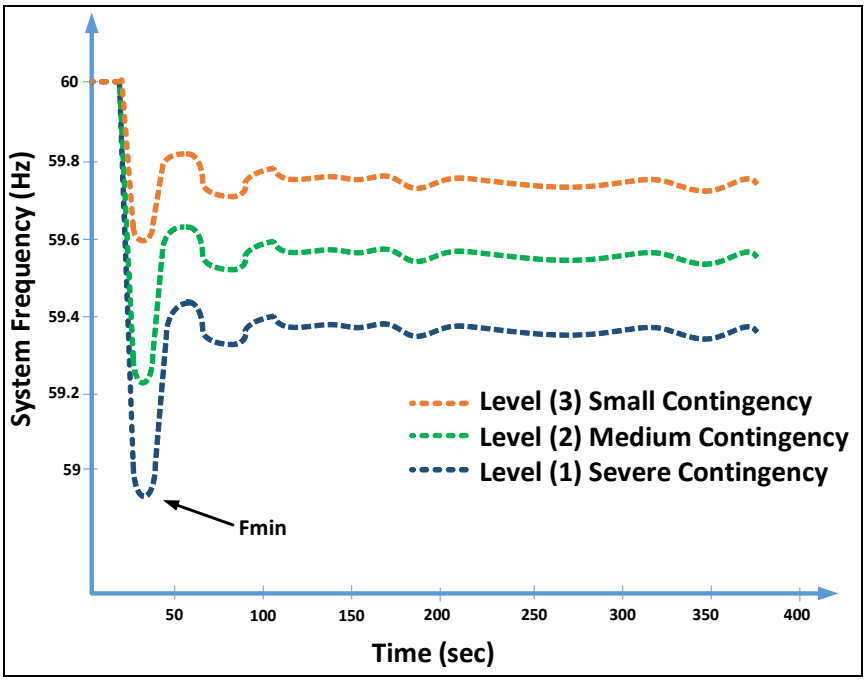

Figure 4.1 Three-level frequency response curves after contingencies

4.2.2 Frequency restoration scheme

To maintain the frequency in safe fluctuations, ISO needs to balance the load and generation. This can be carried out with DR, LS and reserve to avoid frequency drops and excessive load shedding after contingency occurrence. When a contingency occurs the frequency will decrease due to frequency-sensitive loads. The frequency restoration scheme includes several frequency drop levels. These are divided into three-level frequency drop levels like in (Chang-Chien et al., 2012); level one (frequency below 59.2 Hz), level two (frequency between 59.2 Hz and 59.5 Hz) and level three (frequency between 59.5 Hz and 59.7 Hz), which are considered crucial frequency drop levels for severe, medium and small contingencies, respectively (*see Figure 4.1*). In this study, the safe frequency level is fixed at 59.7 Hz. Coordination between DR and reserve will be beneficial for the system at these three levels of frequency restoration.

Minimum system frequency (f_{min}) can be obtained when (4.4) is zero. After simplification, f_{min} is calculated as follows (Chang-Chien et al., 2012):

$$f_{min} = f_o - \frac{R \times P^{GL}}{\mathrm{D} \times R + K_m}(1 + ae^{-\zeta\omega_n t_z}\sin(\omega_r t_z + \varphi)) \tag{4.8}$$

where f_0 is the pre-contingency frequency and P^{GL} is the magnitude of generation loss by the contingency defined by the contingency analysis. t_z is calculated as follows (Anderson et Mirheydar, 1990):

$$t_z = \frac{1}{\omega_r} tan^{-1}\left(\frac{\omega_r T_R}{T_R \zeta \omega_r - 1}\right) \tag{4.9}$$

After calculation of f_{min} by the contingency analysis in the SOPF approach, a three-level frequency restoration scheme is obtained to coordinate DR, LS and reserve as follows:

4.2.2.1 Level one (frequency below 59.2 Hz)

At this frequency restoration level, first minimum DR should be calculated to increase the frequency to 59.2 Hz. Minimum DR (P^{DR1}) and minimum LS (P^{LS1}) that is deployed in the system is as follows:

$$P^{DR1} + P^{LS1} = P^{GL} - P^{FD1} \tag{4.10}$$

where P^{FD1} which is deficit power by the frequency drop from 60 Hz to 59.2 Hz obtained in pu:

$$P^{FD1} = \frac{(\frac{f^{FD1}}{60}) \times (D \times R + K_m)}{R \times (1 + ae^{-\zeta\omega_n t_z}\sin(\omega_r t_z + \varphi))} pu \tag{4.11}$$

In this frequency restoration level, f^{FD1} is defined equal to $f_{nom} - f_{min}$ where f_{min} and f_{nom} are considered 59.2 Hz and 60 Hz, respectively. Then, next remedial action is carried out to return frequency back to 59.7 Hz based on availability of fast instantaneous reserve (FIR) and/or DR and/or LS. The formula of coordination between FIR, DR and LS is:

$$P^{DR2} + P^{LS2} + R^f = P^{GL} - P^{DR1} - P^{LS1} - \left(\frac{60 - 59.7}{60}\right)(D + 1/R) \tag{4.12}$$

In (4.12), where R^f is FIR and P^{DR2} is the second part of DR deployment in the frequency restoration scheme. If there are not enough DR and FIR resources, the second part of LS (P^{LS2}) will be deployed to complete the frequency restoration scheme. In the last step of frequency restoration, sustained instantaneous reserve (SIR) is applied to restore frequency back to 60 Hz as follows:

$$R^s = P^{GL} - (P^{DR1} + P^{LS1} + P^{DR2} + P^{LS2} + R^f) \tag{4.13}$$

4.2.2.2 Level two (frequency between 59.2 Hz and 59.5 Hz)

At this level, minimum DR is obtained to increase the frequency to 59.7 Hz according to (4.10). Note that in (4.11) f_{min} and f_{nom} are considered 59.5 Hz and 60 Hz, respectively. Then, the procedure of frequency restoration will be the same as level one. FIR and/or DR and/or LS are carried out to return frequency back to 59.7 Hz and finally SIR is applied to restore frequency back to 60 Hz.

4.2.2.3 Level three (frequency between 59.5 Hz and 59.7 Hz)

As mentioned before, small contingencies can create the level three of frequency drops. In this level, the first part of FIR and/or DR and/or LS will be zero. Equation (4.12) is only considered at this level to restore frequency back to 59.7 Hz. Finally SIR is applied to increase frequency to 60 Hz.

4.2.3 EL-Index calculation

The EL-Index was proposed by Yang *et al.* (Yang et al., 2013). A comparison between this index and several other indices has been rigorously carried out in this thesis. The EL-index utilized as a voltage stability index can detect precisely the voltage instability. This index considers the generator equivalent model (GEM) in its formula. The L-index models a generator only as a voltage source. On the other hand, the EL-index models a generator as a voltage source (E_G) and an internal impedance (Z_g). Z_g is stated as follows:

$$Z_g = \frac{E_G - V_t}{I_t} = \frac{\left[(r_a i_d - (x'_q - x_l) i_q) + j(r_a i_q + (x'_d - x_l) i_d)\right]}{i_d + j i_q} \tag{4.14}$$

where V_t and I_t are the terminal voltage and current of the generator. r_a is the armature resistance, x_l is the leakage reactance. x'_d and x'_q are the transient reactance in direct and quadrature axis. The equation (4.14) has been achieved from the fourth-order generator model. The nodal admittance matrix can be obtained from the well-known Ohm's law as follows:

$$\begin{bmatrix} \mathrm{I_L} \\ \mathrm{I_G} \end{bmatrix} = \begin{bmatrix} \mathrm{Y_{LL}} & \mathrm{Y_{LG}} \\ \mathrm{Y_{GL}} & \mathrm{Y_{GG}} \end{bmatrix} \begin{bmatrix} \mathrm{V_L} \\ \mathrm{V_G} \end{bmatrix} \tag{4.15}$$

Equation (4.15) can be expressed with consideration of GEM as follows:

$$\begin{bmatrix} I_L \\ 0 \\ I_G \end{bmatrix} = \begin{bmatrix} Y_{LL} & Y_{LG} & Y_{LG} \\ Y_{GL} & Y_{GG} + Y_{gg} & -Y_{gg} \\ 0 & -Y_{gg} & Y_{gg} \end{bmatrix} \begin{bmatrix} V_L \\ V_G \\ E_G \end{bmatrix} \tag{4.16}$$

where $\mathrm{Y_{gg}}$ is the diagonal matrix with $(\frac{1}{\mathrm{Z_{g1}}}, \frac{1}{\mathrm{Z_{g2}}}, \dots, \frac{1}{\mathrm{Z_{gm}}})$ values.

Then, the currents at load buses can be obtained from eliminating V_G:

$$I_L = (Y_{LL} - Y_{LG}(Y_{GG} + Y_{gg})^{-1} Y_{GL}) V_L + Y_{LG}(Y_{GG} + Y_{gg})^{-1} Y_{gg} E_G \tag{4.17}$$

After some simplifications, (4.17) can be rewritten as:

$$V_L = Z'_{LL} I_L + F'_{LG} E_G \tag{4.18}$$

where $Z'_{LL} = (Y_{LL} - Y_{LG}(Y_{GG} + Y_{gg})^{-1} Y_{GL})^{-1}$ and $F'_{LG} = -Z'_{LL}(Y_{LG}(Y_{GG} + Y_{gg})^{-1} Y_{gg})$.

As mentioned before, E_{Gb_G} is the internal voltage source at generator bus b_G. Considering the critical operating point, the EL-index can be defined in (4.19) at load buses b_L:

$$EL_{b_L} = \left| 1 - \frac{\sum_{b_G \in \alpha_{b_G}} F'_{b_L b_G} E_{G b_G}}{V_{b_L}} \right| \tag{4.19}$$

The range of variation of the EL-index is [0,1]. If it reaches 1.0, it shows the closeness to the voltage instability condition. Thus, the maximum value EL-index value in the load buses is chosen to be employed by the proposed SOPF in the next section.

4.3 Proposed frequency and voltage constrained SOPF

The proposed SOPF guarantees to maintain frequency and voltage at a safe level. To reach the purposes, the frequency restoration scheme and EL-index are used as constraints in the SOPF. The objective function used in this study is the minimization of the operating cost function. These costs are obtained based on wind scenario cost corresponding to its probability. The objective function is stated as follows:

$$Min \sum_{u \in \alpha_U} \pi_u \sum_{t \in \alpha_T} \left[\sum_{i \in \alpha_I} [C_G(p_{t,i,u}) + C_R(r_{t,i,u})] + \sum_{i \in \alpha_W} C_W \left({p^C}_{t,w,u} \right) + \sum_{b \in \alpha_{B_{DR}}} C_{DR} \left({p^{DR}}_{t,b,u} \right) + \sum_{b \in \alpha_B} C_{LS} \left({p^{LS}}_{t,b,u} \right) \right] \tag{4.20}$$

$$\underline{P_i} \leq p_{t,i,u} \leq \bar{P}_i \quad \forall t \in \alpha_T, u \in \alpha_U, i \in \alpha_I \tag{4.21}$$

$$\underline{Q_i} \leq q_{t,i,u} \leq \bar{Q}_i \quad \forall t \in \alpha_T, u \in \alpha_U, i \in \alpha_I \tag{4.22}$$

$$-RD_i \leq p_{t,i,u} - p_{t-1,i,u} \leq RU_i \quad \forall t \in \alpha_T, u \in \alpha_U, i \in \alpha_I \tag{4.23}$$

$$\sum_{i \in \alpha_B} p_{t,i,u} + \sum_{w \in \alpha_B} ({P^W}_{t,w,u} - {p^C}_{t,w,u}) - V_{t,b,u} \tag{4.24}$$

$$\sum_{\{b,m\}\in\alpha_L} V_{t,m,u}\, Y_{bm} \cos\left(\theta_{t,b,u} - \theta_{t,m,u} - \phi_{bm}\right)$$
$$= P^D{}_{t,b} + p^{DR}{}_{t,b,u} + p^{LS}{}_{t,b,u} + \frac{ch_{t,b,u}}{\eta_{ch}} - dis_{t,b,u}\eta_{dis}$$
$$\forall t \in \alpha_T, u \in \alpha_U, b \in \alpha_B$$

$$\sum_{i\in\alpha_B} q_{t,i,u} + \sum_{w\in\alpha_B} q^W{}_{t,w,u} - V_{t,b,u} \tag{4.25}$$
$$\sum_{\{b,m\}\in\Omega_L} V_{t,m,u}\, Y_{bm} \sin\left(\theta_{t,b,u} - \theta_{t,m,u} - \phi_{bm}\right)$$
$$= Q^D{}_{t,b} + q^{DR}{}_{t,b,u} + q^{LS}{}_{t,b,u} + q^{BS}{}_{t,b,u}$$
$$\forall t \in \alpha_T, u \in \alpha_U, b \in \alpha_B$$

$$0 \le p^C{}_{t,w,u} \le P^W{}_{t,w,u} \quad \forall t \in \alpha_T, u \in \alpha_U, w \in \alpha_W \tag{4.26}$$

$$\underline{Q_w^W} \le q^W{}_{t,w,u} \le \overline{Q_w^W} \quad \forall t \in \alpha_T, u \in \alpha_U, w \in \alpha_W \tag{4.27}$$

$$-\bar{S}_l \le S_{t,l,u} \le \bar{S}_l \quad \forall t \in \alpha_T, u \in \alpha_U, l \in \alpha_L \tag{4.28}$$

$$\underline{V_b} \le V_{t,b,u} \le \bar{V}_b \quad \forall t \in \alpha_T, u \in \alpha_U, b \in \alpha_B \tag{4.29}$$

$$-\pi \le \theta_{t,b,u} \le \pi \quad \forall t \in \alpha_T, u \in \alpha_U, b \in \alpha_B \tag{4.30}$$

$$\mathrm{P^{GL}}_t \le \textstyle\sum_{i\in\alpha_I} r_{t,i,u} + \sum_{i\in\alpha_I} r^f{}_{t,i,u} \quad \forall t \in \alpha_T, u \in \alpha_U, i \in \alpha_I \tag{4.31}$$

$$r_{t,i,u} + r^f{}_{t,i,u} \le \bar{P}_i - p_{t,i,u} \quad \forall t \in \alpha_T, u \in \alpha_U, i \in \alpha_I \tag{4.32}$$

$$r_{t,i,u} + r^f{}_{t,i,u} \le RU_i \quad \forall t \in \alpha_T, u \in \alpha_U, i \in \alpha_I \tag{4.33}$$

$$0 \le p^{DR}{}_{t,b,u} \le \overline{P}^{DR}{}_b \le P^D{}_{t,b} \quad \forall t \in \alpha_T, u \in \alpha_U, b \in \alpha_{B_{DR}} \tag{4.34}$$

$$0 \le q^{DR}{}_{t,b,u} \le \overline{Q}^{DR}{}_b \le Q^D{}_{t,b} \quad \forall t \in \alpha_T, u \in \alpha_U, b \in \alpha_{B_{DR}} \tag{4.35}$$

$$-RD^{DR}{}_i \le p^{DR}{}_{t,b,u} - p^{DR}{}_{t-1,b,u} \le RU^{DR}{}_i \qquad (4.36)$$
$$\forall t \in \alpha_T, u \in \alpha_U, b \in \alpha_{B_{DR}}$$

$$soc_{t,b,u} = soc_{t-1,b,u} + ch_{t,b,u}\Delta t - dis_{t,b,u}\Delta t \qquad (4.37)$$
$$\forall t \in \alpha_T, u \in \alpha_U, b \in \alpha_{B_{ST}}$$

$$soc_{t,b,u} \le \overline{soc}_b \qquad \forall t \in \alpha_T, u \in \alpha_U, b \in \alpha_{B_{ST}} \qquad (4.38)$$

$$ch_{t,b,u} \le \overline{ch}_b \qquad \forall t \in \alpha_T, u \in \alpha_U, b \in \alpha_{B_{ST}} \qquad (4.39)$$

$$dis_{t,b,u} \le \overline{dis}_b \qquad \forall t \in \alpha_T, u \in \alpha_U, b \in \alpha_{B_{ST}} \qquad (4.40)$$

If $\mathrm{P^{GL}{}_t} \ge P^{FD1}{}_t \sum_{b\in\alpha_B} P^D{}_{t,b}$ → **Level one**

Then $\sum_{b\in\alpha_{B_{DR}}} \mathrm{p^{DR}{}_{t,b,u}} + \sum_{i\in\alpha_B} \mathrm{r^f{}_{t,i,u}} + \sum_{b\in\alpha_B} \mathrm{p^{LS}{}_{t,b,u}} \ge \mathrm{P^{GL}{}_t} - \left(\frac{60-59.7}{60}\right)\left(\mathrm{D} + \frac{1}{\mathrm{R}}\right)\sum_{b\in\alpha_B} P^D{}_{t,b}$ (4.41)
$$\forall t \in \alpha_T, u \in \alpha_U, i \in \alpha_I, b \in \alpha_B$$

and $\sum_{i\in\alpha_B} \mathrm{r^f{}_{t,i,u}} / \sum_{b\in\alpha_B} P^D{}_{t,b} \le P^{FD1}{}_t - \left(\frac{60-59.7}{60}\right)(\mathrm{D} + 1/\mathrm{R})$ (4.42)
$$\forall t \in \alpha_T, u \in \alpha_U, i \in \alpha_I, b \in \alpha_B$$

If $P^{FD1}{}_t \ge \mathrm{P^{GL}{}_t} / \sum_{b\in\alpha_B} P^D{}_{t,b} \ge P^{FD2}{}_t$ → **Level two**

Then $\sum_{b\in\alpha_{B_{DR}}} \mathrm{p^{DR}{}_{t,b,u}} + \sum_{i\in\alpha_B} \mathrm{r^f{}_{t,i,u}} + \sum_{b\in\alpha_B} \mathrm{p^{LS}{}_{t,b,u}} \ge \mathrm{P^{GL}{}_t} - \left(\frac{60-59.7}{60}\right)(\mathrm{D} + 1/\mathrm{R})\sum_{b\in\alpha_B} P^D{}_{t,b}$ (4.43)
$$\forall t \in \alpha_T, u \in \alpha_U, i \in \alpha_I, b \in \alpha_B$$

and $\sum_{i\in\alpha_B} \mathrm{r^f{}_{t,i,u}} / \sum_{b\in\alpha_B} P^D{}_{t,b} \le P^{FD2}{}_t - \left(\frac{60-59.7}{60}\right)(\mathrm{D} + 1/\mathrm{R})$ (4.44)
$$\forall t \in \alpha_T, u \in \alpha_U, i \in \alpha_I, b \in \alpha_B$$

If $P^{FD2}{}_t \geq \mathrm{P^{GL}{}_t} / \sum_{b\in\alpha_B} P^D{}_{t,b} \geq P^{FD3}{}_t \rightarrow$ **Level three**

Then $\sum_{\mathrm{b}\in\alpha_{\mathrm{B_{DR}}}} \mathrm{p^{DR}{}_{t,b,u}} + \sum_{\mathrm{i}\in\alpha_{\mathrm{B}}} \mathrm{r^{f}{}_{t,i,u}} + \sum_{\mathrm{b}\in\alpha_{\mathrm{B}}} \mathrm{p^{LS}{}_{t,b,u}} \geq \mathrm{P^{GL}{}_t} - \left(\frac{60-59.7}{60}\right)(\mathrm{D} + 1/\mathrm{R}) \sum_{b\in\alpha_B} P^D{}_{t,b}$ (4.45)

$$el_{t,b,u} \leq EL_{des} \qquad \forall \mathrm{t} \in \alpha_T, u \in \alpha_U, b \in \alpha_B \tag{4.46}$$

Constraints (4.21)-(4.22) show the min/maximum limits of active and reactive power output of generators. Constraint (4.23) shows the limits of minimum up and down ramp rate. Equations (4.24)-(4.25) are the active and reactive power balance. Constraints (4.26)-(4.30) enforce the active and reactive wind spillage value, power flow and voltage magnitude and angle limits, respectively. Constraints (4.31)-(4.33) are reserve limits. Constraints (4.34)-(4.35) enforce min/maximum limits active and reactive DR deployment. Constraint (4.36) shows min/maximum limits of inc/decrement of DR deployment. Equation (4.37) is the charging and discharging balance in ESSs. Constraints (4.38)-(4.40) enforce maximum limits of the state of charge, rates of charge and discharge, respectively.

In accordance with the frequency restoration scheme (level one), if the magnitude of generation loss by the contingency is bigger than the magnitude of generation loss by the frequency drop from 60 Hz to 59.2 Hz; DR will be allocated as seen in (4.41). Constraint (4.42) enforces the limit of FIR in case of availability. Constraints (4.41)-(4.42) have been obtained according to (4.10) and (4.12). Constraints (4.43)-(4.44) represent frequency restoration constraints at level two. Note that DR may not be deployed at level three in (4.45), if there is sufficient amount of FIR. Constraint (4.46) enforces the desired EL-index, which is set by an ISO. In the optimization problem, SIR is assumed spinning reserve ($r_{t,i,u}$) for simplification. Note that (4.31) provides enough spinning reserve, so it does not need to consider another constraint for (4.13) to restore frequency back from 59.7 Hz to 60 Hz.

4.4 Numerical analysis

In this section, the proposed SOPF approach has been tested on the IEEE RTS-96 (Grigg et al., 1999) which consists of three areas. The optimization problem is solved by using GAMS (GAMS - A User's Guide). 19 wind farms have been added in this system. 10 scenarios are selected to be considered in the optimization problem based on reference (Pand et al., 2016). The two ESSs are installed at buses 121 and 325 (Pandžić et al., 2015).

The costs of spinning reserve and FIR are assumed 0.1 and 0.3 cost of power output, respectively. The costs of the DR and LS programs are assumed to be 5 times and 50 times of the base-case locational marginal prices (LMP) of buses. It is assumed that loads at buses 106, 118, 209, 305, 316, 320 can participate in the DR program and generators 12, 13, 14, 23, 30, 31, 32, 44, 45, 46, 55, 76, 77, 78, 86 and 87 can provide FIR. The desired value of the EL-index is assumed to be 0.9. To provide the stress conditions the loading factor of the system has been increased to 1.6 p.u. By applying the proposed model in 24 hours, the results of the frequency and voltage constrained SOPF approach are presented for two sample contingencies.

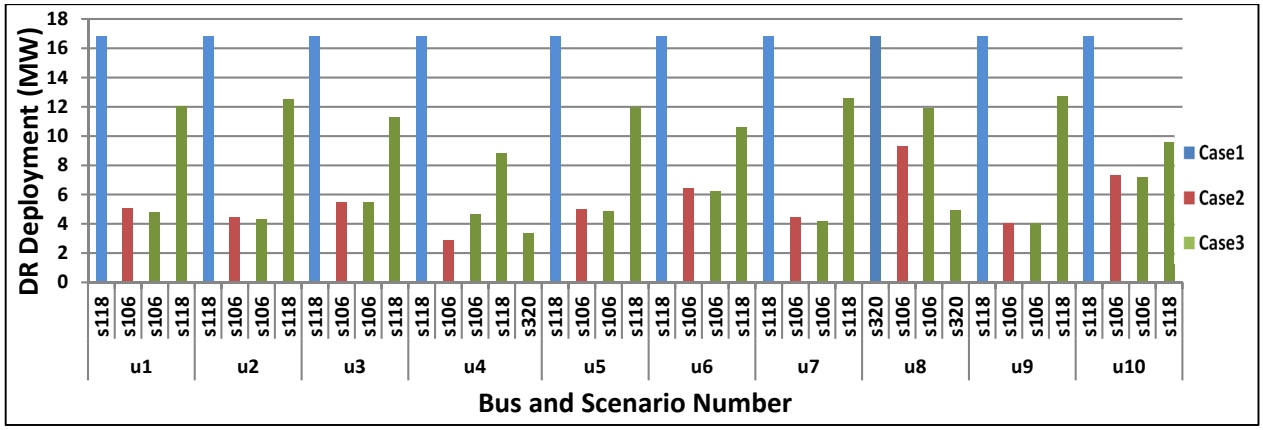

Figure 4.2 DR deployment of buses cooperated in DR program for three cases under all scenarios

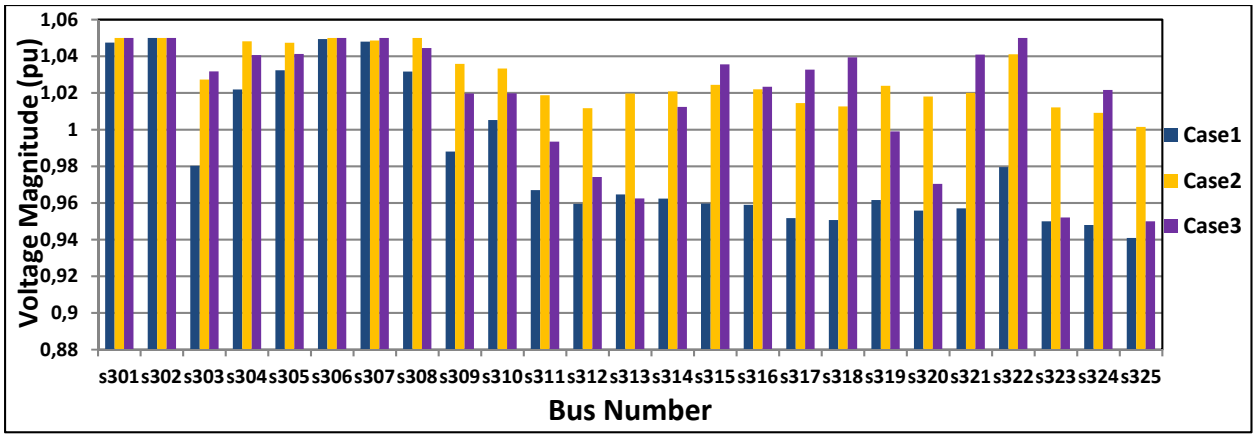

Figure 4.3 Voltage magnitude of buses in area three for three cases under scenario #1

4.4.1.1 Maximum single contingency

The modified IEEE RTS-96 system with the occurrence of maximum single contingency is investigated in this section. The value of maximum single contingency is 400 MW, which is obtained from the outage of generating unit number 22 at bus 118. As an example, P^{FD1} and P^{FD2} at hour three are obtained 613.13 MW and 383.21 MW respectively. Thus, the system activates the frequency restoration plan at level two ($P^{GL} \geq P^{FD2}$).

In voltage stability analysis, maximum value of the EL-index will be more than the desired value due to this contingency occurrence and (46) should be satisfied. Figure 4.2 shows DR deployment for three cases in all scenarios at hour two. Cases are as follows:

CASE 1: SOPF with frequency constraint.

CASE 2: SOPF with voltage constraint.

CASE 3: SOPF with both frequency and voltage constraints.

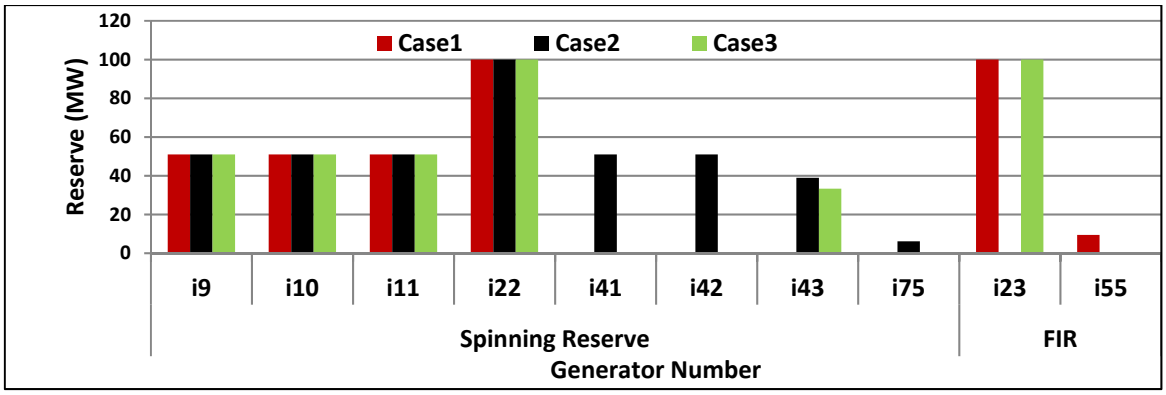

Figure 4.4 Spinning reserve and FIR under scenario #1

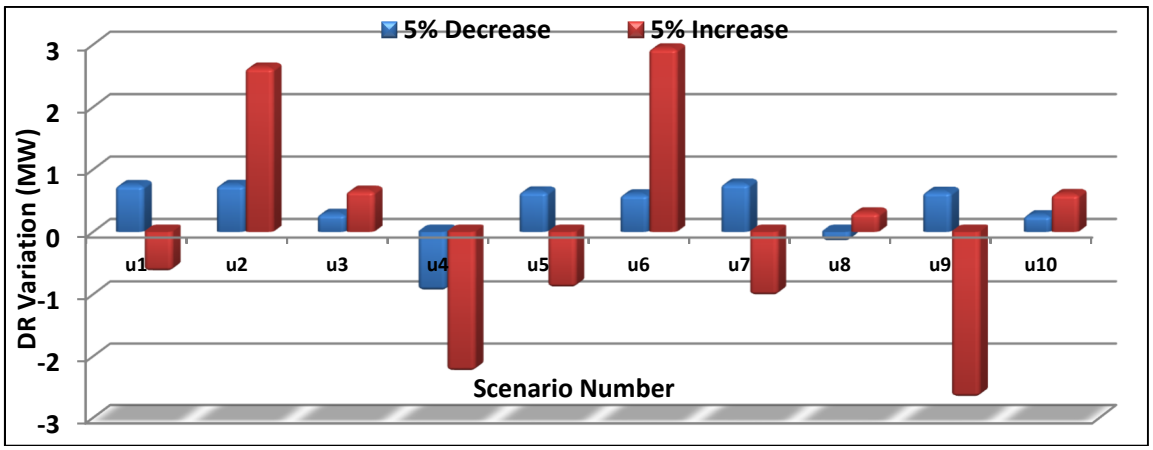

Figure 4.5 Variation of DR deployment with 5% inc/decrement in wind power penetration at bus 106

With this DR deployment seen in Figure 4.2, the system will be stable from the viewpoint of frequency and voltage due to the maximum single contingency occurrence. The results of this contingency show that there is no load shedding at hour two in all cases and scenarios. Figure 4.3 presents voltage magnitude of buses in the area three for three cases in scenario one at hour two. It shows that the cases 2 and 3 provide a higher voltage profile than the case 1 due to the voltage constraint in (4.46). To show reserves variation in the three cases, Figure 4.4 shows spinning reserve and FIR under scenario one during hour two. As is expected, FIR is employed in the cases 1 and 3 due to frequency constraints in (4.41)-(4.45).

To show the effect of the wind penetration level, this value is varied to 45% and 55%. Note that the wind penetration level of the base case is 50%. Figure 4.5 shows the variations of DR deployment at bus 106 with a change in the wind penetration level. The state of charge for two installed EESs at buses 121 and 325 is shown in Figure 4.6.

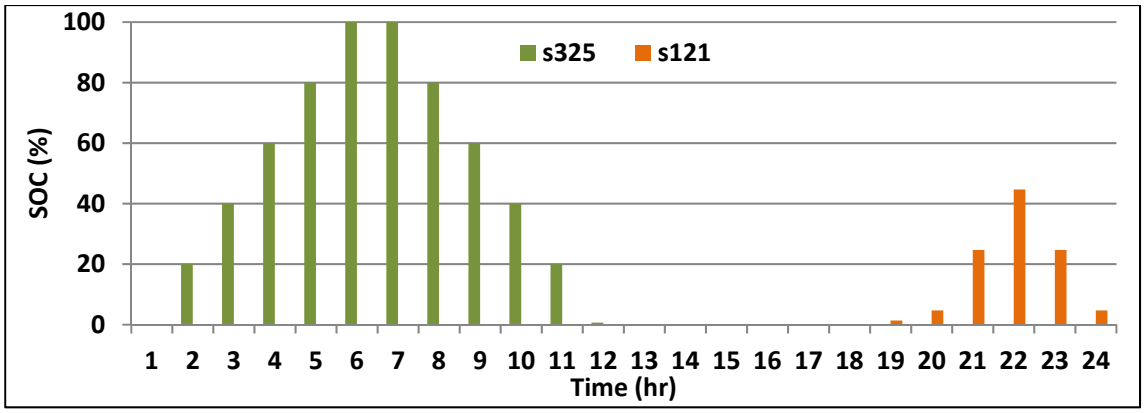

Figure 4.6 State of charge in ESSs during 24 hours under scenario #1

4.4.1.2 Double contingency

To show the sensitivity of the proposed method to the contingencies, a double-contingency case is investigated in this section which are simultaneous outages of generating unit number 22 at bus 118 and the line 59 between the buses 212 and 223.

In this type of contingency, the results show that the system should activate the frequency restoration plan at level one ($P^{GL} \geq P^{FD1}$) during hour two. From the viewpoint of the voltage stability assessment, the system will be unstable due to this double contingency occurrence.

It can be observed from Table 4.1 that DR and LS deployment will be considerably increased to maintain the system stable from frequency fluctuations and voltage instability.

Table 4.1 DR and LS deployment (MW) in double-contingency case

Scenario	$p^{DR}_{t,b,u}$				$p^{LS}_{t,b,u}$	
	Bus					
	$s106$	$s118$	$s209$	$s320$	$s210$	$s212$
$u1$	5.01	32.36	33.91	0	56.08	53.03
$u2$	4.41	15.67	0	0	12.79	72
$u3$	5.41	0	26.1	0	48.27	82.88
$u4$	4.76	72.93	0	41.8	0	19.37
$u5$	0	119.44	0	0	3.4	20.2
$u6$	6.28	70.86	0	0	11.12	43.6
$u7$	4.34	99.84	0	0	7.59	30.1
$u8$	10.62	0	115.41	0	137.58	170.69
$u9$	4.02	0	7.12	0	29.29	80.25
$u10$	7.18	0	0	0	0	79.24

Table 4.2 Active and reactive power of wind farms in all scenarios

Scenario	$P^{W}_{t,w,u} - p^{C}_{t,w,u}$				$q^{W}_{t,w,u}$			
	Wind farm							
	w1	w2	w3	w4	w1	w2	w3	w4
u1	47.14	118.41	231.69	219.03	9.3	-69.87	117.7	20.88
u2	10.56	134.35	165.46	90.81	7.81	-75.97	63.33	108.73
u3	67.81	108.85	284.61	166.68	14.68	-71.3	117.7	68.6
u4	17.76	167.66	198.41	172.97	1.31	-42.54	32.15	-47.98
u5	63.5	119.39	271.52	253.32	15.8	-34.67	49.09	-29.72
u6	28.95	89.66	183.92	88.76	1	-70.01	-0.31	95.84
u7	60.8	132.70	204.78	268.82	-10.38	-33.32	58.48	-32.52
u8	8.43	127.49	264.69	251.01	6.75	-59.43	-87.1	-17.38
u9	6.1	140.98	203.24	154.04	7.36	-68.75	0.23	80.42
u10	2.4	68.50	258.27	178.31	14.37	-70.8	117.7	88.38

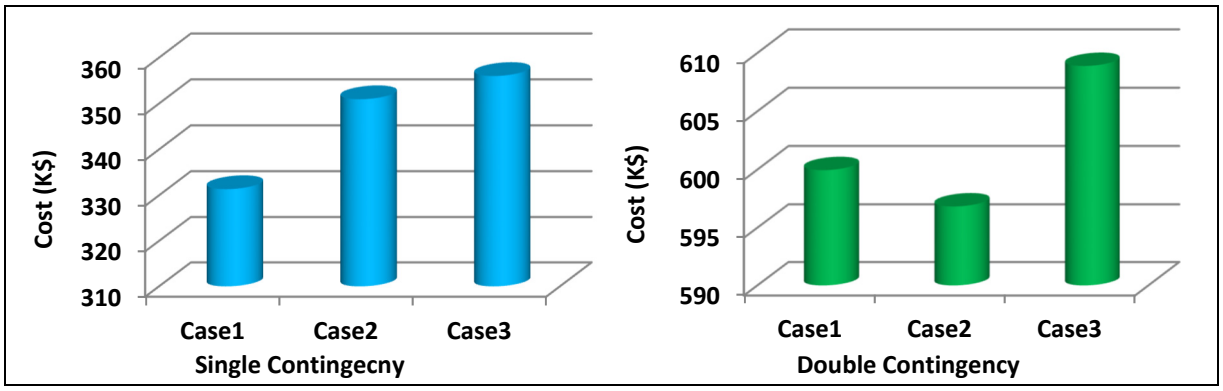

Figure 4.7 Comparison between the costs in different cases in single and double contingency occurrence

Table 4.2 presents active and reactive power dispatches of four wind farms in all scenarios. Comparison between the costs in different cases in single and double contingency occurrence has been carried out in Figure 4.7. As seen, the cost will be higher in case 3 due to enforcing the frequency and voltage constraints.

4.5 Conclusion

In this chapter, a new frequency and voltage constrained SOPF approach is proposed with the presence of uncertain wind power generations and energy storage systems (ESSs). The proposed approach is able to protect the system from frequency fluctuations and voltage instability after contingency occurrence. The wind uncertainty is considered as a scenario-based model. The frequency restoration scheme cooperates with DR and reserve to stop frequency drops. This scheme consists of three levels based on severity of contingencies. The EL index is used as a voltage stability index to prevent voltage collapse after contingency occurrence. The EL-index considers GEM in its formula. Several constraints are added to the traditional SOPF due to obtaining the frequency and voltage stability. This approach is tested on the IEEE RTS-96. The results demonstrate that the cost increases when a system is stable from the viewpoint of voltage and frequency evaluation due to DR and LS deployment.

Consideration of both frequency and voltage constraints in one optimization problem can decrease DR and LS deployment rather than consideration of them in two independent problems. An ISO can find a trade-off between cost and stability issues with choosing the value of the contingency in the system. The results also show that the proposed approach can be implemented easily, and it is compatible with the other technical constraints of the system.

CONCLUSION

Due to a large number of blackouts in different countries, the importance of voltage stability analysis is appearing more and more in the OPF approach. Modeling of elements and control ways like a wind generator, DR, OXL and OLTC can be helpful to control voltage stability in the OPF formulation. The main goal of an ISO is to run the power system operation without any voltage stability collapse at low cost or high revenue. The thesis reaches to this goal with a comprehensive SOPF approach with the presence of uncertain wind power generations.

Among different types of voltage stability presented in Chapter 1, long term voltage stability is considered in this thesis. Main effects on long term voltage stability like reactive power limits, OLTCs and load models has been also evaluated in this chapter. Moreover, several VSIs have been presented that have a role to evaluate the voltage instability risk and to predict the voltage collapse point. Finally, a literature review of DR program and ESSs have been investigated in detail.

In Chapter 2, an improved IB voltage stability index is presented which can predict accurately the voltage instability. The reactive power limit of DFIG has been modeled in this index as a variable virtual impedance. The IB index is considered as a constraint in a OPF approach to form a VSC-OPF approach. The OLTCs is also modeled in the IB index, if it is available in the system. The results have been divided into two parts that are voltage stability monitoring and VSC-OPF. First, the comparison between the improved and traditional IB index has been carried out after a contingency occurrence to monitor voltage stability. Second, the proposed VSC-OPF approach is compared with L-index, VCPI and MSV. The results reveal that the improved IB index has the lowest operating cost.

A multi-objective SOPF approach with the presence of uncertain wind power generations and DR is presented in Chapter 3. The multi-objective SOPF have three objective functions, namely the operating cost, voltage stability and emission effects. A scenario-based technique is used to model the wind uncertainty. To obtain single objective function, the fuzzification

technique is applied. A new LVSI is with accurate voltage collapse detection is presented in this chapter. The comparisons between different LVSIs as the objective function are given in the multi-objective SOPF. The results demonstrate that multi-objective SOPF with proposed LVSI improves the voltage profile and reduces the costs.

In Chapter 4, a new frequency and voltage constrained SOPF approach is proposed with the presence of uncertain wind power generations and ESSs. The frequency restoration scheme cooperates with DR and reserve to stop frequency drops. This scheme consists of three levels based on severity of contingencies. The EL index is used as a voltage stability index to prevent voltage collapse after contingency occurrence. The EL-index considers GEM in its formula. Several constraints are added to the traditional SOPF approach due to obtaining the frequency and voltage stability. The results demonstrate that consideration of both frequency and voltage constraints in one optimization problem can decrease DR and LS deployment rather than consideration of them in two independent problems. The results also show that the proposed approach can be implemented easily, and it is compatible with the other technical constraints of the system.

Future Works

The present research can be continued by some ideas are listed as follows:

A new VSC-SOPF approach compatible with electricity market regulations

The objective function in the presented VSC-SOPF is minimization of the operating costs. This objective function can be changed by the characteristics of an electricity market such as reactive power market. Therefore, it would be compatible with the electricity market regulations. In this approach, the loads and generators can have their own bids to participate in active and reactive power markets.

Multi-objective SOPF considering voltage stability, demand response and transmission switching

Optimal transmission switching improves the stabilities and reduces the costs in power systems. It also affects on voltage profile, so formulating the multi-objective SOPF can be beneficial for ISOs. This formulation will be a mixed integer nonlinear program (MINLP) due to binary variables in transmission switching. This approach provides the voltage stability for power systems after N-1 contingency occurrence and it can also improve the social welfare.

A new VSC-SOPF approach considering multi terminal DC (MTDC)

Multi terminal DC (MTDC) systems can improve the voltage and frequency stabilities after a contingency occurrence. Also, MTDC is an appropriate option to integrate power systems to wind farms. To formulate this new SOPF approach, some constraints from MTDC should be added to the main VSC-SOPF problem.

APPENDIX I

IMPEDANCE MATCHING THEORY

An impedance matching is a proper way to estimate the maximum power transferred for a load bus. As is known, Thevenin impedance is a criterion for the voltage stability assessment. The Thevenin equivalent circuit from a load bus viewpoint is shown in Figure-A I-1. The impedance matching can be determined as the formula below:

$$|Z_L| = |Z_{eq}| \qquad \text{(A I-1)}$$

where Z_L and Z_{eq} are the impedance of the load and the Thevenin equivalent circuit, respectively.

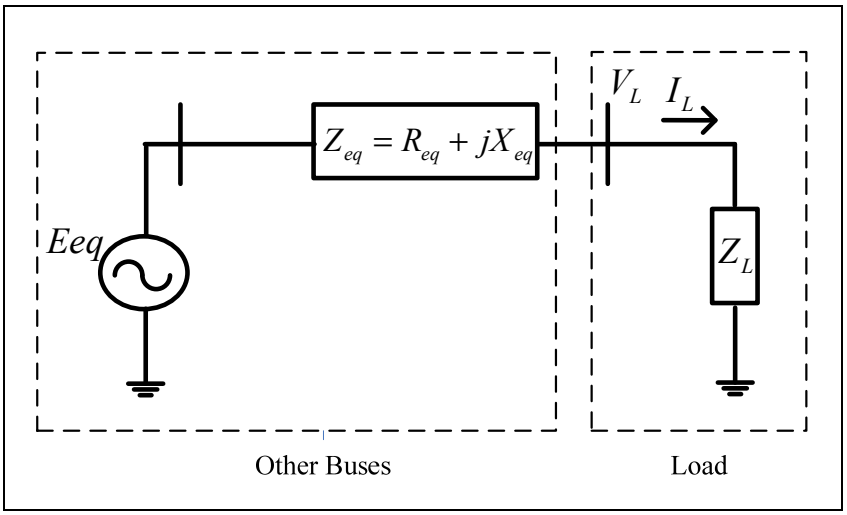

Figure-A I-1 Thevenin equivalent circuit for a load bus

The voltage of the Thevenin equivalent circuit can be defined as follows:

$$E_{eq} = V_L + I_L Z_{eq} \qquad \text{(A I-2)}$$

where V_L and I_L are the load voltage and current, respectively.

The accurate calculation of this impedance is very complicated, so there are some methods to simplify the large network.

The impedance matching in the R-X diagram is shown in Figure-A I-2. If load impedance (Z_L) locates inside of the circle with radius $|Z_{eq}|$, the system will be unstable. To consider the circle of radius $|Z_{eq}|$ is not accurate due to the dynamic behavior of power systems.

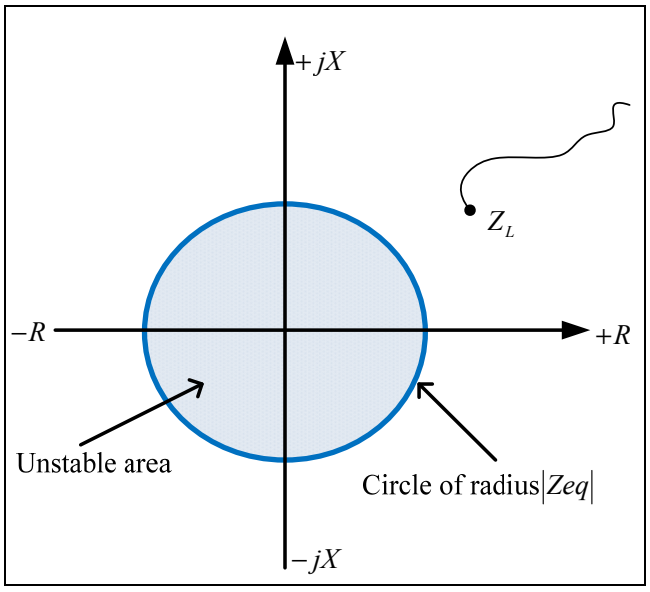

Figure-A I-2 Mapping of stability in the R-X diagram

APPENDIX II

INPUT DATA FOR SOPF APPROACH

Table-A II-I presents probability of each scenario. 10 scenarios are considered in this chapter. Table-A II-II shows the value of parameters used in the frequency restoration scheme.

Table-A II-I
Wind scenarios and their probabilities

Scenario	π_u
u_1	0.02
u_2	0.16
u_3	0.107273
u_4	0.241818
u_5	0.107273
u_6	0.15
u_7	0.086364
u_8	0.000909
u_9	0.125455
u_{10}	0.000909

Table-A II-II
Parameters of frequency restoration scheme

Parameter	4	0.95	0.5	8	0.28	0.19
	H	K_m	D	T_R	F_H	R

APPENDIX III

IEEE RTS 96-BUS SYSTEM

In this section, the proposed SOPF approach has been tested on the IEEE RTS-96 (Grigg et al., 1999) which consists of three areas. 19 wind farms have been added to this system. It also consists of 73 buses, 96 generators, 51 loads, and 120 transmission lines as seen in Figure-A III-1.

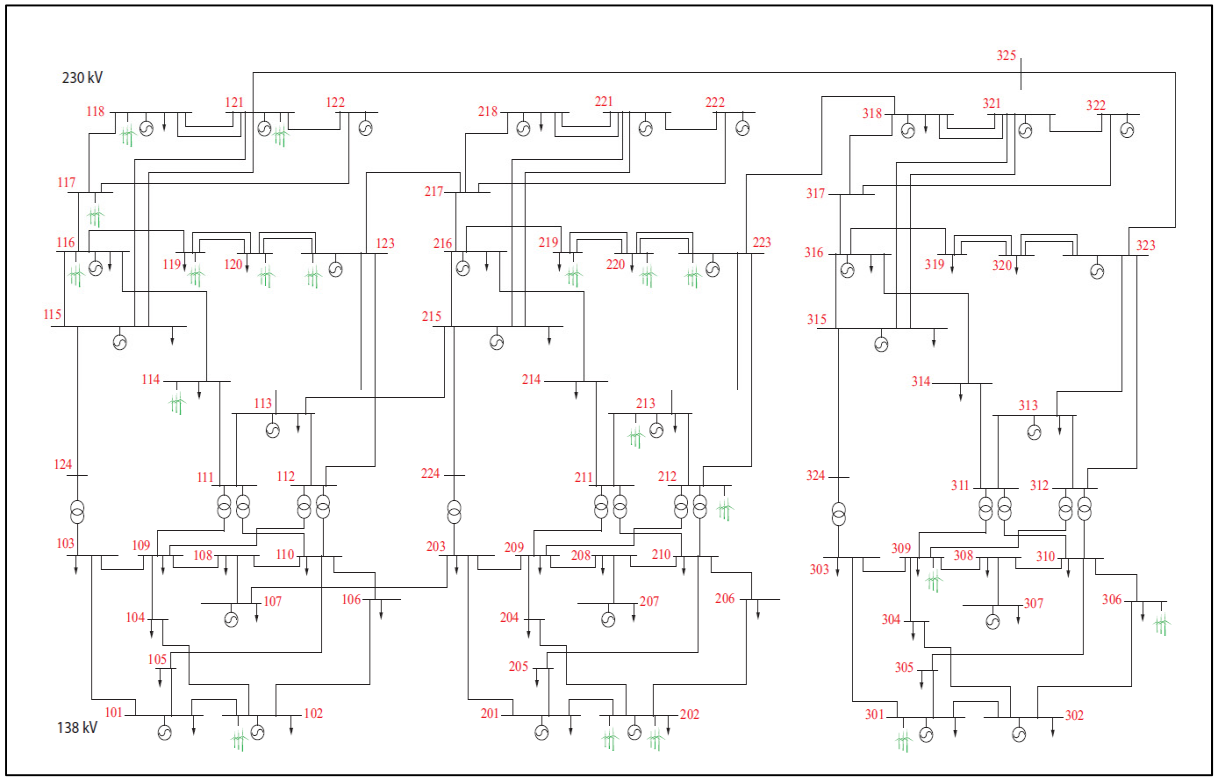

Figure-A III-1 Modified IEEE RTS 96-bus system
Taken from Pandžić, Wang et al. (2015)

APPENDIX IV

IEEE 39-BUS SYSTEM

The IEEE 39-bus system is also named New-England Power System consists of ten generators. Generator 1 at bus 31 is assumed the slack bus. This system is presented in Figure-A IV-1.

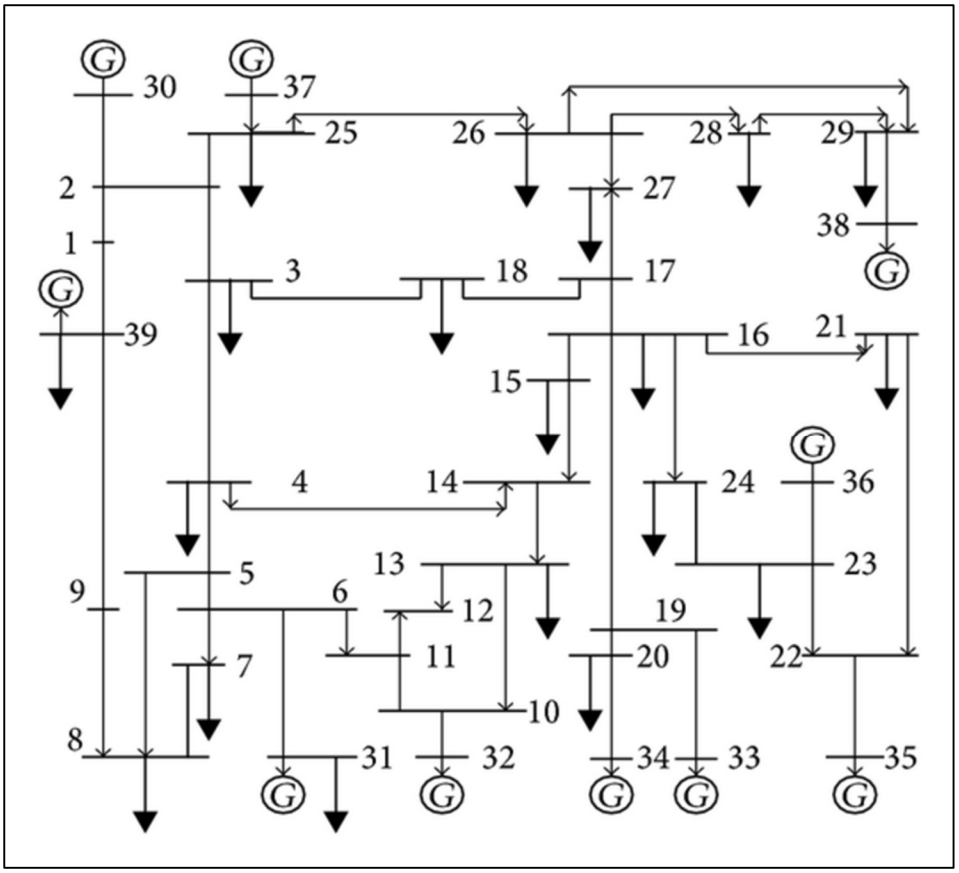

Figure-A IV-1 IEEE 39-bus (New-England) system
Taken from Athay, Podomore et al. (1979)

APPENDIX V

IEEE 57-BUS SYSTEM

The IEEE 57-bus system consists of 7 generators and 42 loads. This system shows a part of the American Electric Power System in 1965. This system is presented in Figure-A V-1.

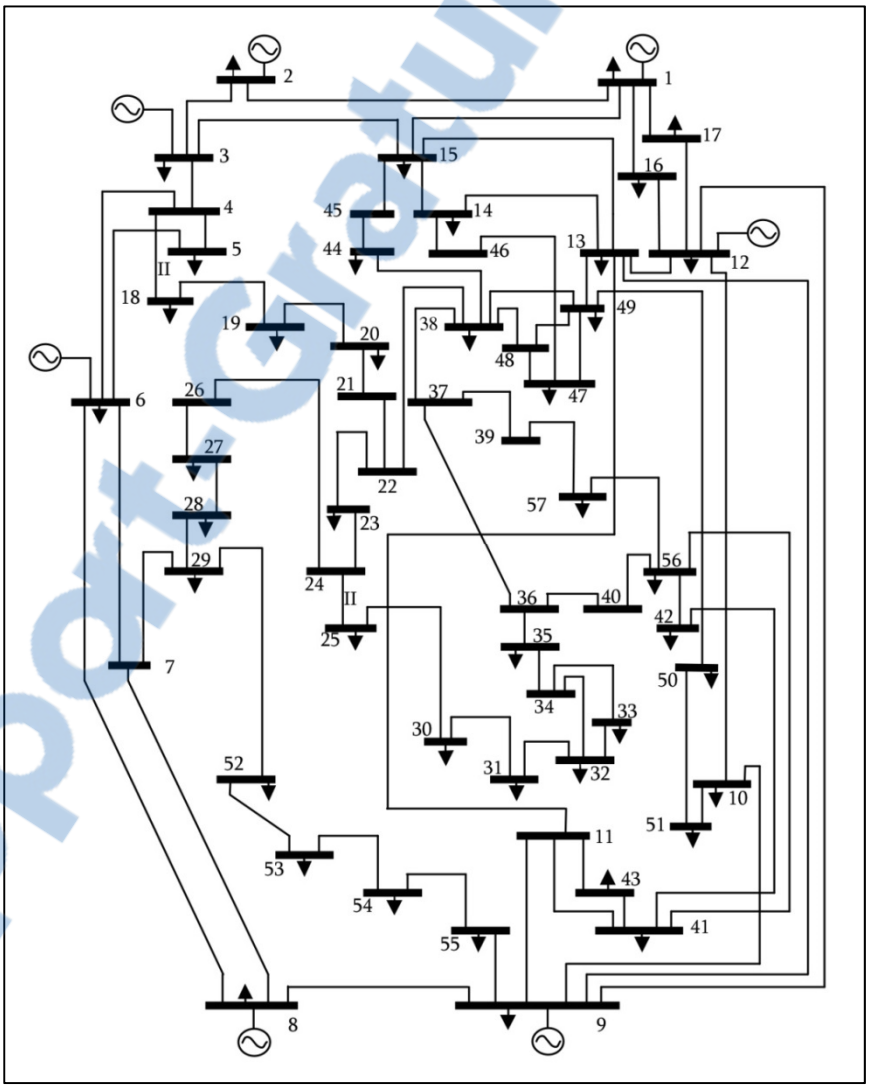

Figure-A V-1 IEEE 57-bus system

LIST OF REFERENCES

Abdelkader, S. M., et D. J. Morrow. 2012. « Online Tracking of Thevenin Equivalent Parameters Using PMU Measurements ». *Power Systems, IEEE Transactions on,* vol. 27, nº 2, p. 975-983.

Abdelkader, S. M., et D. J. Morrow. 2015. « Online Thevenin Equivalent Determination Considering System Side Changes and Measurement Errors ». *Power Systems, IEEE Transactions on,* vol. 30, nº 5, p. 2716-2725.

Al Dessi, S. A., A. H. Osman et A. I. Ibrahim. 2013. « Voltage stability assessment of a real power system using a detailed dynamic load model ». In *Electric Power and Energy Conversion Systems (EPECS), 2013 3rd International Conference on*. (2-4 Oct. 2013), p. 1-6.

Anaya-Lara, O., N. Jenkins, J. Ekanayake, P. Cartwright et M. Hughes. 2009. *Wind Generation, Modeling and Control*. New York, NY, USA: Wiley.

Anderson, P. M., et M. Mirheydar. 1990. « A low-order system frequency response model ». *IEEE Transactions on Power Systems,* vol. 5, nº 3, p. 720-729.

Andersson, Göran. 2004. « Modelling and analysis of electric power systems ». *EEH-Power Systems Laboratory, Swiss Federal Institute of Technology (ETH), Zürich, Switzerland*.

Assessment of demand response and advanced metering. 2012. FERC Report,. <https://www.ferc.gov/ >.

Athay, T., R. Podmore et S. Virmani. 1979. « A Practical Method for the Direct Analysis of Transient Stability ». *Power Apparatus and Systems, IEEE Transactions on,* vol. PAS-98, nº 2, p. 573-584.

Atwa, Y. M., et E. F. El-Saadany. 2010. « Optimal Allocation of ESS in Distribution Systems With a High Penetration of Wind Energy ». *IEEE Transactions on Power Systems,* vol. 25, nº 4, p. 1815-1822.

Atwa, Yasser M, et Ehab F El-Saadany. 2011. « Probabilistic approach for optimal allocation of wind-based distributed generation in distribution systems ». *IET Renewable Power Generation,* vol. 5, nº 1, p. 79-88.

Atwa, YM, EF El-Saadany, MMA Salama et R Seethapathy. 2010. « Optimal renewable resources mix for distribution system energy loss minimization ». *IEEE Transactions on Power Systems,* vol. 25, nº 1, p. 360-370.

Avalos, R. J. 2008. « Analysis and Application of Optimization Techniques to Power System Security and Electricity Markets ». University of Waterloo, 185 p.

Avalos, R. J., C. A. Canizares et M. F. Anjos. 2008. « A practical voltage-stability-constrained optimal power flow ». In *Power and Energy Society General Meeting - Conversion and Delivery of Electrical Energy in the 21st Century, 2008 IEEE*. (20-24 July 2008), p. 1-6.

Barbier, C., et J.P. Barret. 1980. « Analyse des phenomenes d'ecroulement de tension sur un reseau de transport ». *Rev. Generale d'Elect.,* vol. 89, nº 10, p. 672-690.

Bienstock, Daniel, Michael Chertkov et Sean Harnett. 2014. « Chance-Constrained Optimal Power Flow: Risk-Aware Network Control under Uncertainty ». *SIAM Review,* vol. 56, nº 3, p. 461-495.

Bouffard, F., F. D. Galiana et A. J. Conejo. 2005. « Market-clearing with stochastic security-part II: case studies ». *IEEE Transactions on Power Systems,* vol. 20, nº 4, p. 1827-1835.

Breiman, Leo. 2001. « Random forests ». *Machine learning,* vol. 45, nº 1, p. 5-32.

Cain, Mary B., Richard P. O'Neill et Anya Castillo. December, 2012. *History of Optimal Power Flow and Formulations*. Federal Energy Regulatory Commission (FERC).

Canizares, C., W. Rosehart, A. Berizzi et C. Bovo. 2001. « Comparison of voltage security constrained optimal power flow techniques ». In *Power Engineering Society Summer Meeting, 2001*. (2001) Vol. 3, p. 1680-1685 vol.3.

Canizares, Claudio A. 2002. « Voltage stability assessment: concepts, practices and tools ». *Power System Stability Subcommittee Special Publication IEEE/PES, Final Document (thunderbox. uwaterloo. ca/~ claudio/claudio. html# VSWG)*.

Carpentier, J. . 1984. « Voltage collapce proximity indicators computed from an optimal power flow ». In *Proceedings of Systems Computation Conference*. (Helsinki, Finland, September), p. 671-678.

Chacra, Fouad Abou, Patrick Bastard, Gilles Fleury et Régine Clavreul. 2005. « Impact of energy storage costs on economical performance in a distribution substation ». *IEEE Transactions on Power Systems,* vol. 20, nº 2, p. 684-691.

Chandrasekaran, K., et S. P. Simon. 2012. « Multi-objective unit commitment problem with reliability function using fuzzified binary real coded artificial bee colony algorithm ». *IET Generation, Transmission & Distribution,* vol. 6, nº 10, p. 1060-1073.

Chang-Chien, L. R., L. N. An, T. W. Lin et W. J. Lee. 2012. « Incorporating Demand Response With Spinning Reserve to Realize an Adaptive Frequency Restoration Plan for System Contingencies ». *IEEE Transactions on Smart Grid,* vol. 3, nº 3, p. 1145-1153.

Chilvers, I., N. Jenkins et P. Crossley. 2005. « Distance relaying of 11 kV circuits to increase the installed capacity of distributed generation ». *IEE Proceedings - Generation, Transmission and Distribution,* vol. 152, nº 1, p. 40-46.

Chow, J. C., R. Fischl et H. Yan. 1990. « On the evaluation of voltage collapse criteria ». *Power Systems, IEEE Transactions on,* vol. 5, nº 2, p. 612-620.

Chowdhury, Badrul H, et Carson W Taylor. 2000. « Voltage stability analysis: VQ power flow simulation versus dynamic simulation ». *Power Systems, IEEE Transactions on,* vol. 15, nº 4, p. 1354-1359.

Chu, Steven, et Arun Majumdar. 2012. « Opportunities and challenges for a sustainable energy future ». *nature,* vol. 488, nº 7411, p. 294-303.

Cohon, J.L. 2013. *Multiobjective Programming and Planning*. Dover Publications.

Condren, J., T. W. Gedra et P. Damrongkulkamjorn. 2006. « Optimal power flow with expected security costs ». *IEEE Transactions on Power Systems,* vol. 21, nº 2, p. 541-547.

Corsi, S., et G. N. Taranto. 2008. « A Real-Time Voltage Instability Identification Algorithm Based on Local Phasor Measurements ». *Power Systems, IEEE Transactions on,* vol. 23, nº 3, p. 1271-1279.

Cupelli, M, C Doig Cardet et A Monti. 2012. « Comparison of line voltage stability indices using dynamic real time simulation ». In *Innovative Smart Grid Technologies (ISGT Europe), 2012 3rd IEEE PES International Conference and Exhibition on*. p. 1-8. IEEE.

Cutsem, Thierry Van, et Costas Vournas. 1998. *Voltage stability of electric power systems*. Coll. « The Kluwer international series in engineering and computer science », 441. Boston: Kluwer Academic Publishers, xi, 378 p. p.

Delille, Gauthier, Bruno Francois, Gilles Malarange et Jean-Luc Fraisse. 2009. « Energy storage systems in distribution grids: New assets to upgrade distribution network abilities ». In *Electricity Distribution-Part 1, 2009. CIRED 2009. 20th International Conference and Exhibition on*. p. 1-4. IET.

Devaraj, D., et J. Preetha Roselyn. 2010. « Genetic algorithm based reactive power dispatch for voltage stability improvement ». *International Journal of Electrical Power & Energy Systems,* vol. 32, nº 10, p. 1151-1156.

Duman, S., So, x, Y. nmez, Gu, x, venc, x, U., Yo, x, ru, x et N. keren. 2012a. « Optimal reactive power dispatch using a gravitational search algorithm ». *Generation, Transmission & Distribution, IET,* vol. 6, nº 6, p. 563-576.

Duman, Serhat, Uğur Güvenç, Yusuf Sönmez et Nuran Yörükeren. 2012b. « Optimal power flow using gravitational search algorithm ». *Energy Conversion and Management,* vol. 59, p. 86-95.

Dupačová, Jitka, Nicole Gröwe-Kuska et Werner Römisch. 2003. « Scenario reduction in stochastic programming ». *Mathematical programming,* vol. 95, nº 3, p. 493-511.

Dvorkin, Yury, Yishen Wang, Hrvoje Pandzic et Daniel Kirschen. 2014. « Comparison of scenario reduction techniques for the stochastic unit commitment ». In *PES General Meeting| Conference & Exposition, 2014 IEEE*. p. 1-5. IEEE.

El-Sadek, M. Z., M. S. Abdel-Salam, A. A. Ibraheem et A. A. Hussien. 1997. « CRITERIA FOR DETECTION OF STEADY-STATE VOLTAGE STABILITY OF POWER SYSTEMS ». *Electric Machines & Power Systems,* vol. 25, nº 8, p. 851-864.

El-Sadek, M. Z., G. A. Mahmoud, M. M. Dessouky et W. I. Rashed. 1999. « Tap changing transformer role in voltage stability enhancement ». *Electric Power Systems Research,* vol. 50, nº 2, p. 115-118.

Engelhardt, S., I. Erlich, C. Feltes, J. Kretschmann et F. Shewarega. 2011. « Reactive Power Capability of Wind Turbines Based on Doubly Fed Induction Generators ». *IEEE Transactions on Energy Conversion,* vol. 26, nº 1, p. 364-372.

Eremia, M., et M. Shahidehpour. 2013. *Handbook of Electrical Power System Dynamics: Modeling, Stability, and Control*. Wiley.

Esmaili, M. 2013. « Placement of minimum distributed generation units observing power losses and voltage stability with network constraints ». *IET Generation, Transmission & Distribution,* vol. 7, nº 8, p. 813-821.

Gabash, A., et P. Li. 2012. « Active-Reactive Optimal Power Flow in Distribution Networks With Embedded Generation and Battery Storage ». *IEEE Transactions on Power Systems,* vol. 27, nº 4, p. 2026-2035.

« GAMS - A User's Guide ». < www.gams.com/dd/docs/bigdocs/GAMSUsersGuide.pdf >.

Gan, D, Robert J Thomas et Ray D Zimmerman. 1998. « A transient stability constrained optimal power flow ». *Proc. of the Bulk Power Systems Dynamics and Control IV-Restructuring*.

Gear, C.W. 1971. *Numerical initial value problems in ordinary differential equations*. Prentice-Hall.

Goel, L., Wu Qiuwei et Wang Peng. 2006. « Reliability enhancement of a deregulated power system considering demand response ». In *2006 IEEE Power Engineering Society General Meeting*. (0-0 0), p. 6 pp.

Gomez-Exposito, A., A.J. Conejo et C. Canizares. 2008. *Electric Energy Systems: Analysis and Operation*. Taylor & Francis.

Grenier, M. E., D. Lefebvre et T. Van Cutsem. 2005. « Quasi steady-state models for long-term voltage and frequency dynamics simulation ». In *Power Tech, 2005 IEEE Russia*. (27-30 June 2005), p. 1-8.

Grigg, C., P. Wong, P. Albrecht, R. Allan, M. Bhavaraju, R. Billinton, Q. Chen, C. Fong, S. Haddad, S. Kuruganty, W. Li, R. Mukerji, D. Patton, N. Rau, D. Reppen, A. Schneider, M. Shahidehpour et C. Singh. 1999. « The IEEE Reliability Test System-1996. A report prepared by the Reliability Test System Task Force of the Application of Probability Methods Subcommittee ». *IEEE Transactions on Power Systems,* vol. 14, n^{o} 3, p. 1010-1020.

Gröwe-Kuska, Nicole, Krzysztof C. Kiwiel, Matthias P. Nowak, Werner Römisch et Isabel Wegner. 2002. « Power Management in a Hydro-Thermal System under Uncertainty by Lagrangian Relaxation ». In *Decision Making Under Uncertainty: Energy and Power*, sous la dir. de Greengard, Claude, et Andrzej Ruszczynski. Gröwe-Kuska2002. p. 39-70. New York, NY: Springer New York. <http://dx.doi.org/10.1007/978-1-4684-9256-9_3 >.

Guo-yun, Cao, Chen Luo-nan et K. Aihara. 2015. « Power System Voltage Stability Assessment Based on Branch Active Powers ». *Power Systems, IEEE Transactions on,* vol. 30, n^{o} 2, p. 989-996.

Haoyu, Yuan, et Li Fangxing. 2014. « A comparative study of measurement-based Thevenin equivalents identification methods ». In *North American Power Symposium (NAPS), 2014*. (7-9 Sept. 2014), p. 1-6.

Harsha, Pavithra, et Munther Dahleh. 2015. « Optimal management and sizing of energy storage under dynamic pricing for the efficient integration of renewable energy ». *IEEE Transactions on Power Systems,* vol. 30, nº 3, p. 1164-1181.

Hatipoglu, Kenan. 2014. « Dynamic voltage stability enhancement of a microgrid with different types of distributed energy resources ». TENNESSEE TECHNOLOGICAL UNIVERSITY.

Horta, R., J. Espinosa et J. Pati. 2015. « Frequency and voltage control of a power system with information about grid topology ». In *Automatic Control (CCAC), 2015 IEEE 2nd Colombian Conference on*. (14-16 Oct. 2015), p. 1-6.

Ilić, M., et J. Zaborszky. 2000. *Dynamics and Control of Large Electric Power Systems*. Wiley.

Jabr, R. A., et B. C. Pal. 2009. « Intermittent wind generation in optimal power flow dispatching ». *IET Generation, Transmission & Distribution,* vol. 3, nº 1, p. 66-74.

Jalboub, Mohamed K., Haile S. Rajamani, Darwin T. W. Liang, Raed A. Abd-Alhameed et Abdulbassat M. Ihbal. 2012. « Investigation of Voltage Stability Indices to Identify Weakest Bus (TBC) ». In *Mobile Multimedia Communications: 6th International ICST Conference, MOBIMEDIA 2010, Lisbon, Portugal, September 6-8, 2010. Revised Selected Papers*, sous la dir. de Rodriguez, Jonathan, Rahim Tafazolli et Christos Verikoukis. Jalboub2012. p. 682-687. Berlin, Heidelberg: Springer Berlin Heidelberg. < http://dx.doi.org/10.1007/978-3-642-35155-6_56 >.

Jarjis, J., et F. D. Galiana. 1981. « Quantitative Analysis of Steady State Stability in Power Networks ». *Power Apparatus and Systems, IEEE Transactions on,* vol. PAS-100, nº 1, p. 318-326.

Jian-Hong, Liu, et Chu Chia-Chi. 2014. « Wide-Area Measurement-Based Voltage Stability Indicators by Modified Coupled Single-Port Models ». *Power Systems, IEEE Transactions on,* vol. 29, nº 2, p. 756-764.

Joskow, Paul, et Jean Tirole. 2006. « Retail electricity competition ». *The Rand Journal of Economics,* vol. 37, nº 4, p. 799-815.

Joskow, Paul, et Jean Tirole. 2007. « Reliability and competitive electricity markets ». *The Rand Journal of Economics,* vol. 38, nº 1, p. 60-84.

Kayikci, M., et J. V. Milanovic. 2007. « Reactive Power Control Strategies for DFIG-Based Plants ». *IEEE Transactions on Energy Conversion,* vol. 22, nº 2, p. 389-396.

Kessel, P., et H. Glavitsch. 1986. « Estimating the Voltage Stability of a Power System ». *Power Delivery, IEEE Transactions on,* vol. 1, nº 3, p. 346-354.

Konopinski, R. J., P. Vijayan et V. Ajjarapu. 2009. « Extended Reactive Capability of DFIG Wind Parks for Enhanced System Performance ». *IEEE Transactions on Power Systems,* vol. 24, nº 3, p. 1346-1355.

Kraning, Matt, Yang Wang, Ekine Akuiyibo et Stephen Boyd. 2011. « Operation and configuration of a storage portfolio via convex optimization ». *IFAC Proceedings Volumes,* vol. 44, nº 1, p. 10487-10492.

Kundur, P., J. Paserba, V. Ajjarapu, G. Andersson, A. Bose, C. Canizares, N. Hatziargyriou, D. Hill, A. Stankovic, C. Taylor, T. Van Cutsem et V. Vittal. 2004. « Definition and classification of power system stability ». *Ieee Transactions on Power Systems,* vol. 19, nº 3, p. 1387-1401.

Kusiak, Andrew, et Zijun Zhang. 2010. « Short-horizon prediction of wind power: A data-driven approach ». *IEEE Transactions on Energy Conversion,* vol. 25, nº 4, p. 1112-1122.

« Kyoto Protocol to the United Nations Framework Convention on Climate Change ». 1992. < http://www.unfccc.int. >.

Lage, G. G., G. R. M. da Costa et C. A. Canizares. 2012. « Limitations of assigning general critical values to voltage stability indices in Voltage-Stability-Constrained optimal power flows ». In *Power System Technology (POWERCON), 2012 IEEE International Conference on*. (Oct. 30 2012-Nov. 2 2012), p. 1-6.

Lee, Byung Ha, et Kwang Y Lee. 1993. « Dynamic and static voltage stability enhancement of power systems ». *Power Systems, IEEE Transactions on,* vol. 8, nº 1, p. 231-238.

Lee, D. H. A. 2015. « Voltage Stability Assessment Using Equivalent Nodal Analysis ». *Power Systems, IEEE Transactions on,* vol. PP, nº 99, p. 1-10.

Lee, M, O Aslam, B Foster, D Kathan, J Kwok, L Medearis, R Palmer, P Sporborg et M Tita. 2013. « Assessment of demand response and advanced metering ». *Federal Energy Regulatory Commission, Tech. Rep*.

Lian, S, S Morii, T Ishii et S Kawamoto. 2010. « Voltage stability and sensitivity analysis considering dynamic load for smart grid ». In *Innovative Smart Grid Technologies (ISGT), 2010*. p. 1-6. IEEE.

Lin, Yashen, Johanna L Mathieu et Jeremiah X Johnson. 2016. « Stochastic optimal power flow formulation to achieve emissions objectives with energy storage ». In *Power Systems Computation Conference (PSCC), 2016*. p. 1-7. IEEE.

Lof, P. A., G. Andersson et D. J. Hill. 1993. « Voltage stability indices for stressed power systems ». *Power Systems, IEEE Transactions on,* vol. 8, nº 1, p. 326-335.

Londero, R. R., C. d. M. Affonso et J. P. A. Vieira. 2015. « Long-Term Voltage Stability Analysis of Variable Speed Wind Generators ». *IEEE Transactions on Power Systems,* vol. 30, nº 1, p. 439-447.

Lu, S., S. Lou, Y. Wu et X. Yin. 2013. « Power system economic dispatch under low-carbon economy with carbon capture plants considered ». *IET Generation, Transmission & Distribution,* vol. 7, nº 9, p. 991-1001.

Lu, S., N. Samaan, R. Diao, M. Elizondo, C. Jin, E. Mayhorn, Y. Zhang et H. Kirkham. 2011. « Centralized and decentralized control for demand response ». In *Innovative Smart Grid Technologies (ISGT), 2011 IEEE PES*. (17-19 Jan. 2011), p. 1-8.

Lund, Torsten, Poul Sørensen et Jarle Eek. 2007. « Reactive power capability of a wind turbine with doubly fed induction generator ». *Wind Energy,* vol. 10, nº 4, p. 379-394.

Mathieu, J. L., M. G. Vay, x00E et G. Andersson. 2013. « Uncertainty in the flexibility of aggregations of demand response resources ». In *Industrial Electronics Society, IECON 2013 - 39th Annual Conference of the IEEE*. (10-13 Nov. 2013), p. 8052-8057.

McLinn, James. 2009. « Major Power Outages in the US, and around the World ». *IEEE Reliability Society*.

Meegahapola, L. G., T. Littler et D. Flynn. 2010. « Decoupled-DFIG Fault Ride-Through Strategy for Enhanced Stability Performance During Grid Faults ». *IEEE Transactions on Sustainable Energy,* vol. 1, nº 3, p. 152-162.

Meegahapola, Lasantha, Tim Littler et Sarath Perera. 2013. « Capability curve based enhanced reactive power control strategy for stability enhancement and network voltage management ». *International Journal of Electrical Power & Energy Systems,* vol. 52, p. 96-106.

Meyer-Huebner, Nico, Frederik Gielnik, Michael Suriyah et Thomas Leibfried. 2016. «Dynamic optimal power flow in AC networks with multi-terminal HVDC and energy storage ». In *Innovative Smart Grid Technologies-Asia (ISGT-Asia), 2016 IEEE*. p. 300-305. IEEE.

Milano, F. 2005. « An Open Source Power System Analysis Toolbox ». *Power Systems, IEEE Transactions on,* vol. 20, nº 3, p. 1199-1206.

Milano, F., C. A. Canizares et M. Invernizzi. 2005. « Voltage stability constrained OPF market models considering N-1 contingency criteria ». *Electric Power Systems Research,* vol. 74, nº 1, p. 27-36.

Mo, N, ZY Zou, KW Chan et TYG Pong. 2007. « Transient stability constrained optimal power flow using particle swarm optimisation ». *Generation, Transmission & Distribution, IET,* vol. 1, nº 3, p. 476-483.

Moghavvemi, M, et FM Omar. 1998. « Technique for contingency monitoring and voltage collapse prediction ». *IEE Proceedings-Generation, Transmission and Distribution,* vol. 145, nº 6, p. 634-640.

Moghavvemi, M., et O. Faruque. 1998. « Real-time contingency evaluation and ranking technique ». *Generation, Transmission and Distribution, IEE Proceedings-,* vol. 145, nº 5, p. 517-524.

Mohamed, A, GB Jasmon et S Yusoff. 1989. « A static voltage collapse indicator using line stability factors ». *Journal of industrial technology,* vol. 7, nº 1, p. 73-85.

Morales, Juan M, Salvador Pineda, Antonio J Conejo et Miguel Carrion. 2009. « Scenario reduction for futures market trading in electricity markets ». *IEEE Transactions on Power Systems,* vol. 24, nº 2, p. 878-888.

Musirin, Ismail, et TK Abdul Rahman. 2002. « On-line voltage stability based contingency ranking using fast voltage stability index (FVSI) ». In *Transmission and Distribution Conference and Exhibition 2002: Asia Pacific. IEEE/PES.* Vol. 2, p. 1118-1123. IEEE.

Nath, Sudipta, et Shrabani Pal. 2010. « A novel technique for determination of voltage stability margin ».

« National Emission Ceilings for Certain Atmospheric Pollutants, Directive 2001/81/EC of the European Parliament and of the Council ». 2001. < http://www.europa.int.eu >.

Niknam, T., M. R. Narimani, J. Aghaei et R. Azizipanah-Abarghooee. 2012. « Improved particle swarm optimisation for multi-objective optimal power flow considering the cost, loss, emission and voltage stability index ». *IET Generation, Transmission & Distribution,* vol. 6, nº 6, p. 515-527.

Pal, Mrinal K. 1992. « Voltage stability conditions considering load characteristics ». *Power Systems, IEEE Transactions on,* vol. 7, nº 1, p. 243-249.

Pan, Yang, Libao Shi, Yajie Liu, Jinqing Luo et Ren Wang. 2016. « Study on optimal power flow in a wind-storage system ». In *Power and Energy Engineering Conference (APPEEC), 2016 IEEE PES Asia-Pacific*. p. 1709-1713. IEEE.

Pand, H., Y. Dvorkin, T. Qiu, Y. Wang et D. S. Kirschen. 2016. « Toward Cost-Efficient and Reliable Unit Commitment Under Uncertainty ». *IEEE Transactions on Power Systems,* vol. 31, nº 2, p. 970-982.

Pandžić, H., Y. Wang, T. Qiu, Y. Dvorkin et D. S. Kirschen. 2015. « Near-Optimal Method for Siting and Sizing of Distributed Storage in a Transmission Network ». *IEEE Transactions on Power Systems,* vol. 30, nº 5, p. 2288-2300.

Papavasiliou, A., et S. S. Oren. 2012. « A stochastic unit commitment model for integrating renewable supply and demand response ». In *2012 IEEE Power and Energy Society General Meeting*. (22-26 July 2012), p. 1-6.

Papavasiliou, A., S. S. Oren et R. P. O' Neill. 2011. « Reserve Requirements for Wind Power Integration: A Scenario-Based Stochastic Programming Framework ». *IEEE Transactions on Power Systems,* vol. 26, nº 4, p. 2197-2206.

Papavasiliou, Anthony, et Shmuel S Oren. 2013. « Multiarea stochastic unit commitment for high wind penetration in a transmission constrained network ». *Operations Research,* vol. 61, nº 3, p. 578-592.

Polak, E. 1971. *Computational Methods in Optimization: A Unified Approach*. Elsevier Science.

Potter, Cameron, Debra Lew, Jim McCaa, Sam Cheng, Scott Eichelberger et Eric Grimit. 2008. « Creating the dataset for the western wind and solar integration study (USA) ». *Wind Engineering,* vol. 32, nº 4, p. 325-338.

Rabiee, A., A. Soroudi, B. Mohammadi-ivatloo et M. Parniani. 2014. « Corrective Voltage Control Scheme Considering Demand Response and Stochastic Wind Power ». *IEEE Transactions on Power Systems,* vol. 29, nº 6, p. 2965-2973.

Rashedi, Esmat, Hossein Nezamabadi-pour et Saeid Saryazdi. 2009. « GSA: A Gravitational Search Algorithm ». *Information Sciences,* vol. 179, nº 13, p. 2232-2248.

Rastler, DM. 2010. *Electricity energy storage technology options: a white paper primer on applications, costs and benefits*. Electric Power Research Institute.

Rebours, Y. G., D. S. Kirschen, M. Trotignon et S. Rossignol. 2007. « A Survey of Frequency and Voltage Control Ancillary Services—Part I: Technical Features ». *IEEE Transactions on Power Systems,* vol. 22, nº 1, p. 350-357.

Regulski, Pawel Adam. 2012. « Estimation of parameters of dynamic load models for voltage stability studies ». University of Manchester.

Rezaei Adaryani, M., et A. Karami. 2013. « Artificial bee colony algorithm for solving multi-objective optimal power flow problem ». *International Journal of Electrical Power & Energy Systems,* vol. 53, p. 219-230.

Roald, Line, Sidhant Misra, Michael Chertkov, Scott Backhaus et Göran Andersson. 2016. «Chance Constrained Optimal Power Flow with Curtailment and Reserves from Wind Power Plants ». *arXiv preprint arXiv:1601.04321*.

Rosehart, W. D., C. A. Canizares et V. H. Quintana. 2003a. « Effect of detailed power system models in traditional and voltage-stability-constrained optimal power-flow problems ». *Power Systems, IEEE Transactions on,* vol. 18, nº 1, p. 27-35.

Rosehart, W. D., C. A. Canizares et V. H. Quintana. 2003b. « Multiobjective optimal power flows to evaluate voltage security costs in power networks ». *Power Systems, IEEE Transactions on,* vol. 18, nº 2, p. 578-587.

Salama, MM, EM Saied et SM Abdel-Maksoud. 1999. « Steady state voltage instability assessment in a power system ». *Energy conversion and management,* vol. 40, nº 1, p. 59-69.

Sioshansi, Ramteen. 2012. « OR Forum—modeling the impacts of electricity tariffs on plug-in hybrid electric vehicle charging, costs, and emissions ». *Operations Research,* vol. 60, nº 3, p. 506-516.

Sioshansi, Ramteen, et Walter Short. 2009. « Evaluating the impacts of real-time pricing on the usage of wind generation ». *IEEE Transactions on Power Systems,* vol. 24, nº 2, p. 516-524.

Sjödin, Emma, Dennice F Gayme et Ufuk Topcu. 2012. « Risk-mitigated optimal power flow for wind powered grids ». In *American Control Conference (ACC), 2012*. p. 4431-4437. IEEE.

Smon, I., G. Verbic et F. Gubina. 2006. « Local voltage-stability index using tellegen's Theorem ». *Power Systems, IEEE Transactions on,* vol. 21, nº 3, p. 1267-1275.

Steen, D., S. Al-Yami, L. A. Tuan, O. Carlson et L. Bertling. 2011. « Optimal load management of electric heating and PEV loads in a residential distribution system in Sweden ». In *Innovative Smart Grid Technologies (ISGT Europe), 2011 2nd IEEE PES International Conference and Exhibition on*. (5-7 Dec. 2011), p. 1-7.

Su, Han-I, et Abbas El Gamal. 2011. « Modeling and analysis of the role of fast-response energy storage in the smart grid ». In *Communication, Control, and Computing (Allerton), 2011 49th Annual Allerton Conference on*. p. 719-726. IEEE.

Summers, T., J. Warrington, M. Morari et J. Lygeros. 2014. « Stochastic optimal power flow based on convex approximations of chance constraints ». In *Power Systems Computation Conference (PSCC), 2014*. (18-22 Aug. 2014), p. 1-7.

Tamimi, Behnam, Claudio A Canizares et Sadegh Vaez-Zadeh. 2010. « Effect of reactive power limit modeling on maximum system loading and active and reactive power markets ». *Power Systems, IEEE Transactions on,* vol. 25, nº 2, p. 1106-1116.

Tamura, Y., H. Mori et S. Iwamoto. 1983. « Relationship Between Voltage Instability and Multiple Load Flow Solutions in Electric Power Systems ». *Power Engineering Review, IEEE,* vol. PER-3, nº 5, p. 30-31.

Taylor, C.W., N.J. Balu et D. Maratukulam. 1994. *Power system voltage stability*. McGraw-Hill Ryerson, Limited.

Thukaram, Bansilal D., et K. Parthasarathy. 1996. « Optimal reactive power dispatch algorithm for voltage stability improvement ». *International Journal of Electrical Power & Energy Systems,* vol. 18, nº 7, p. 461-468.

Thukaram, D., Lawrence Jenkins, H. P. Khincha, G. Yesuratnam et B. R. Kumar. 2004. «Monitoring the effects of on-load tap changing transformers on voltage stability ». In *Power System Technology, 2004. PowerCon 2004. 2004 International Conference on*. (21-24 Nov. 2004) Vol. 1, p. 419-424 Vol.1.

Tiranuchit, A., et R. J. Thomas. 1988. « A posturing strategy against voltage instabilities in electric power systems ». *Power Systems, IEEE Transactions on,* vol. 3, nº 1, p. 87-93.

V, Jorge Esteban Tobón, Rosa E. Correa Gutiérrez et Juan M. Ramirez. 2014. « Voltage collapse detection based on local measurements ». *Electric Power Systems Research,* vol. 107, p. 77-84.

Van Cutsem, T., et R. Mailhot. 1997. « Validation of a fast voltage stability analysis method on the Hydro-Quebec system ». *Power Systems, IEEE Transactions on,* vol. 12, nº 1, p. 282-292.

Van Cutsem, T., et C. D. Vournas. 1996. « Voltage stability analysis in transient and mid-term time scales ». *Power Systems, IEEE Transactions on,* vol. 11, nº 1, p. 146-154.

Venkatesh, B., A. Arunagiri et H. B. Gooi. 2003. « Unified OPF method for maximizing voltage stability margin using successive fuzzy LP ». *Electric Power Systems Research,* vol. 64, nº 2, p. 119-128.

Vittal, E., M. O' Malley et A. Keane. 2010. « A Steady-State Voltage Stability Analysis of Power Systems With High Penetrations of Wind ». *IEEE Transactions on Power Systems,* vol. 25, nº 1, p. 433-442.

Vournas, C. D., et M. Karystianos. 2002. « Transmission system tap changer settings to maximize loadability margin ». In *Proc. 14th Power Syst. Comput. Conf.* (Sevilla, Spain).

Vournas, C., et M. Karystianos. 2004. « Load tap changers in emergency and preventive voltage stability control ». *Power Systems, IEEE Transactions on,* vol. 19, nº 1, p. 492-498.

Vrakopoulou, M., K. Margellos, J. Lygeros et G. Andersson. 2012. « A probabilistic framework for security constrained reserve scheduling of networks with wind power generation ». In *Energy Conference and Exhibition (ENERGYCON), 2012 IEEE International*. (9-12 Sept. 2012), p. 452-457.

Vrakopoulou, M., J. L. Mathieu et G. Andersson. 2014. « Stochastic Optimal Power Flow with Uncertain Reserves from Demand Response ». In *2014 47th Hawaii International Conference on System Sciences*. (6-9 Jan. 2014), p. 2353-2362.

Vrakopoulou, Maria, Kostas Margellos, John Lygeros et Göran Andersson. 2013. «Probabilistic guarantees for the N-1 security of systems with wind power generation». In *Reliability and Risk Evaluation of Wind Integrated Power Systems*. p. 59-73. Springer.

Vrettos, E., et G. Andersson. 2013. « Combined Load Frequency Control and active distribution network management with Thermostatically Controlled Loads ». In *Smart Grid Communications (SmartGridComm), 2013 IEEE International Conference on*. (21-24 Oct. 2013), p. 247-252.

Vu, K., M. M. Begovic, D. Novosel et M. M. Saha. 1999. « Use of local measurements to estimate voltage-stability margin ». *Power Systems, IEEE Transactions on,* vol. 14, nº 3, p. 1029-1035.

Wang, Y. H., Y. Y. Wang, K. W. Chan et T. Y. G. Pong. 2011. « Dynamic voltage security constrained optimal coordinated voltage control using enhanced particle swarm optimisation ». *Generation, Transmission & Distribution, IET,* vol. 5, nº 2, p. 239-248.

Wang, Yang, Wenyuan Li et Jiping Lu. 2009. « A new node voltage stability index based on local voltage phasors ». *Electric Power Systems Research,* vol. 79, nº 1, p. 265-271.

Wang, Zhongwei, Jin Zhong, Dong Chen, Yuefeng Lu et Kun Men. 2013. « A multi-period optimal power flow model including battery energy storage ». In *Power and Energy Society General Meeting (PES), 2013 IEEE*. p. 1-5. IEEE.

Warrington, Joseph, Paul Goulart, Sébastien Mariéthoz et Manfred Morari. 2013. « Policy-based reserves for power systems ». *IEEE Transactions on Power Systems,* vol. 28, nº 4, p. 4427-4437.

Weedy, B.M., B.J. Cory, N. Jenkins, J.B. Ekanayake et G. Strbac. 2012. *Electric Power Systems*. Wiley.

Wikipedia. 2017. « List of Major Power Outages ».
<http://en.wikipedia.org/wiki/List_of_power_outages. >.

Wu, GY, CY Chung, KP Wong et CW Yu. 2007. « Voltage stability constrained optimal dispatch in deregulated power systems ». *IET Generation, Transmission & Distribution,* vol. 1, nº 5, p. 761-768.

Xie, D., Z. Xu, L. Yang, J, x00D, stergaard, Y. Xue et K. P. Wong. 2013. « A Comprehensive LVRT Control Strategy for DFIG Wind Turbines With Enhanced Reactive Power Support ». *IEEE Transactions on Power Systems,* vol. 28, nº 3, p. 3302-3310.

Xie, L., H. D. Chiang et S. H. Li. 2011. « Optimal power flow calculation of power system with wind farms ». In *2011 IEEE Power and Energy Society General Meeting*. (24-29 July 2011), p. 1-6.

Yang, Chien-Feng, Gordon G. Lai, Chia-Hau Lee, Ching-Tzong Su et Gary W. Chang. 2012. « Optimal setting of reactive compensation devices with an improved voltage stability index for voltage stability enhancement ». *International Journal of Electrical Power & Energy Systems,* vol. 37, nº 1, p. 50-57.

Yang, Wang, Wang Caisheng, Lin Feng, Li Wenyuan, Wang Le Yi et Zhao Junhui. 2013. «Incorporating Generator Equivalent Model Into Voltage Stability Analysis ». *Power Systems, IEEE Transactions on,* vol. 28, nº 4, p. 4857-4866.

Yau, Timothy, Lewis N Walker, Huber L Graham, Avijit Gupta et Richard Raithel. 1981. «Effects of battery storage devices on power system dispatch ». *IEEE transactions on power apparatus and systems*, nº 1, p. 375-383.

Youssef, E., R. M. El Azab et A. M. Amin. 2015. « Comparative study of voltage stability analysis for renewable energy grid-connected systems using PSS/E ». In *SoutheastCon 2015*. (9-12 April 2015), p. 1-6.

Yunfei, Wang, I. R. Pordanjani, Li Weixing, Xu Wilsun, Chen Tongwen, E. Vaahedi et J. Gurney. 2011. « Voltage Stability Monitoring Based on the Concept of Coupled Single-Port Circuit ». *Power Systems, IEEE Transactions on,* vol. 26, nº 4, p. 2154-2163.

Zabaiou, T., L. A. Dessaint et I. Kamwa. 2014. « Preventive control approach for voltage stability improvement using voltage stability constrained optimal power flow based on static line voltage stability indices ». *Generation, Transmission & Distribution, IET,* vol. 8, nº 5, p. 924-934.

Zeng, YG, G Berizzi et P Marannino. 1997. « Voltage stability analysis considering dynamic load model ».

Zimmerman, R. D., et C. Murillo-Sánchez. « MATPOWER ». <http://www.pserc.cornell.edu//matpower/ >.